Effect of Si and Other Elements Modification on the Photocatalytic Activities of Titanias Prepared by the Glycothermal Method

Hirotaka Ozaki

2008

Contents

General Introduction

Since Honda and Fujishima first reported the photosensitization effect of titanium dioxide (TiO_2) electrode on the electrolysis of water to form H_2 and O_2 [1], the photocatalytic dissociation of water has been extensively studied [2–8]. Many studies in the early stages of this research were devoted to the elucidation of the basic feature of the reaction, and a general mechanism for the heterogeneous photocatalysis on TiO_2 was explained, as illustrated in Fig. 1. The irradiation of a semiconductor with a photon of energy *hv* that exceeds its bandgap energy E_g results in the excitation of an electron from the valence band (V.B.) to the conduction band (C.B.), leaving a positive hole behind. The excited-state conduction-band electrons and valence-band holes recombine and dissipate the input energy as heat, get trapped in the metastable surface states, or react with electron acceptors and electron donors adsorbed on the surface of the semiconductor. In the absence of suitable electron and hole scavengers, the stored energy is dissipated within a few nanoseconds by recombination. In the presence of water, the photogenerated electrons reduce the water molecules to produce H_2, while the positive holes oxidize them to produce O_2, leading to overall water splitting. For this reaction, the lowest level of the conduction band of the semiconductor must be higher (i.e., more negative) on the electrochemical scale than the potential of H^+/H_2 (0 V vs. NHE), and the top level of the valence band must be lower (more positive) than the potential of O_2/H_2O (1.23 V vs. NHE). Since this reaction is regarded as a conversion of light energy into chemical energy, which potentially provides an environmentally benign energy supply system using solar energy, it has been attracting considerable attention. Since the reverse reaction expressed

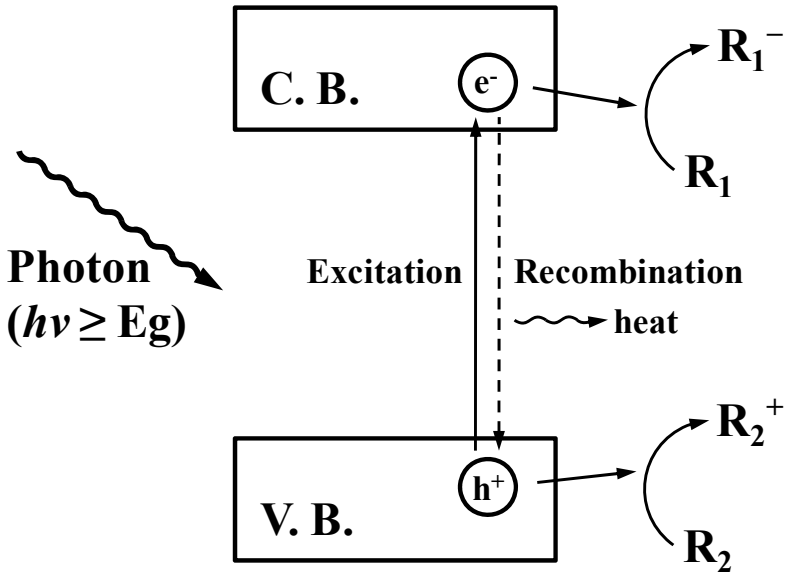

Fig. 1. General scheme for photocatalytic reaction

in Eq. (1)

$$2H_2 + O_2 \rightarrow 2H_2O \quad (1)$$

proceeds easily, quantum yields on bare TiO_2 photocatalysts are usually very low. To improve the efficiency for the photocatalytic dissociation of water, developments of novel photocatalytic materials with different compositions and crystal structures, and the effects of promoters are actively studied [4–8].

Several years after the discovery of the photoelectrolysis of water on TiO_2, Frank and Bard first reported the decomposition of cyanide in water using TiO_2 under ultraviolet (UV) light irradiation [9,10]. Their results were of considerable importance because they demonstrated a potential application of photocatalysis in the field of environmental purification. The redox potential for photogenerated holes in the valence band of TiO_2 is sufficiently positive for the production of hydroxyl radicals (·OH) from water. In addition, the photogenerated electrons excited to the conduction band can reduce oxygen molecules to superoxide O_2^-. In the presence of organic substances, these active oxygen species and/or photogenerated holes react with the organic molecules adsorbed on the surface of the catalysts. To date, a significant number of noteworthy performances of the TiO_2 photocatalysts for the oxidation of a wide range of organic materials (e.g., phenols, chlorophenols, halocarbons, surfactants, pesticides, cyanides, and textile dyes) have been reported. It should be noted that in many cases, the organic compounds could be completely mineralized into harmless compounds such as CO_2 and H_2O. Recently, photocatalysis on TiO_2 for the destruction of microorganisms such as bacteria and viruses and for the inactivation of cancer cells have also been reported [11–13].

It is well known that photocatalytic activity strongly depends on the bulk and surface properties of the TiO_2 samples. Ohtani et al. studied the relationship between the nature and the photocatalytic activity of various TiO_2 photocatalysts; they pointed out that TiO_2 particles having both large surface area (to adsorb a substrate) and a high degree of crystallinity (or few surface and bulk defects) exhibited higher photocatalytic activity [14,15]. Kominami et al. prepared highly active TiO_2 photocatalysts possessing the abovementioned two properties by a novel method known as hydrothermal crystallization in organic media [16].

Modification of titania photocatalysts with other components in order to improve the photocatalytic activity has been investigated. It was previously reported that the photocatalytic activity of TiO_2 was remarkably enhanced by the addition of small amounts of a noble metal such as Pt [17–19]. In a Pt-loaded TiO_2 photocatalyst, the electrons excited by UV-light irradiation were transferred to the Pt particles loaded onto the TiO_2 surface, and the charge separation of the electrons and holes effectively suppresses their recombination, leading to a marked improvement in the photocatalytic activity.

The addition of modifiers that enhance the amount of substrate near the surface of the TiO_2 photocatalysts is also effective. For this purpose, SiO_2, Al_2O_3, phosphate, etc. are used [20–25]. For example, Tada et al. examined the photocatalytic oxidation of cetylpyridinium bromide in aqueous solutions and reported a remarkable improvement in the activity using SiO_2/TiO_2 photocatalysts. They discussed the increase in the electrostatic attraction between the catalyst surface and the cetylpyridinium ion [21].

However, TiO_2 exhibits photocatalytic activities only under UV-light irradiation

because the bandgap energies of titanium dioxides are relatively wide, for instance, 3.0 eV for rutile and 3.2 eV for anatase. This implies that only approximately 3% of the incoming solar energy on the earth's surface can be utilized for photocatalytic reactions on TiO_2 photocatalysts. A number of studies were carried out for the development of photocatalytic materials that exhibit photocatalytic activities under visible-light irradiation. The earliest studies for this purpose date back to the late 1970s, when TiO_2 doped with 3d transition metals were used [26–34]. However, as pointed out by several groups, the photocatalytic activities of the doped titanias under UV-light irradiation were lower than that of pure TiO_2 [35–37]. Pichat et al. discussed the formation of oxygen defects by substituting Cr^{3+} ions for Ti^{4+} ions in titania for maintaining the charge balance and explained the effect of the defect sites that act as recombination centers for photoexcited electrons and photogenerated holes. Recently, Kudo et al. reported a remarkably high photocatalytic activity of TiO_2 and $SrTiO_3$ photocatalysts co-doped with antimony and chromium [38]. They emphasized that the high activities are due to the maintenance of charge balance by the co-doped Sb^{5+} and Cr^{3+} ions without the formation of Cr^{6+} ions and oxygen defects in the lattice. Anpo et al. successfully prepared various transition-metal-ion-doped TiO_2 photocatalysts by a metal-ion-implantation method [39,40]. They reported that the electronic properties of bulk TiO_2 photocatalysts were modified by this method and that the photocatalytic reactivity of the original TiO_2 catalyst under UV-light irradiation ($\lambda < 380$ nm) was preserved even after metal ion doping.

Another approach for the photosensitization of TiO_2 under visible-light irradiation is the doping of anionic species such as C [41–43], F [44,45], S [46–48], and most importantly, N [49–65]. Approximately two decades ago, Sato briefly reported that the calcination of $Ti(OH)_4$ involving ammonium compounds yielded yellowish powders that

exhibited photocatalytic activities for the oxidation of CO and ethane under visible-light irradiation [49]. Recently, Asahi et al. reported the visible-light-induced photocatalytic activity of N-doped titania films and N-doped TiO_2 powders prepared by sputtering a TiO_2 target in an N_2/Ar gas mixture and by treating anatase powder in an NH_3 atmosphere, respectively [50]. They also showed the results of XPS analysis on the doped nitrogen and calculation of the densities of states of the anionic species doped in the anatase TiO_2 crystal. The durability of the catalysts in acid and alkaline solvents and their stable photocatalytic performances during long-term use under mercury lamp irradiation were also reported.

Following the report by Asahi et al., N-doped titanias attracted considerable attention, and a lot of studies, both fundamental and practical, were conducted. Although the mechanism of the emergence of the visible-light-induced photocatalytic activity by N doping and the state of N atoms in the N-doped titania still remain controversial [49–53], the nitrogen-doping in TiO_2 has been proved to be an effective method to induce a visible-light sensitivity to TiO_2. Hashimoto et al. prepared N-doped titanias with varied nitrogen concentrations by changing the NH_3 treatment temperatures (550, 575, and 600 °C) and examined their photocatalytic activities for the decomposition of 2-propanol under visible-light irradiation [51]. They found that the quantum yield significantly decreased when the amount of nitrogen atoms doped in the TiO_2 lattice increased from 0.005 to 0.019. They pointed out that an increase in the amount of nitrogen doped increased oxygen vacancies, which promoted the recombination of holes and electrons, and suggested a difficulty to improve the photoefficiency under visible-light irradiation in the ternary Ti-O-N system.

Titanium oxides are widely used as catalyst supports for the selective catalytic reduction of NO with NH_3 and selective oxidation of hydrocarbons; hence, the preparation method of titania is a subject of considerable importance. Various preparation methods for titanias as well as titania-based mixed oxides have been investigated, for example, the sol-gel method, coprecipitation, and hydrothermal synthesis. Inoue et al. developed a novel technique for the preparation of inorganic materials by treating appropriate starting materials in organic media at elevated temperatures (200–300 °C) under autogeneous pressures [66–68]. Instead of water, which is the common solvent used in well-known hydrothermal methods, they used various organic solvents; therefore, this synthetic technique is referred to as the solvothermal method. With regard to titanias, it was reported that anatase-type nanocrystalline titanias were directly obtained by thermal reactions of titanium alkoxides in 1,4-butanediol and toluene [69]. Kominami et al. applied the solvothermal method to synthesize TiO_2 nanocrystals having high degree of crystallinity and reported their superior photocatalytic activities for various reactions under UV-light irradiation [70,71].

Recently, Iwamoto et al. reported that the thermal reaction of titanium tetraisopropoxide and tetraethyl orthosilicate in 1,4-butanediol (glycothermal reaction) afforded nanocrystalline Si-modified titanias with the anatase structure having significantly large surface areas and high thermal stabilities [72,73]. They also showed that xerogels of the Si-modified titanias prepared by flash evaporation after the glycothermal reaction exhibited enhanced activities for the photocatalytic oxidation of acetic acid under UV-light irradiation [74]. Furthermore, the author of this thesis examined the photocatalytic properties of the xerogels of the Si-modified titanias for various reactions, and he also investigated the photocatalytic activities of nitrified

Si-modified titanias under visible-light irradiation. In this thesis, the results obtained during his doctoral course study are described.

This thesis includes 6 chapters. In chapter 1, the physicochemical properties of Si-modified titania xerogels having higher Si contents and their photocatalytic activities for the degradation of several organic dyes are described.

In chapter 2, the nitrification of Si-modified titanias and their photocatalytic activities under visible-light irradiation are described. It was demonstrated that higher amounts of nitrogen were doped in Si-modified titanias compared to non-modified titanias, and the mechanism of the stabilization of N-doping was discussed.

The author prepared various N- and Si-co-doped titanias by changing the amount of Si added and annealing temperature after the nitrification, and characterized the obtained products by several methods. In chapter 3, effects of the amount of added Si and annealing treatment on the photocatalytic activities of N- and Si-co-doped titanias under visible-light irradiation are mentioned.

Chapter 4 deals with the photocatalytic activities of NH_3-treated titanias modified with elements other than Si. Titanias modified with B, Mg, Al, P, Zn, and Ga were prepared by the glycothermal method, and the products were subjected to nitrification. The photocatalytic decomposition of acetaldehyde using the obtained co-doped titanias under visible-light irradiation was examined.

In order to improve the visible-light responsive photocatalytic activity of the N- and Si-co-doped titanias, as mentioned in the previous chapters, the addition of small amounts of transition metals were examined. In chapter 5, the effect of the addition of a small amount of V on the photocatalytic activities of N- and Si-co-doped titanias under visible-light irradiation is described. By ESR analysis, the electron transfer behavior on

the catalyst under illumination is examined.

Chapter 6 describes the addition of a small amount of Fe to N- and Si-co-doped titanias. A marked enhancement of more than 10 times in the visible-light-induced photocatalytic activity was achieved on an optimized catalyst. The mechanism of the promotive effect of Fe^{3+} cations is discussed.

References

[1] K. Honda and A. Fujishima, *Nature* **1972**, *238*, 37.

[2] M. Grätzel, *Acc. Chem. Res.* **1981**, *20*, 987.

[3] D. Duonghong, E. Borgarello, and M. Grätzel, *J. Am. Chem. Soc.* **1981**, *103*, 4685.

[4] A. Kudo, *Catal. Surv. Asia.* **2003**, *7*, 31.

[5] A. Fujishima, T. N. Rao, and D. A. Tryk, *J. Photochem. Photobiol. C: Photochem. Rev.* **2000**, *1*, 1.

[6] Z. Zou, J. Ye, K. Sayama, and H. Arakawa, *Nature* **2001**, *414*, 625.

[7] H. Hagiwara, N. Ono, T. Inoue, H. Matsumoto, and T. Ishihara, *Angew. Chem. Int. Ed.* **2006**, *45*, 1420.

[8] K. Maeda, K. Teramura, D. Lu, T. Takata, N. Saito, Y. Inoue, and K. Domen, *Nature* **2006**, *440*, 295.

[9] S. N. Frank and A. J. Bard, *J. Am. Chem. Soc.* **1977**, *99*, 303.

[10] S. N. Frank and A. J. Bard, *J. Phys. Chem.* **1977**, *81*, 1484.

[11] H. Sakai, R. Baba, K. Hashimoto, Y. Kubota, and A. Fujishima, *Chem. Lett.* **1995**, 185.

[12] Y. Kikuchi, K. Sunada, T. Iyoda, K. Hashimoto, and A. Fujishima, *J. Photochem. Photobiol. A: Chem.* **1997**, *106*, 51.

[13] K. Sunada, Y. Kikuchi, K. Hashimoto, and A. Fujishima, *Environ. Sci. Technol.* **1998**, *32*, 726.

[14] B. Ohtani and S.-i. Nishimoto, *J. Phys. Chem.* **1993**, *97*, 920.

[15] H. Kominami, S.-y. Murakami, Y. Kera, and B. Ohtani, "Design, Preparation and Characterization of Highly Active Metal Oxide Photocatalysts" in *Photocatalysis: Science and Technology*, Eds. M. Kaneko, I. Okura, Kodansha, Tokyo, **2002**.

[16] H. Kominami, M. Kohno, Y. Takada, M. Inoue, T. Inui, and Y. Kera, *Ind. Eng. Chem. Res.* **1999**, *38*, 3925.

[17] H. Gerischer and A. Heller, *J. Electrochem. Soc.* **1992**, *139*, 113.

[18] H. Einaga, S. Futamura, and T. Ibusuki, *Environ. Sci. Technol.* **2001**, *35*, 1880.

[19] H. Furube, T. Asachi, H. Masuhara, Y. Yamashita, and M. Anpo, *Chem. Phys. Lett.* **2001**, *336*, 424.

[20] C. Anderson and A. J. Bard, *J. Phys. Chem.* **1995**, *99*, 9882.

[21] H. Tada, M. Akazawa, Y. Kubo, and S. Ito, *J. Phys. Chem. B* **1998**, *102*, 6360.

[22] H. Chun, W. Yizhong, and T. Hongxiao, *Appl. Catal. B: Environmental* **2001**, *30*, 277.

[23] C. Anderson and A. J. Bard, *J. Phys. Chem. B* **1997**, *101*, 2611.

[24] M. Wakamura, K. Hashimoto, and T. Watanabe, *Langmuir* **2003**, *19*, 3428.

[25] L. Körösi, S. Papp, I. Bertótti, and I. Dékány, *Chem. Mater.* **2007**, *19*, 4811.

[26] A. K. Ghosh and H. P. Maruska, *J. Electrochem. Soc.* **1977**, *124*, 1516.

[27] H. P. Maruska and A. K. Ghosh, *Solar Energy Mater.* **1979**, *1*, 237.

[28] A. Monnier and J. Augustynski, *J. Electrochem. Soc.* **1980**, *127*, 1576.

[29] Y. Matsumoto, J. Kurimoto, T. Shimizu, and E. Sato, *J. Electrochem. Soc.* **1981**, *128*, 1040.

[30] E. Borgarello, J. Kiwi, M. Grätzel, E. Pelizzetti, and M. Visca, *J. Am. Chem. Soc.* **1982**, *104*, 2996.

[31] W. Choi, A. Termin, and M. R. Hoffman, *J. Phys. Chem.* **1994**, *98*, 13669.

[32] J. A. Navio, G. Colon, M.I. Litter, and G. N. Bianco, *J. Mol. Catal. A: Chem.* **1996**, *106*, 267.

[33] S. Klosek and D. Raftery, *J. Phys. Chem. B* **2001**, *105*, 2815.

[34] J. C.-S. Wu and C.-H. Chen, *J. Photochem. Photobiol. A: Chem.* **2004**, *163*, 509.

[35] J.-M. Herrmann, J. Disdier, and P. Pichat, *Chem. Phys. Lett.* **1984**, *108*, 618.

[36] Z. Luo and Q.-H. Gao, *J. Photochem. Photobiol. A: Chem.* **1992**, *63*, 367.

[37] N. Serpone, D. Lawless, J. Disdier, and J.-M. Herrmann, *Langmuir* **1994**, *10*, 643.

[38] H. Kato and A. Kudo, *J. Phys. Chem. B* **2002**, *106*, 5029.

[39] M. Takeuchi, H. Yamashita, M. Matsuoka, M. Anpo, T. Hirao, N. Itoh, and N. Iwamoto, *Catal. Lett.* **2000**, *67*, 135.

[40] H. Yamashita, M. Harada, J. Misaka, M. Takeuchi, K. Ikeue, and M. Anpo, *J. Photochem. Photobiol. A: Chem.* **2002**, *148*, 257.

[41] S. U. M. Khan, M. A.-Shahry, and W. B. Ingler Jr., *Science* **2002**, *297*, 2243.

[42] C. Lettmann, K. Hildenbrand, H. Kisch, W. Macyk, and W. F. Maier, *Appl. Catal. B: Environmental* **2001**, *32*, 215.

[43] H. Irie, Y. Watanabe, and K. Hashimoto, *Chem. Lett.* **2003**, *32*, 772.

[44] J. C. Yu, J. Yu, W. Ho, Z. Jiang, and L. Zhang, *Chem. Mater.* **2002**, *14*, 3808.

[45] D. Li, H. Haneda, N. K. Labhsetwar, S. Hishita, and N. Ohashi, *Chem. Phys. Lett.* **2005**, *401*, 579.

[46] T. Umebayashi, T. Yamaki, S. Tanaka, and K. Asai, C*hem. Lett.* **2003**, *32*, 330.

[47] T. Umebayashi, T. Yamaki, H. Itoh, and K. Asai, *Appl. Phys. Lett.* **2002**, *81*, 454.

[48] T. Ohno, M. Akiyoshi, T. Umebayashi, K. Asai, T. Mitsui, and M. Matsumura, *Appl. Catal. A:General* **2004**, *265*, 115.

[49] S. Sato, *Chem. Phys. Lett.* **1986**, *123*, 126.

[50] R. Asahi, T. Morikawa, T. Ohwaki, K. Aoki, and Y. Taga, *Science* **2001**, *293*, 269.

[51] H. Irie, Y. Watanabe, and K. Hashimoto, *J. Phys. Chem. B* **2003**, *107*, 5483.

[52] S. Sato, R. Nakamura, and S. Abe, *Appl. Catal. A: General* **2005**, *284*, 131.

[53] T. Ihara, M. Miyoshi, Y. Iriyama, O. Matsumoto, and S. Sugihara, *Appl. Catal. B: Environmental* **2003**, *42*, 403.

[54] T. Morikawa, R. Asahi, T. Ohwaki, K. Aoki, and Y. Taga, *Jpn. J. Appl. Phys.* **2001**, *40*, L561.

[55] T. Lindgren, J. M. Mwabora, E. Avendaño, J. Jonsson, A. Hoel, C.-G. Granqvist, and S.-E. Lindquist, *J. Phys. Chem. B* **2003**, *107*, 5709.

[56] O. Diwald, T. L. Thompson, E. G. Goralski, S. D. Walck, and J. T. Yartes, *J. Phys. Chem. B* **2004**, *108*, 52.

[57] S.-Z. Chen, P.-Y. Zhang, D.-M. Zhuang, and W.-P. Zhu, *Catal. Commun*. **2004**, *5*, 677.

[58] S. Yin, H. Yamaki, M. Komatsu, Q. Zhang, J. Wang, Q. Tang, F. Saito, and T. Sato, *J. Mater. Chem.* **2003**, *13*, 2996.

[59] Y. Suda, H. Kawasaki, T. Ueda, and T. Ohshima, *Thin Solid Films* **2004**, *453–454*, 162.

[60] S. Yin, Y. Aita, M. Komatsu, J. Wang, Q. Tang, and T. Sato, *J. Mater. Chem.* **2005**, *15*, 674.

[61] K. Kobayakawa, Y. Murakami, and Y. Sato, *J. Photochem. Photobiol. A: Chem.* **2005**, *170*, 177.

[62] Y. Nosaka, M. Matsushita, J. Nishino, and A. Y. Nosaka, *Sci. Technol. Adv. Mater.* **2005**, *6*, 143.

[63] M. Miyauchi, A. Ikezawa, H. Tobimatsu, H. Irie, and K. Hashimoto, *Phys. Chem. Chem. Phys.* **2004**, *6*, 865.

[64] Y. Sakatani, H. Ando, K. Okusako, H. Koike, J. Nunoshige, T. Takata, J. N. Kondo, M. Hara, and K. Domen, *J. Mater. Res.* **2004**, *19*, 2100.

[65] H. Wei, Y. Wu, N. Lun, and F. Zhao, *J. Mater. Sci.* **2004**, *39*, 1305.

[66] M. Inoue, Y. Kondo, and T. Inui, *Chem. Lett.* **1986**, 1421.

[67] M. Inoue, in "Chemical Processing of Ceramics 2nd Ed." (Taylor & Francis, Boca Raton. FL., **2005**) p. 21.

[68] M. Inoue, *J. Phys.: Condens. Matter* **2004**, *16*, S1291.

[69] M. Inoue, H. Kominami, H. Otsu, and T. Inui, *Nippon Kagaku Kaishi (J. Chem. Soc. Jpn)* **1991**, 1364.

[70] H. Kominami, J. Kato, Y. Takada, Y. Doushi, B. Ohtani, S. Nishimoto, M. Inoue, T. Inui, and Y. Kera, *Catal. Lett.* **1997**, *46*, 235.

[71] H. Kominami, J. Kato, S. Murakami, Y. Kera, M. Inoue, T. Inui, and B. Ohtani, *J. Mol. Catal. A: Chem.* **1999**, *144*, 165.

[72] S. Iwamoto, W. Tanakulrungsank, M. Inoue, K. Kagawa, and P. Praserthdam, *J. Mater. Sci. Lett.* **2000**, *19*, 1439.

[73] Sh. Iwamoto, Se. Iwamoto, M. Inoue, S. Uemura, K. Kagawa, W. Tanakulrungsank, and P. Praserthdam, *Ceram. Trans.* **2000**, *115*, 643.

[74] S. Iwamoto, K. Saito, M. Inoue, and K. Kagawa, *Nano Lett.* **2001**, *1*, 417.

Chapter 1

Photocatalytic activities of nanocrystalline Si-modified titania xerogels prepared by the glycothermal method

1.1 Introduction

Semiconductor photocatalysts have attracted great attention because they can be utilized for air purification, water purification, anti-bacteria, self-cleaning materials, etc. Among various photocatalyst materials, titanium dioxide (TiO_2) has been most widely used and investigated [1–3], because it has advantages in inexpensiveness, chemical stability, and nontoxicity in addition to its favorable optoelectronic property.

In order to improve the photocatalytic activity of titania photocatalysts, various dopants have been explored. Among them, SiO_2 exhibited the most promising results. For example, Tada et al. examined the photocatalytic oxidation of cetylpyridinium bromide in aqueous solutions using SiO_x/TiO_2 photocatalysts and reported that the activity was improved with the SiO_x monolayer coverage on the surface of TiO_2. They explained the results by the increase in the electrostatic attraction between the catalyst surface and cetylpyridinium ion [4]. Bard et al. found that incorporation of SiO_2 to a TiO_2-based photocatalyst by a sol–gel method improved photocatalytic activities for decomposition of Rhodamine 6G and explained that the higher activity of the TiO_2/SiO_2 catalysts than bare TiO_2 is due to an increase in the amount of the substrate near the

catalyst surface [5].

M. Inoue et al. previously reported direct synthesis of anatase-type nanocrystalline titanias by thermal reaction of titanium alkoxides in organic media [6–8]. Recently, they also reported that the thermal reaction of titanium tetraisopropoxide (TIP) and tetraethyl orthosilicate (TEOS) in 1,4-butanediol (glycothermal reaction) afforded nanocrystalline Si-modified titanias with the anatase structure having quite large surface areas and high thermal stabilities [9–11]. Furthermore, xerogels of Si-modified titania were prepared by flash evaporation of the glycothermal solvent, and it was demonstrated that the obtained xerogel catalysts exhibited enhanced activities for photocatalytic oxidation of acetic acid [12]. In this chapter, the present author describes the physicochemical properties of Si-modified titania xerogels having higher Si contents and their photocatalytic activities for degradation of several organic dyes.

1.2 Experimental

1.2.1 Preparation of the catalysts

Titania and Si-modified titanias were prepared by the glycothermal method [8]: TIP (25 g) and an appropriate amount of TEOS (Si/Ti atomic ratio of 0–0.5) were added to 100 mL of 1,4-butanediol and this mixture was placed in a 300 mL autoclave. After the atmosphere inside the autoclave was replaced with nitrogen, the assembly was heated to 300 °C at a rate of 2.3 °C/min and kept at that temperature for 2 h. After the glycothermal reaction, the assembly was cooled and the resulting powders were collected by centrifugation, washed with methanol and then air-dried. The product was calcined in a box furnace in air at 600 °C for 30 min to remove the surface organic moieties. The thus-obtained products are designated as GT(x), where x is the Si/Ti

charged ratio. Xerogel titania and Si-modified titanias were prepared according to the procedure reported previously [12]: After the glycothermal reaction, one of the valves of the autoclave was slightly opened to remove the organic matter in the autoclave by flash evaporation while keeping the autoclave temperature at 300 °C. After all the volatile compounds were eliminated, the autoclave was cooled, and then bulky solid products were directly obtained. The products were calcined in a box furnace in air at 600 °C for 30 min. The thus-obtained products are designated as XG(x), where x is the Si/Ti charged ratio.

1.2.2 Characterizations

The UV–vis absorption spectra of the samples were recorded on a Shimadzu MPS-2000 spectrophotometer. Powder X-ray diffraction (XRD) patterns were recorded on a Shimadzu XD-D1 diffractometer using CuKα radiation and a carbon-monochromator. The specific surface areas of the samples were calculated by the BET single-point method on the basis of the nitrogen uptake measured at 77 K. X-ray photoelectron spectroscopy (XPS) measurement was performed on an ULVAC-PHI Model 5500 spectrometer with 15 kV - 400 W MgKα emission as the X-ray source. The zeta potentials were measured on an electrophoretic light scattering spectrophotometer, Otsuka Electronics, ELS-800. A small amount of the sample was dispersed in a 10 mmol/L NaCl solution and then pH of the suspension was adjusted by adding 0.1 N NaOH or 0.1 N HCl. The measurement was conducted after ultrasonic treatment of the suspension for 10 min. The particle size distribution was determined by measuring the dynamic light scattering on the same electrophoretic light scattering spectrometer, ELS-800. A portion of the catalyst (20 mg) was added in 100 mL of

distilled water and pH of the suspension was adjusted to 5.0 with 0.1 N NaOH or 0.1 N HCl. The measurement was carried out after ultrasonic treatment for 10 min.

1.2.3 Photocatalytic reaction and adsorption isotherm

Photocatalytic activity was evaluated by degradation of six organic dyes, Rhodamine 6G (Rh6G), Rhodamine B (RhB), Eosin Y (EY), Orange G (OG), Acid Orange 7 (AO7) and Acid Yellow 23 (AY23), whose structures are shown in Fig. 1-1. Among these dyes, Rh6G and RhB are cationic dyes and other four are anionic dyes. A portion of the catalyst (20 mg) was dispersed in a 100 mL solution of a dye, and the obtained suspension was irradiated with a 500 W high-pressure mercury arc lamp at 25 °C under magnetic stirring. Initial concentrations of the dyes in the solutions were 1.0×10^{-4} mol/L for Rh6G and RhB, 2.0×10^{-4} mol/L for EY, OG and AY23, and 3.0×10^{-4} mol/L for AO7. After a certain period of irradiation, a portion of the suspension was taken out and filtered. The solution was then analyzed by a UV–vis spectrometer, Shimadzu MPS-2000, to measure the concentration of the remaining organic dye. JRC-TIO-4 (equivalent to Degussa P-25; rutile/anatase = 3/7; BET surface area = 49 m^2/g) was used as a reference to compare the photocatalytic activity of the catalysts.

Adsorption isotherms were measured for the suspensions containing 50 mg of the sample and 100 mL of the dye solution with various concentrations. After stirring in the dark for 1 h, the concentration of the dye in the solution was measured with the UV–vis spectrometer.

1.3 Results and discussion

Figure 1-2 depicted the XRD patterns of XG(x)'s with various Si/Ti ratios, which

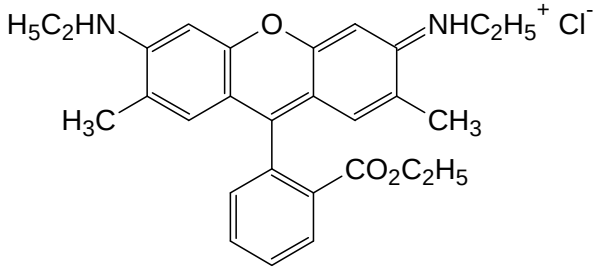

Rhodamine 6G (Rh6G)

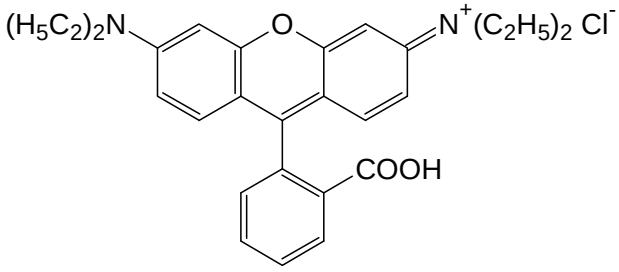

Rhodamine B (RhB)

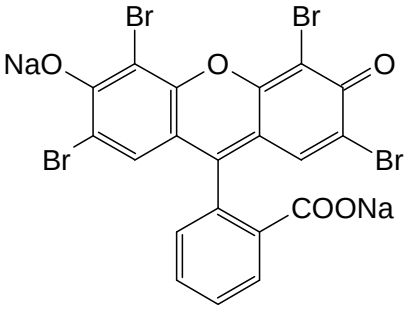

Eosin Y (EY)

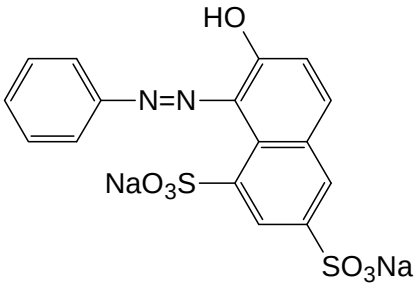

Orange G (OG)

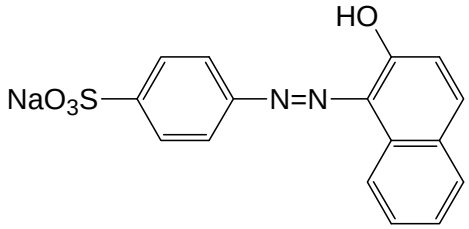

Acid Orange 7 (AO7)

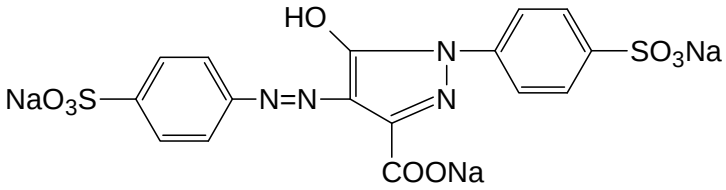

Acid Yellow 23 (AY23)

Fig. 1-1 Structures of organic dyes.

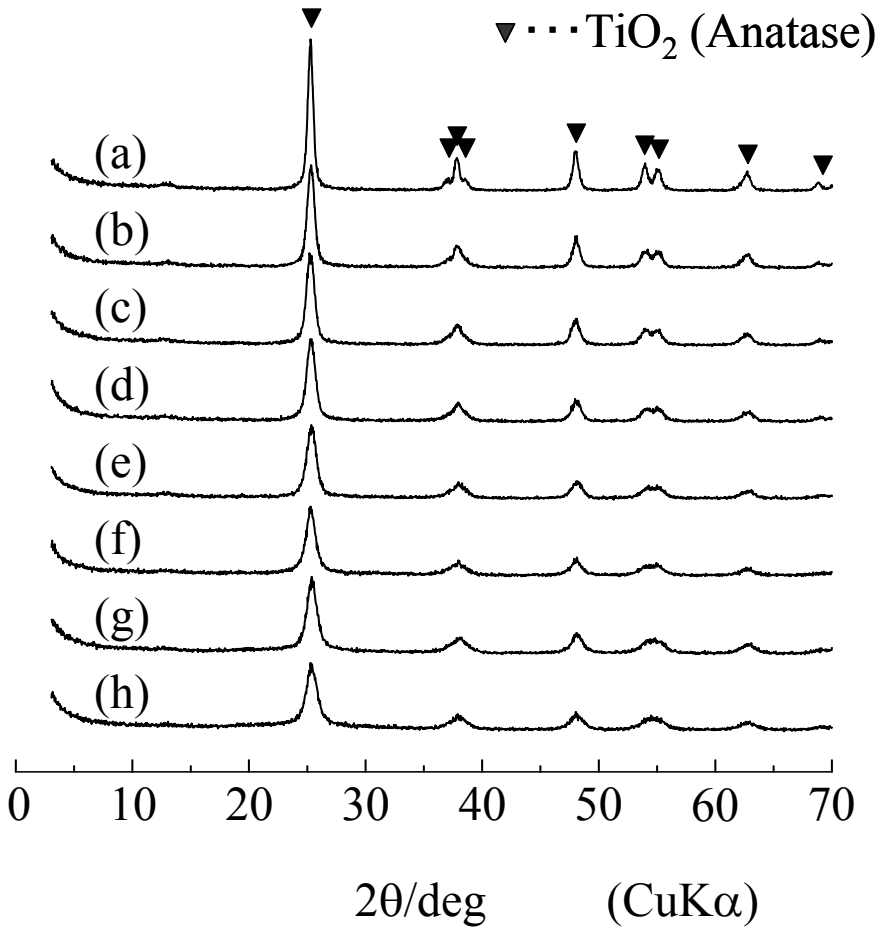

Fig. 1-2 XRD patterns of: (a) XG(0), (b) XG(0.02), (c) XG(0.06), (d) XG(0.1), (e) XG(0.2), (f) XG(0.3), (g) XG(0.4), and (h) XG(0.5).

show that all the products had the anatase structure. The BET surface areas and crystallite sizes of XG(x)'s are listed in Table 1-1. The crystallite size of XG(0) was 18 nm, and by the addition of a small amount of Si, the crystallite size significantly decreased. With further increase in the amount of Si addition, the crystallite size decreased gradually. For XG(0.5), quite a small crystallite size, 8 nm, was obtained. The BET surface areas increased from 75 m^2/g to 140 m^2/g with the increase in the amount of Si modification up to Si/Ti = 0.2. However, the BET surface area reached a plateau level for Si/Ti = 0.2–0.4, and for XG(0.5) it rather decreased. By increasing the Si/Ti charged ratio, the maximum intensity as well as the area of the XRD peak decreased gradually, suggesting the presence of non-crystalline components in the samples. We have previously examined the surface properties of GT(x)'s by TPD methods and found that GT(x) samples with x smaller than 0.1 has the surface property similar to that of pure TiO_2 and in the case of GT(x) with x higher than 0.2, a part of the surface was covered with SiO_2-like components [10].

The results of XPS of XG(x)'s are shown in Table 1-2. The Si/Ti ratios of the samples determined by XPS increased with increasing the amount of Si modification. The Si/Ti ratios measured by XPS were always larger than those charged for the glycothermal reaction, indicating that Si was enriched in the surface region of the samples. The O1s XPS spectra of XG(x)'s are shown in Fig. 1-3. In the O1s XPS spectrum of XG(0), a peak was observed at 530 eV, which corresponds to the oxygen in TiO_2. For the Si-modified titanias, another component was recognized at 532 eV. This component is due to the oxygen associated with the Si–O–Ti bridging bond [13,14]. These results indicate the absence of pure SiO_2 clusters on the surface of the product particles, since the O1s peak of oxygen in pure SiO_2 is observed at around 533 eV [15].

Table 1-1 Physical properties of the catalysts

Sample	Crystallite size (nm)	BET surface area (m^2/g)	Isoelectric point	Zeta potential [a] (mV)
JRC-TIO-4	–	49	7.0	25.4
XG(0)	20	76	6.5	20.1
XG(0.02)	16	95	6.2	19.6
XG(0.06)	13	129	6.1	14.4
XG(0.1)	11	142	5.7	7.6
XG(0.2)	10	146	4.3	-7.4
XG(0.3)	9	124	3.9	-10.1
XG(0.4)	9	145	3.6	-12.5
XG(0.5)	8	90	3.4	-15.2

[a] The value at pH 5

Table 1-2 Binding energy of core electrons for XG(x)'s

Sample	Si/Ti[a]	O 1s (eV)	Si $2p_{1/2}$ (eV)	Ti $2p_{3/2}$ (eV)
XG(0)		529.8		458.7
XG(0.02)	0.055	529.9 (84)[b]	101.9	458.9
		531.8 (16)		
XG(0.06)	0.130	530.0 (76)	102.1	458.7
		531.8 (24)		
XG(0.1)	0.171	529.9 (71)	102.1	458.7
		531.6 (29)		
XG(0.2)	0.412	530.0 (63)	102.4	458.7
		532.0 (37)		
XG(0.3)	0.653	530.1 (54)	102.7	458.8
		532.1 (46)		
XG(0.4)	0.748	530.2 (52)	102.9	459.0
		532.3 (48)		
XG(0.5)	1.272	530.2 (40)	102.9	458.9
		532.4 (60)		

[a] Determined by XPS.

[b] The number in parentheses indicates the percentage of the peak.

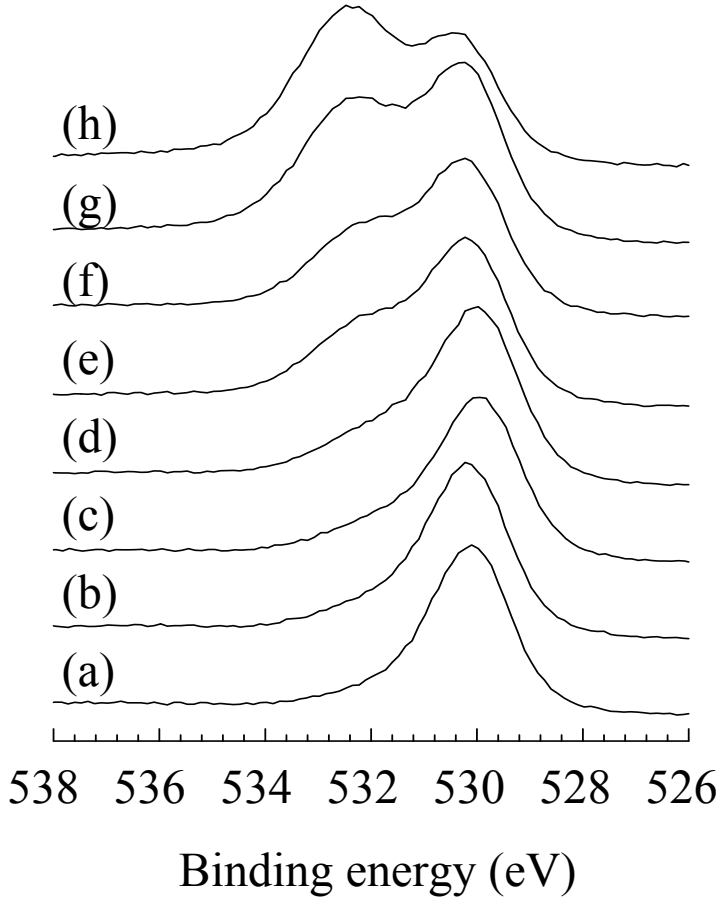

Fig. 1-3 O1s XPS spectra of: (a) XG(0), (b) XG(0.02), (c) XG(0.06), (d) XG(0.1), (e) XG(0.2), (f) XG(0.3), (g) XG(0.4), and (h) XG(0.5).

Figure 1-4 shows the zeta potentials of XG(x)'s as a function of pH. The isoelectric point of the samples as well as the zeta potentials at pH 5.0 estimated from the results shown in Fig. 1-4 are listed in Table 1-1. The isoelectric point of XG(0) was around 6.5, and the value gradually shifted to the lower pH side with increasing the amount of Si addition. Since the isoelectric point of pure SiO_2 is ca. 2.0 [16], the observed change in the isoelectric point suggests the presence of Si-rich components on the surface of the Si-modified titanias.

Figure 1-5(a) shows the adsorption isotherms of Rh6G (cationic dye). The amount of Rh6G adsorbed on the samples increased significantly by increasing the Si/Ti charged ratio up to 0.4. The pH values of the diluted Rh6G solutions were 5.0–5.5, and in this pH range, the zeta potential of XG(0) was ca. +20 mV, and it gradually decreased by increasing the Si/Ti ratio. Since Rh6G is a cationic dye that is adsorbed preferably on a negatively charged surface, the enhancement of the Rh6G uptake of the Si-modified titanias is explained by the change in the surface charge. Further increase in the Si/Ti ratio to 0.5 resulted in a slight decrease in the amount of the dye adsorbed. This is probably due to the smaller BET surface area of XG(0.5) than that of XG(0.4). As for the OG (anionic dye) adsorption, the highest amount of adsorption was observed for JRC-TIO-4 and the amount of the adsorption gradually decreased with the increase in the amount of Si addition as shown in Fig. 1-5(b). This tendency is completely opposite to that of Rh6G, and is also explained by the change in the zeta potentials of the samples.

The amount of the dyes adsorbed on 50 mg of the catalysts from the 100 mL of 2.0×10^{-5} mol/L dye solution is shown in Fig. 1-6 as a function of the Si/Ti charged ratio.

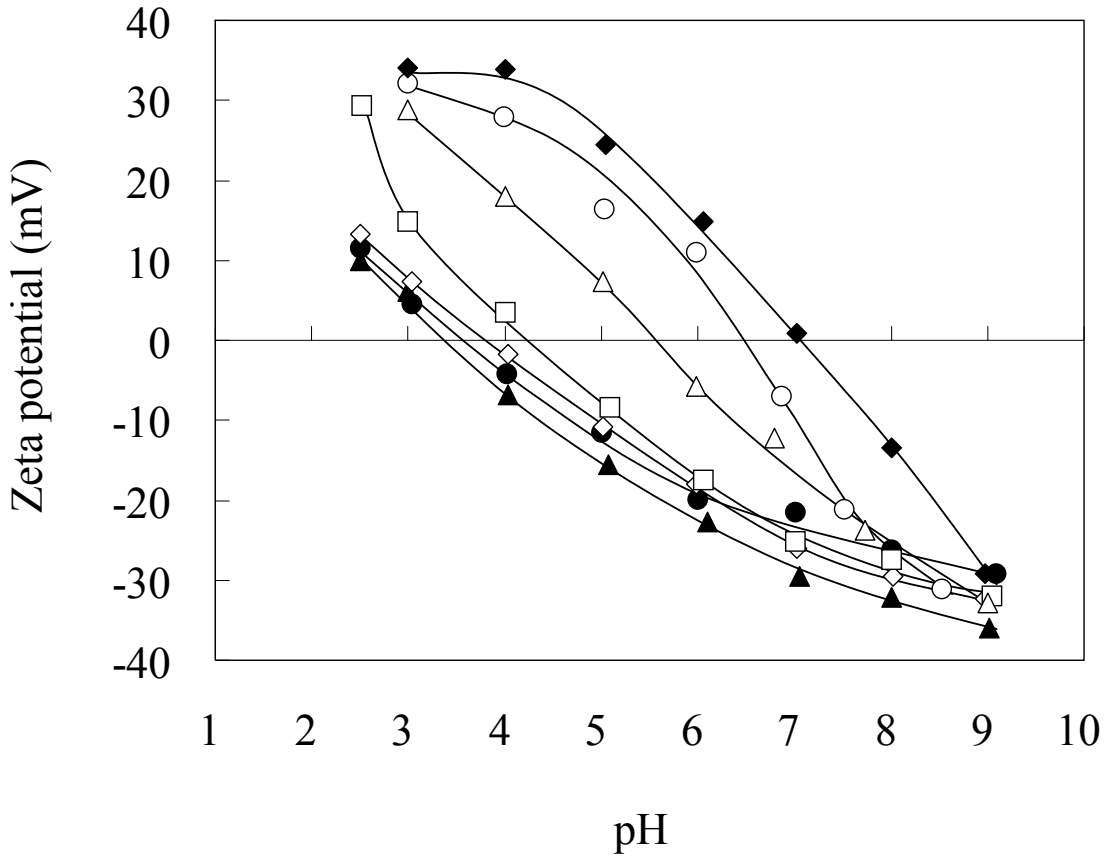

Fig. 1-4 Zeta potentials of: (○) XG(0), (△) XG(0.1), (□) XG(0.2), (◇) XG(0.3), (●) XG(0.4), (▲) XG(0.5), and (◆) JRC-TIO-4; as a function of pH.

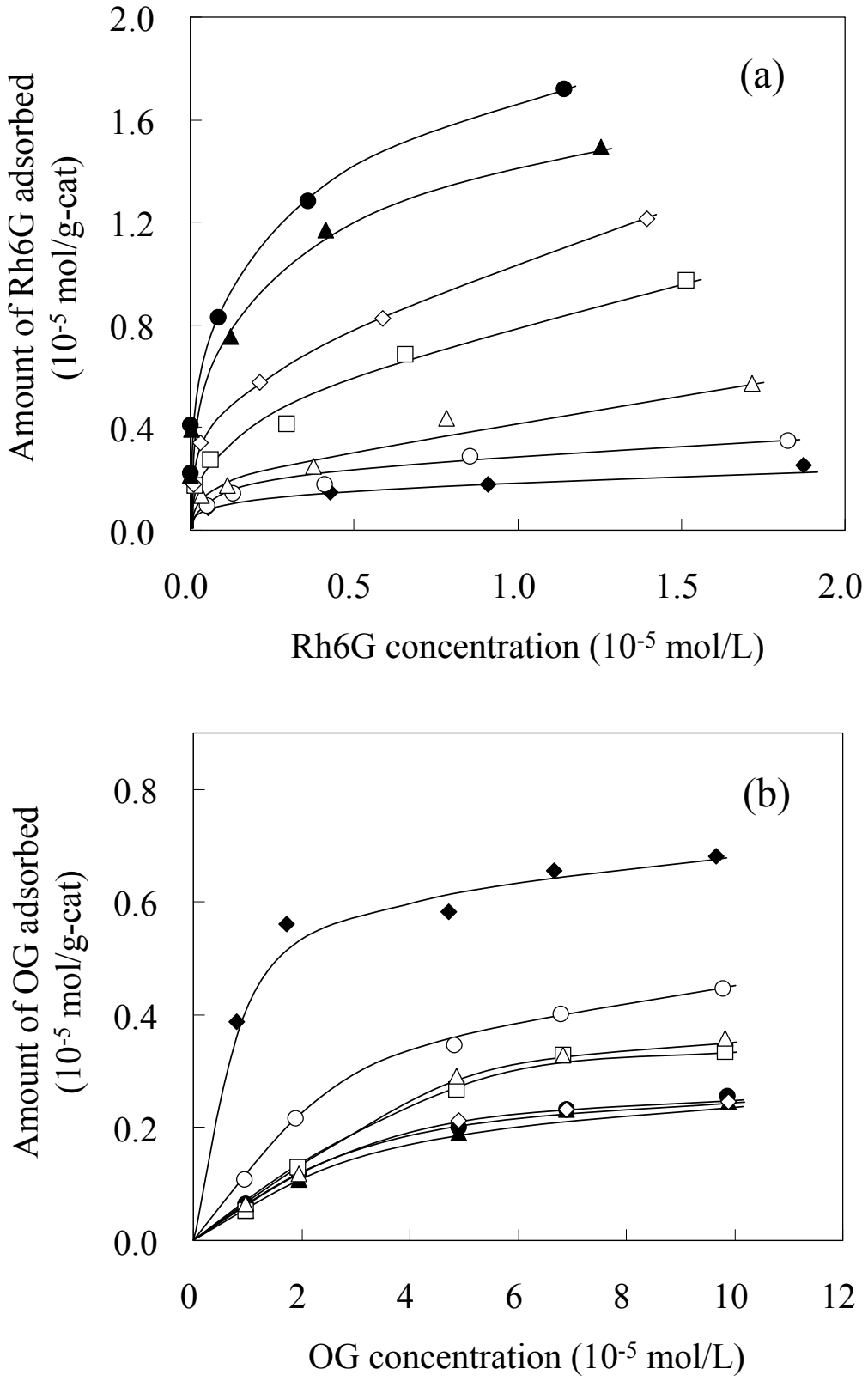

Fig. 1-5 Isotherms for adsorption of: (a) Rh6G and (b) OG; on: (○) XG(0), (△) XG(0.1), (□) XG(0.2), (◇) XG(0.3), (●) XG(0.4), (▲) XG(0.5), and (◆) JRC-TIO-4.

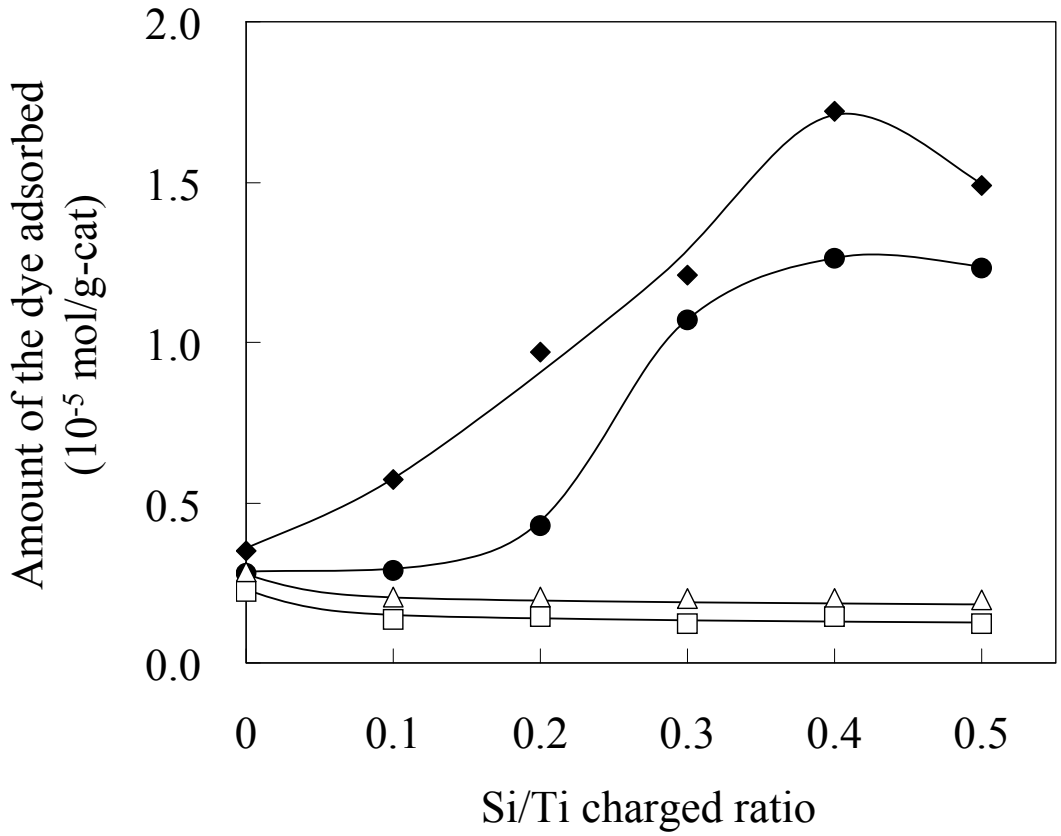

Fig. 1-6 Amounts of the dyes: (◆) Rh6G, (●) RhB, (△) EY and (□) OG; adsorbed on the Si-modified xerogel catalysts with various Si/Ti charged ratios.

For the cationic dyes (RhB and Rh6G), the amounts of the adsorbed dyes markedly increased with the increase in the Si/Ti ratio. On the other hand, the adsorbed amount of the anionic dyes (EY and OG) decreased. In Fig. 1-7, the amounts of the dyes adsorbed on the catalysts are plotted as a function of zeta potential at pH 5. The adsorbed amount of the cationic dyes significantly increased, as the zeta potential of the catalyst changed from +20 mV to -15 mV. On the other hand, for the anionic dyes, the amount of adsorption increased slightly as the surface potential increased. The adsorbability of the cationic dyes is influenced strongly by the surface electric charge, while that of anionic dyes is slightly affected.

Figure 1-8 shows the particle size distributions of XG(x)'s and JRC-TIO-4 in aqueous suspensions at pH 5. For GT(x) samples, we also conducted the measurement; however, when the ultrasonic irradiation was stopped, the particles in the suspensions began to sediment quickly. This result can be attributed to the coagulation of GT(x) particles which occurred during the drying stage by the strong surface tension of the liquid between the fine particles. Even with the prolonged ultrasonic treatment, reliable data were not obtained. In the case of JRC-TIO-4, the suspension was milky and relatively stable for several minutes after the ultrasonic treatment, although a small amount of the sediment was recognized after several hours. The measured particle size of JRC-TIO-4 was distributed in a range from 60 nm to 1 μm, as shown in Fig. 1-8. The crystallite size of this sample, calculated from the XRD peak broadening of the anatase phase, was 31 nm. Therefore, the obtained result suggests that JRC-TIO-4 was comprised of stiff aggregates of smaller primary particles. On the other hand, the suspensions of all of XG(x)'s were quite stable. Especially, XG(x)'s with higher Si/Ti ratios ($x \geq 0.2$) did not sediment even after a couple of days. The suspensions were

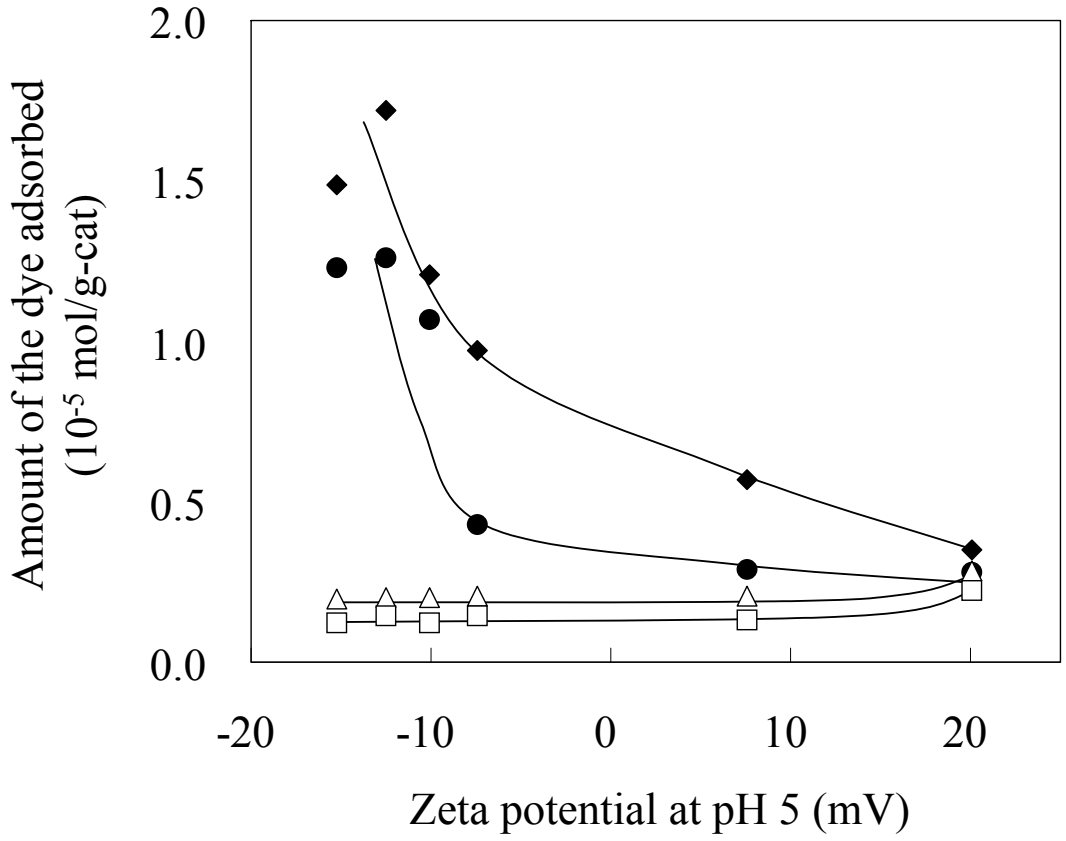

Fig. 1-7 Effect of zeta potential of the catalyst on the amount of the dyes adsorbed at pH 5: (◆) Rh6G, (●) RhB, (△) EY, and (□) OG.

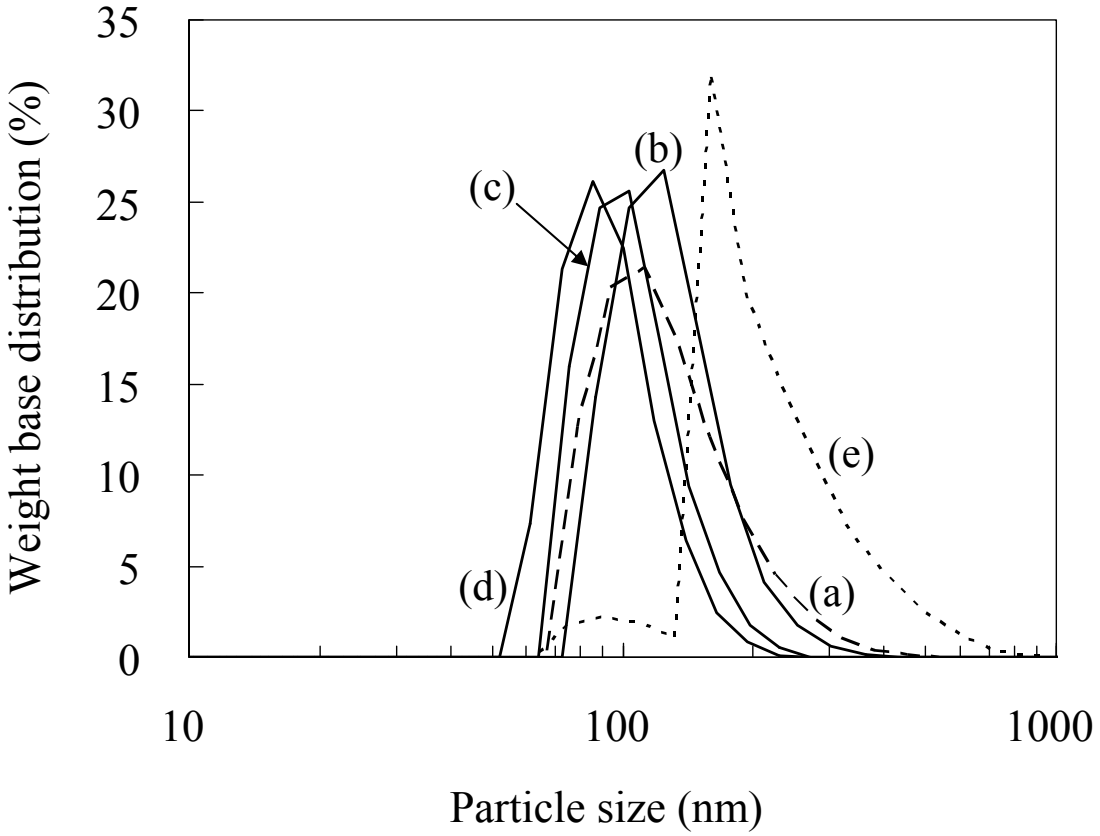

Fig. 1-8 Particle size distributions of: (a) XG(0), (b) XG(0.1), (c) XG(0.2), (d) XG(0.3), and (e) JRC-TIO-4 in aqueous suspensions at pH 5.

translucent, which was also quite different from the case of JRC-TIO-4. The turbidity of the suspension is due to the scattering of visible light by the presence of relatively large particles in the suspension, and therefore, these observations also suggest that XG(x)'s were highly dispersed in the suspension as compared to JRC-TIO-4. Particle sizes of XG(0) measured by the light scattering were ranging from 70 to 550 nm, which was much smaller than that of JRC-TIO-4. By the Si-modification, the particle sizes were further reduced; for examples, 70–450 nm for XG(0.1), 60–300 nm for XG(0.2), and 50–250 nm for XG(0.3). Such high dispersion of XG(x)'s was due to the effective prevention of the coagulation of the ultrafine particles by drying the products via the flash evaporation method.

Figure 1-9 shows the photocatalytic decomposition of various organic dyes using XG(x)'s. Although $\ln(C/C_0)$ vs. time plots were made in order to compare the decomposition rate, in most of the cases they showed quite complex behaviors and linear relationships were not obtained clearly. This is probably because of ignoring the effect of dye-sensitized photocatalytic reactions, which have been observed in various dye-TiO_2 systems [17,18], or not considering the effect of partially decomposed organic intermediates. Therefore, the photocatalytic activities were simply compared from the concentration of the dyes remaining after 60 min of irradiation. XG(0) showed a photocatalytic activity as high as JRC-TIO-4 for degradation of both the cationic and anionic dyes. The photocatalytic activity for degradation of cationic dyes was improved by increasing the amount of Si modification up to 0.2–0.4. The pH values of the initial suspensions were around 5, and they changed into 4–4.5 after the photocatalytic reaction for 2–3 h. In this pH range, the zeta potential was positive for XG(0) and XG(0.1), and negative for XG(x)'s with higher x. Such surface changes strongly affect

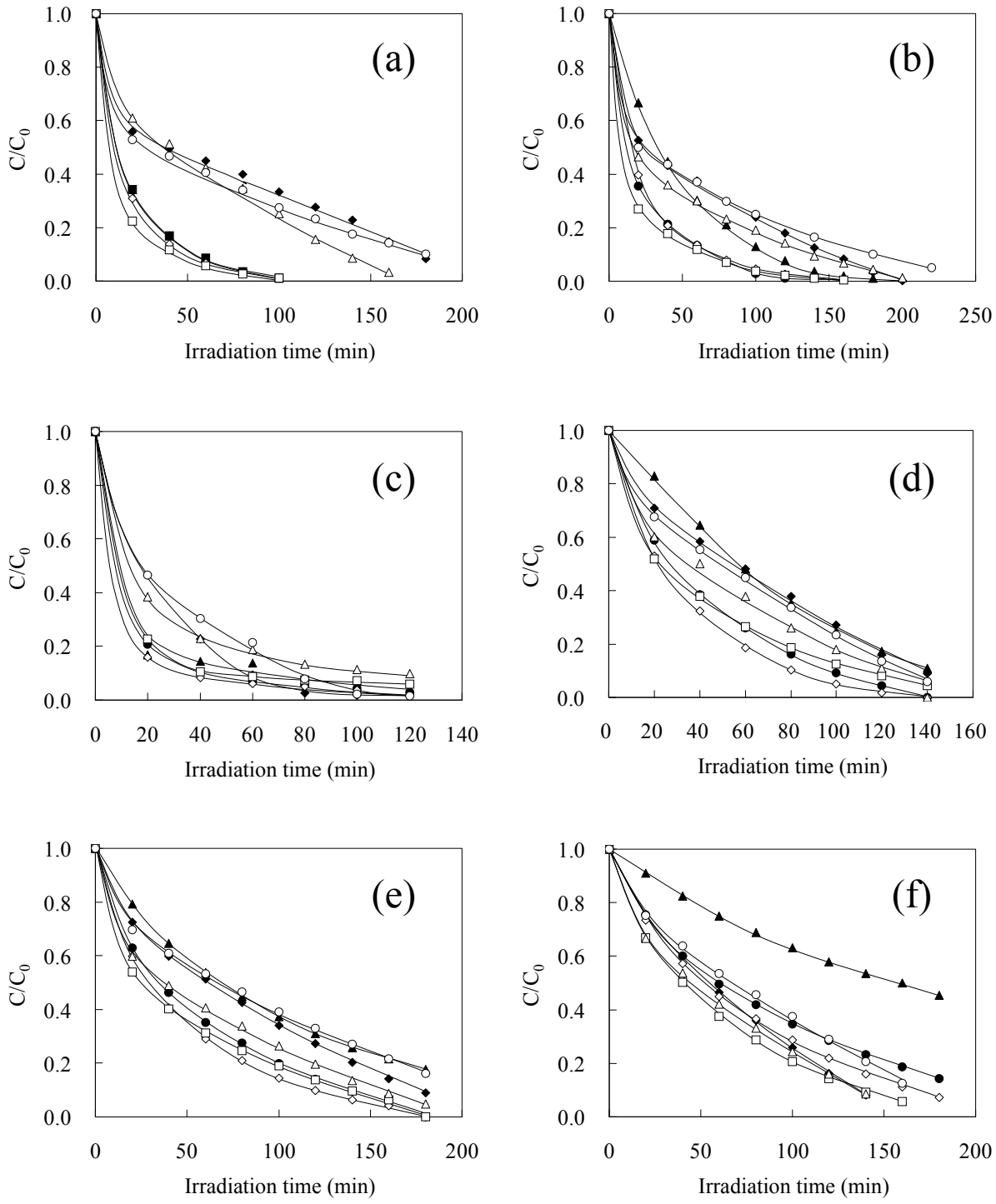

Fig. 1-9 Photocatalytic activities of: (○) XG(0), (△) XG(0.1), (□) XG(0.2), (◇) XG(0.3), (●) XG(0.4), (▲) XG(0.5), and (◆) JRC-TIO-4; for the decompositions of: (a) Rh6G, (b) RhB, (c) EY, (d) OG, (e) AO7, and (f) AY23.

adsorption for Rh6G and RhB and lead to the remarkable enhancements of the photocatalytic activities.

For the degradation of anionic dyes, XG(x)'s were also effective and XG(0.2) and XG(0.3) exhibited relatively higher photocatalytic activities. Although the zeta potential varied from +20.1 mV for XG(0) to -15.2 mV for XG(0.5) at pH 5, these changes in zeta potential slightly decreased the adsorbability of anionic dyes. Therefore, the dispersion of the samples seems to be a more important factor for the enhancement of the photocatalytic activity.

For XG(0.5), the photocatalytic activities were relatively low for both the cationic and anionic dyes. These diminished activities are probably due to surface Si-rich components, which are suggested by XPS analysis and BET surface area measurement described in this study as well as the results of TPD reported previously [10].

The obtained results suggest that the adsorption property as well as the particle size distribution (dispersibility) of the sample affected the photocatalytic activity for decomposition under the experimental condition in this study.

1.4 Conclusions

Xerogels of Si-modified titanias prepared by the glycothermal method were effective for photocatalytic decomposition of various organic dyes. As the amount of Si modification increased, the isoelectric point shifted to the lower pH side and the surface of the catalysts in the suspension became more negatively charged. This increased adsorption for the cationic dyes and led to the enhancement of the decomposition rate. On the other hand, for the anionic dyes, the negative side shift of the zeta potential slightly decreased the dye uptake of the catalysts. However, enhanced photocatalytic

activities were observed for the catalysts with small amounts of Si, and the high dispersibility of xerogel catalysts seems to be the reason for the higher photocatalytic activities of Si-modified titanias.

References

[1] A. Fujishima, T. N. Rao, and D. A. Tryk, *J. Photochem. Photobiol. C* **2000**, *1*, 1.

[2] M. R. Hoffman, S. T. Martin, W. Choi, and D. W. Bahnemann, *Chem. Rev.* **1995**, *95*, 69.

[3] C. Carp, C. L. Huisman, and A. Reller, *Progress Solid State Chem.* **2004**, *32*, 33.

[4] H. Tada, M. Akazawa, Y. Kubo, and S. Ito, *J. Phys. Chem. B* **1998**, *102*, 6360.

[5] C. Anderson and A. J. Bard, *J. Phys. Chem.* **1995**, *99*, 9882.

[6] M. Inoue, in "Chemical Processing of Ceramics 2nd Ed." (Taylor & Francis, Boca Raton. FL., 2005) p. 21.

[7] M. Inoue, *J. Phys.: Condens. Matter* **2004**, *16*, S1291.

[8] M. Inoue, H. Kominami, H. Otsu, and T. Inui, *Nippon Kagaku Kaishi (J. Chem. Soc. Jpn)* **1991**, 1364.

[9] S. Iwamoto, W. Tanakulrungsank, M. Inoue, K. Kagawa, and P. Praserthdam, *J. Mater. Sci. Lett.* **2000**, *19*, 1439.

[10] Sh. Iwamoto, Se. Iwamoto, M. Inoue, S. Uemura, K. Kagawa, W. Tanakulrungsank, and P. Praserthdam, *Ceram. Trans.* **2000**, *115*, 643.

[11] Sh. Iwamoto, Se. Iwamoto, M. Inoue, H. Yoshida, T. Tanaka, and K. Kagawa, *Chem. Mater.* **2005**, *17*, 650.

[12] S. Iwamoto, K. Saito, M. Inoue, and K. Kagawa, *Nano Lett.* **2001**, *1*, 417.

[13] C. U. I. Odenbrand, S. L. T. Andersson, L. A. H. Andersson, J. G. M. Brandin, and G. Busca, *J. Catal.* **1990**, *125*, 541.

[14] A. Y. Stakheev, E. S. Shpiro, and J. Apijok, *J. Phys. Chem.* **1993**, *97*, 5668.

[15] G. E. Muilenberg, in "Handbook of X-ray Photoelectron Spectroscopy" (Perkin-Elmer Corporation, Minnesota, 1979) p. 45.

[16] G. A. Parks, *Chem. Rev.* **1965**, *65*, 177.

[17] T. Wu, G. Liu, J. Zhao, H. Hidaka, and N. Serpone, *J. Phys. Chem. B* **1998**, *102*, 5845.

[18] K. Vinodgopal and P. V. Kamat, *J. Phys. Chem.* **1992**, *96*, 5053.

Chapter 2

Nitrification of Si-modified titanias prepared by the glycothermal method and their photocatalytic activity under visible-light irradiation

2.1 Introduction

In chapter 1, it was demonstrated that xerogels of Si-modified titanias prepared by the glycothermal method were effective for photocatalytic decomposition of various organic dyes. However, the band gap of anatase TiO_2 is 3.2 eV; therefore, the photocatalytic reaction proceeds only by irradiation of ultraviolet (UV) light (wavelength (λ) < 388 nm), which means only about 3% of the incoming solar energy on the earth's surface can be utilized. In recent years, a number of attempts have been made to expand the photosensitivity of TiO_2-based photocatalysts into the visible-light region. One approach is introduction of allowed energy states in the band gap of TiO_2 by doping of transition metal cations such as Cr, V or Fe [1–4]. However, the introduction of these cations causes an increase in the population of recombination centers, which usually results in a low photoefficiency. Another approach is use of anionic species, such as C, N, F and S [5–11]. Nitrogen-doped TiO_2 materials were reported by Sato for the first time in 1986 [5]. He found that the calcination of $Ti(OH)_4$ involving ammonium compounds gave yellowish powders that exhibited photocatalytic activities under visible light irradiation. Recently, several groups also reported the

visible light sensitivity of N-doped TiO_2 materials [6–8]. Asahi et al. reported that nitrogen-doped TiO_2 thin films showed photocatalytic activities under visible light irradiation [6]. They reported that the visible light sensitivity of the nitrogen-doped TiO_2 was due to the narrowing of the energy gap by mixing N 2p and O 2p states. Lindgren et al. prepared nanocrystalline porous nitrogen-doped TiO_2 films by the DC magnetron sputtering method and examined their photoelectrochemical properties [7]. It was reported that although all the nitrogen-doped films showed visible light absorption in the wavelength range from 400 to 535 nm, there was an optimum concentration of nitrogen where the response was highest. Irie et al. compared quantum yields in the photocatalytic decomposition of 2-propanol using TiO_xN_y powders. They found that the highest quantum yield was obtained for a sample with a very low concentration of nitrogen, the N/Ti ratio of 0.005, and that further increase in the nitrogen concentration lowered the quantum yield due to the increase in the recombination rate [8]. Although these reports showed that nitrogen-doping is an effective method to induce a visible light sensitivity to TiO_2, they also suggested that in the ternary Ti-O-N system, an improvement of the photoefficiency under visible light irradiation is difficult.

S. Iwamoto et al. previously reported that the thermal reactions of titanium tetraisopropoxide and tetraethyl orthosilicate in 1,4-butanediol (glycothermal reaction) afforded nanocrystalline Si-modified titanias with the anatase structure having large surface areas and superior thermal stabilities [12]. The obtained Si-modified titanias were characterized by XPS and XANES, and it was found that the Si atoms are inserted in the distorted octahedral vacant sites of the anatase structure [13]. Such insertion of the Si atoms causes unbalanced positive charges. They observed that the concentration of the surface OH groups decreased by the Si modification. These two results are

reasonably explained as follows: substitution of the surface OH groups with surface oxide ions forms negative charge which compensates for the positive charge caused by the insertion of the Si in the vacant sites. From the obtained results, it is expected that substitution of O^{2-} with N^{3-} in the Si-modified titanias would take place more easily because such additional negative charge cancels the extra positive charge caused by the Si incorporation. The author examined, accordingly, the nitrification of the Si-modified titanias and found that the titanias co-doped with Si and N showed a strong absorption in the visible region (400–550 nm) and exhibited high photocatalytic activities for degradation of RhB and decomposition of acetaldehyde under visible-light irradiation. In the present chapter, the author shows the physical properties and the photocatalytic activities of N- and Si-co-doped titania in detail.

2.2 Experimental

2.2.1 Preparation of the catalysts

Titania and Si-modified titania were prepared by the glycothermal method and collected as a xerogel form [14]: titanium tetraisopropoxide (25 g) and an appropriate amount of tetraethyl orthosilicate (Si/Ti atomic ratio of 0 or 0.1) were added to 100 mL of 1,4-butanediol and this mixture was placed in a 300 mL autoclave equipped with two valves, one of which was used as a gas inlet and the other was connected to a Liebig condenser of stainless tubing. After the atmosphere inside the autoclave was replaced with nitrogen, the assembly was heated to 300 °C at a rate of 2.3 °C/min and kept at that temperature for 2 h. After the glycothermal reaction, the valve of the autoclave was slightly opened in order to remove the organic vapor from the autoclave by flash evaporation while keeping the autoclave temperature at 300 °C. After cooling, bulky

solid products were directly obtained. The product was calcined in a box furnace in air at 500 °C for 30 min to remove the surface organic moieties. The thus-obtained products are designated as XG(x), where x is the Si/Ti charged ratio. XG(x) was placed in a quartz tube reactor, heated to a desired temperature (450–700 °C) at a rate of about 10 °C/min in a 100 mL/min flow of argon, and allowed to react in an NH_3 flow (100 mL/min) for 1 h, 3 h or 5 h at that temperature. After the NH_3 treatment, the sample was annealed at 400 °C in air for 30 min using a box furnace in order to eliminate the adsorbed NH_3 on the catalyst. JRC-TIO-4 (a reference catalyst supplied from The Catalysis Society of Japan; equivalent to Degussa P-25; rutile/anatase=3/7; BET surface area=49 m^2/g) was nitrified in the same way.

2.2.2 Characterization

The UV-vis absorption spectra were recorded on a Shimadzu MPS-2000 spectrophotometer. Powder X-ray diffraction (XRD) patterns were recorded on a Shimadzu XD-D1 diffractometer using CuKα radiation and a carbon-monochromator. The specific surface areas of the samples were determined by the BET single-point method on the basis of the nitrogen uptake measured at 77 K using a Micromeritics Flowsorb II 2300. X-ray photoelectron spectroscopy (XPS) measurement was performed on an ULVAC-PHI Model 5500 spectrometer with 15 kV - 400 W MgKα emission as the X-ray source. The zeta potentials were measured on an electrophoretic light scattering spectrophotometer, Otsuka Electronics, ELS-800.

2.2.3 Photocatalytic reaction

Photocatalytic activity was evaluated by degradation of Rhodamine B (RhB) and decomposition of acetaldehyde. As for the RhB degradation, 20 mg of the catalyst was dispersed in 100 mL of 1.0×10^{-5} mol/L RhB solution and the obtained suspension was irradiated with blue-light-emitting diodes (blue LED, NSPB510S, Nichia). The blue LED has an emission wavelength ranging from 420 to 520 nm and a peak wavelength at 470 nm. The power of a blue LED device used in this study was 72 mW, and 96 pieces of the devices were used as a light source (4 panels equipped with 24 devices). After a certain period of irradiation, a portion of the suspension was taken out to measure the concentration of the remaining RhB by using the UV-Vis spectrometer.

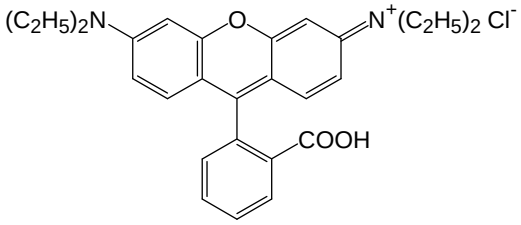

Rhodamine B (RhB)

The decomposition of acetaldehyde was carried out in a closed glass reaction vessel (1.0 L). The catalyst (0.2 g) dispersed on a 90 mmϕ glass filter was placed in the vessel and 0.2 mmol acetaldehyde was injected in it. The vessel was placed in the dark for 1 h and then visible light was irradiated using a 300 W xenon lamp (Optical Modulex SX-UI300XQ, Ushio Inc.) through a UV cut-off filter (L-42, Asahi Technoglass Co. Ltd.) and an infrared cut-off filter (Super Cold Filter, Ushio Inc.). As shown in Fig. 2-1, ultraviolet light under 400 nm was cut-off by the UV-filter. After a certain period of irradiation, the CO_2 concentration was measured by a gas chromatograph, Shimadzu GC-8A. The amount of CO_2 formed was calculated by

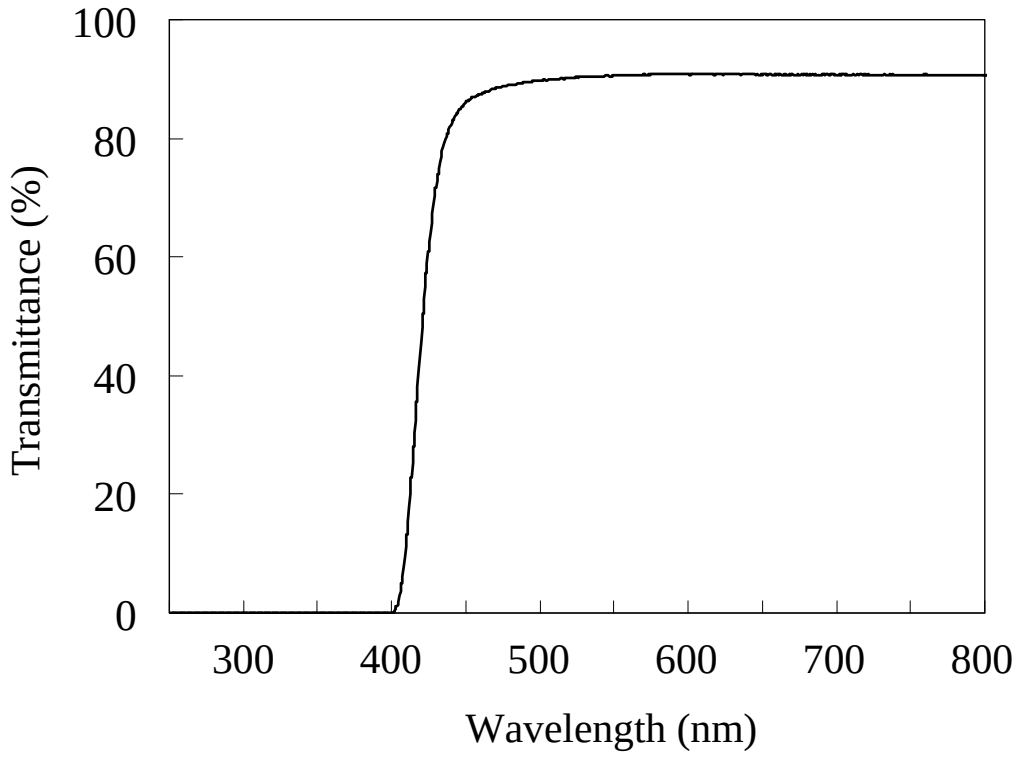

Fig. 2-1 Transmission spectrum of the UV cut-off filter (L-42).

subtracting the initial amount of CO_2 in the vessel.

2.3 Results and discussion

2.3.1 Physical properties of XG(x)'s after NH_3 treatment

White powders of the mother TiO_2, XG(0), turned into gray, dark blue and black by the NH_3 treatment at 600 °C, 650 °C and 700 °C, respectively, while the colors of NH_3-treated XG(0.1) were yellow, yellowish-green and dark blue, respectively. Those colors indicated the samples were nitrified by the NH_3 treatment. When the samples were taken out from the reactor after the NH_3 treatment and exposed to air, a slight decolorization was observed, which indicates that these NH_3-treated samples were partly oxidized in air at room temperature. Figure 2-2 shows the UV-vis absorption spectra of NH_3-treated XG(0)'s. Whereas untreated XG(0) exhibited an absorption only in the UV region (<400 nm), the sample treated at 450 °C in an NH_3 flow showed absorption bands at the visible light region (>400 nm). The absorbance at the visible light region gradually became stronger as the NH_3 treatment temperature increased to 600 °C, and the absorbance abruptly increased at 650 °C. Similar results were reported by several authors [8, 15–17]. The spectra of the NH_3-treated samples had a shoulder absorption band at 400–500 nm and a broad band at higher wavelength (>500 nm). The former band is attributed to the doped nitrogen into the anatase structure and the latter corresponds to the formation of Ti^{3+} [18].

Figure 2-3 shows the absorption spectra of the Si-modified titanias, XG(0.1)'s, heated in an NH_3 flow. As compared with the spectra of NH_3-treated XG(0) shown in Fig. 2-2, NH_3-treated XG(0.1) have a stronger absorption at 400–500 nm. This result clearly indicates that larger amounts of nitrogen were doped in XG(0.1)'s than in

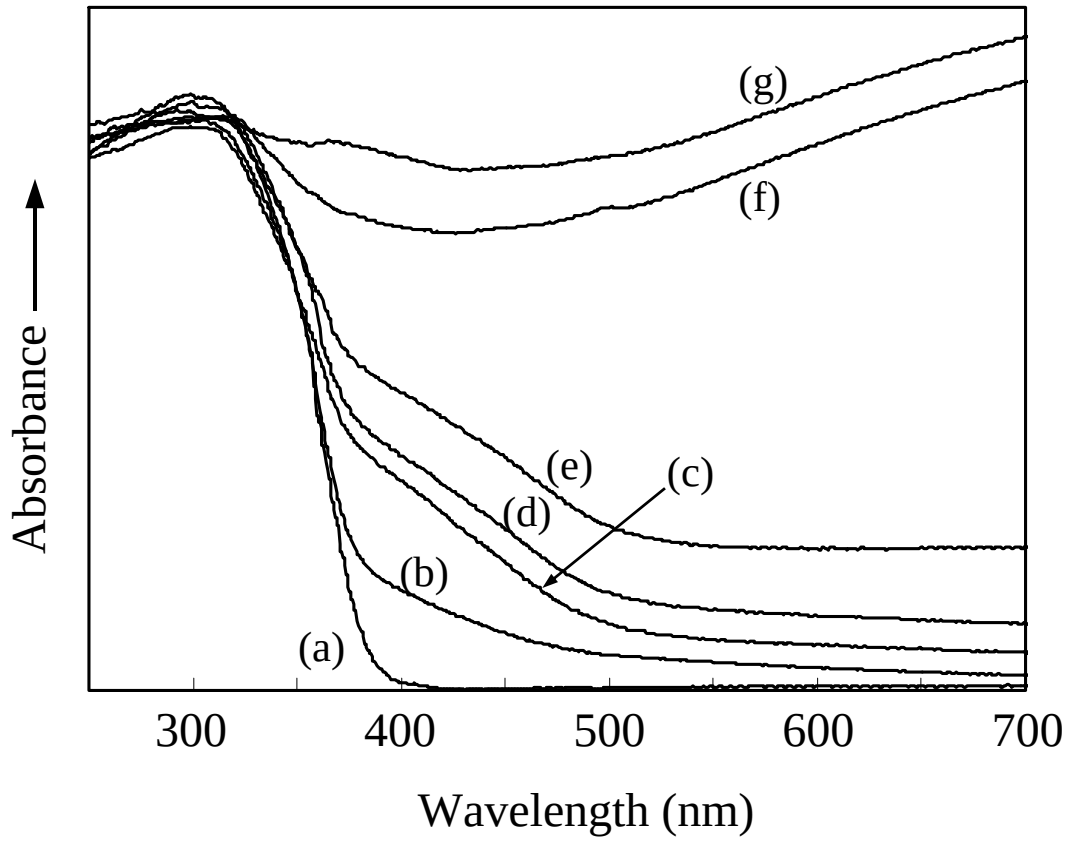

Fig. 2-2 UV-vis spectra of XG(0)'s: (a), without NH_3 treatment; treated in an NH_3 flow at: (b), 450 °C; (c), 500 °C; (d), 550 °C; (e), 600 °C; (f), 650 °C; (g), 700 °C; for 1 h.

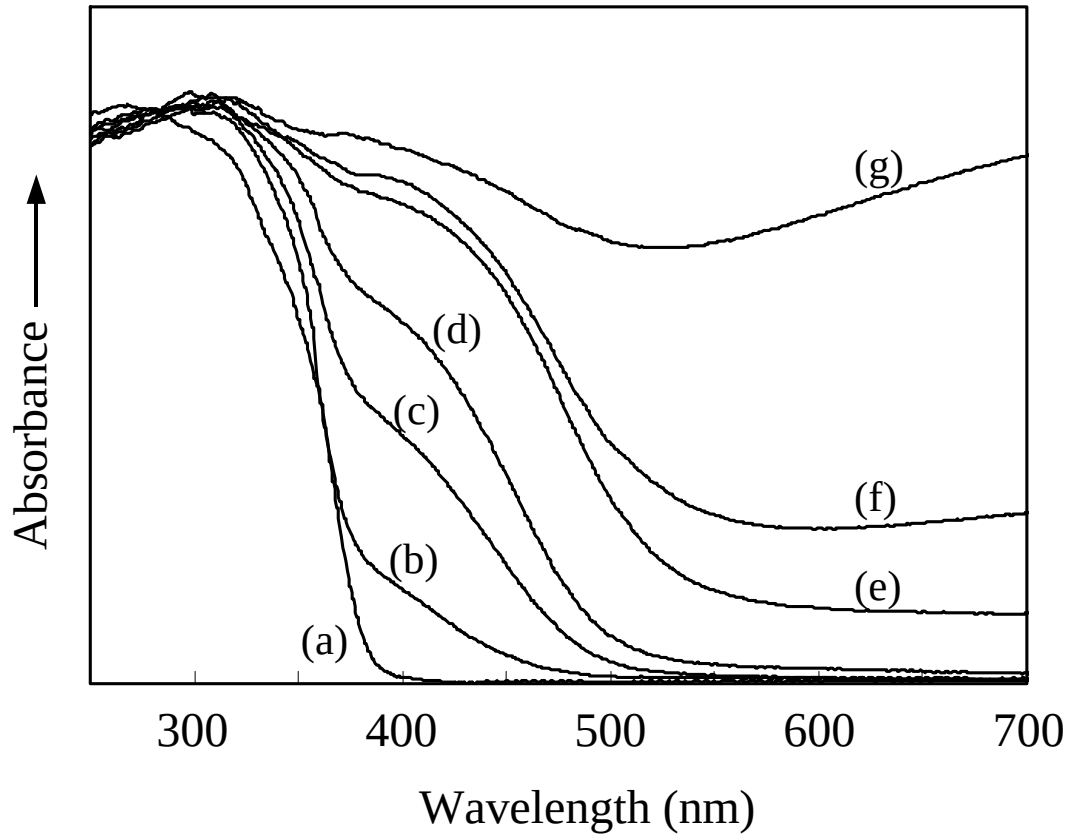

Fig. 2-3 UV-vis spectra of XG(0.1)'s: (a), without NH_3 treatment; treated in an NH_3 flow at: (b), 450 °C; (c), 500 °C; (d), 550 °C; (e), 600 °C; (f), 650 °C; (g), 700 °C; for 1 h.

XG(0)'s. On the other hand, at higher wavelength, the absorptions in XG(0.1)'s were very weak compared with those of XG(0)'s, indicating the reduction of Ti^{4+} to Ti^{3+} was significantly suppressed by the Si modification.

The XRD patterns of the samples are shown in Fig. 2-4. Both XG(0) and XG(0.1) were composed of anatase nanocrystals and their crystallite sizes were 18 nm and 10 nm, respectively. After the NH_3 treatment at 600 °C for 1 h, the samples preserved the anatase structure. For XG(0) treated at 650 °C, a small diffraction peak appeared at 2θ = 43° besides the peaks due to anatase. The sample treated at 700 °C exhibited three peaks at 37°, 43° and 63° and the intensities of the peaks increased with prolonging the treatment time. The diffraction pattern suggests the formation of a rock salt structure, isomorphous to TiN, but the peaks of the samples treated in NH_3 at 700 °C were observed at higher diffraction angles than those observed for a reference TiN specimen (Wako chemicals). The lattice parameter was 0.418 nm for both XG(0) and XG(0.1) treated in NH_3 at 700 °C for 5 h and that of TiN (Wako) was 0.424 nm. Guillot et al. reported that thin films of TiN_xO_y deposited by DC magnetron sputtering had the rock salt structure and its lattice parameter was 0.422 nm, which is smaller than that of pure TiN [19]. Makino et al. also reported that the lattice constant of titanium oxynitride films produced by the arc ion plating method decreased when the content of oxygen in the compounds increased [20]. Therefore, the newly appeared peaks were assigned to a TiN_xO_y phase, which is designated as TiN_xO_y(rock-salt) hereafter. For XG(0.1), the diffraction peaks for TiN_xO_y(rock-salt) were not observed after the NH_3 treatment at 650 °C or lower temperatures. Treatment at 700 °C gave the peaks but their intensities were much lower than those of XG(0), indicating that the Si-modification suppressed the formation of TiN_xO_y(rock-salt).

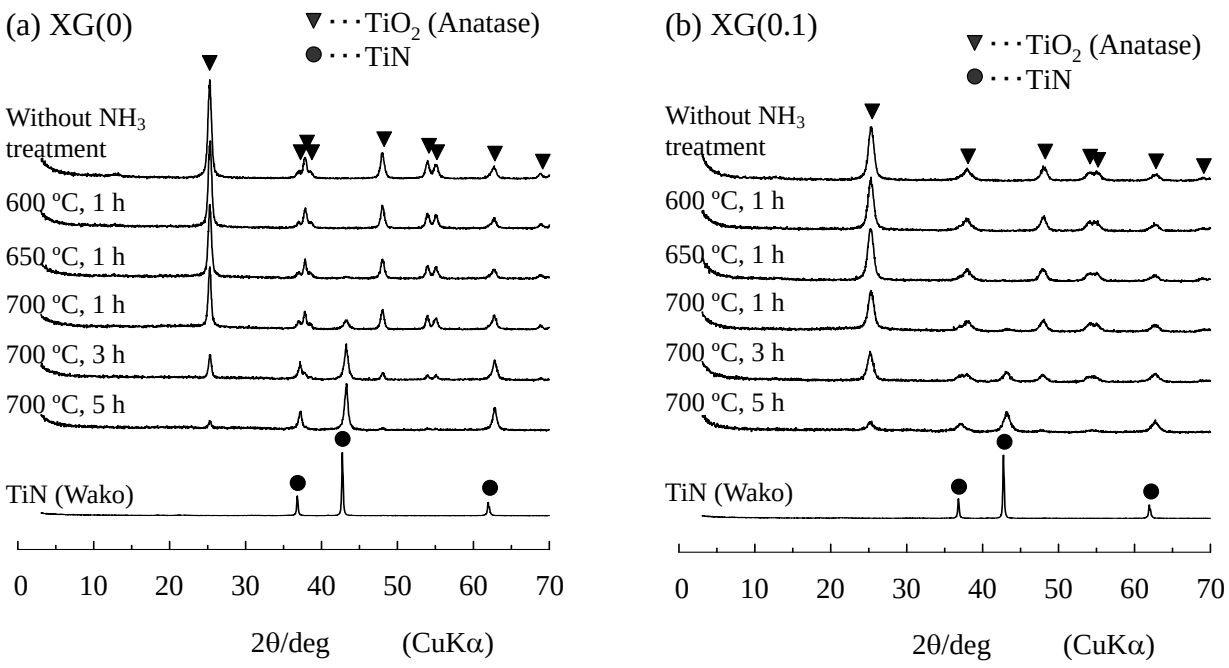

Fig. 2-4 XRD patterns of: (a), XG(0)'s; and (b), XG(0.1)'s.

2.3.2 Physical properties of NH_3-treated and annealed XG(x)'s

The BET surface areas, the crystallite sizes and the colors of NH_3-treated XG(x)'s after annealing are summarized in Table 2-1. XG(0.1) had a smaller crystallite size and a larger surface area than those of XG(0). Even after the NH_3 treatment and annealing, the crystallite sizes and BET surface areas of XG(0.1) did not change significantly, indicating that XG(0.1) had a superior thermal stability as compared to XG(0). The annealing treatment caused a decolorization; for example, black color of XG(0) after the NH_3 treatment at 700 °C turned into pale brown, and dark blue of XG(0.1) became orange. These results indicate that the annealing at 400 °C resulted in not only the desorption of the adsorbed NH_3 from the surface but also the denitrification from the bulk of the samples.

Figure 2-5 shows the UV-vis absorption spectra of nitrified XG(0) with annealing treatment at 400 °C. Compared with the spectra before annealing shown in Fig. 2-2, the absorption in the visible light region decreased, indicating the decrease in the amounts of both the doped nitrogen and the Ti^{3+}. Especially, in the case of XG(0) NH_3-treated at higher temperatures (650 and 700 °C), the absorption decreased significantly. After the annealing in air at 400 °C, the XRD patterns of the samples showed only peaks due to the anatase structure. These results suggest that the TiN_xO_y(rock-salt) phase is not stable under the oxidative conditions at high temperatures. For XG(0), the broad absorption at higher wavelength did not disappear completely, indicating that a certain amount of Ti^{3+} remained in the samples.

Figure 2-6 shows the UV-vis absorption spectra of annealed XG(0.1). On the contrary to the results for XG(0), the absorbance at the higher wavelength region was apparently lower and the shoulder band at 400–500 nm was much stronger. These

Table 2-1 Physical properties of XG(x)'s treated in an NH_3 flow at various temperatures for 1 h and annealed in air at 400 °C for 30 min

Sample	NH_3 treatment temperature (°C)	BET surface area (m^2/g)	Crystallite size (nm)	Color
XG(0)	—	81	18	white
	500	77	18	pale gray
	600	70	21	gray
	700	60	25	pale brown
XG(0.1)	—	152	10	white
	500	145	10	pale yellow
	600	149	10	yellow
	700	142	11	orange

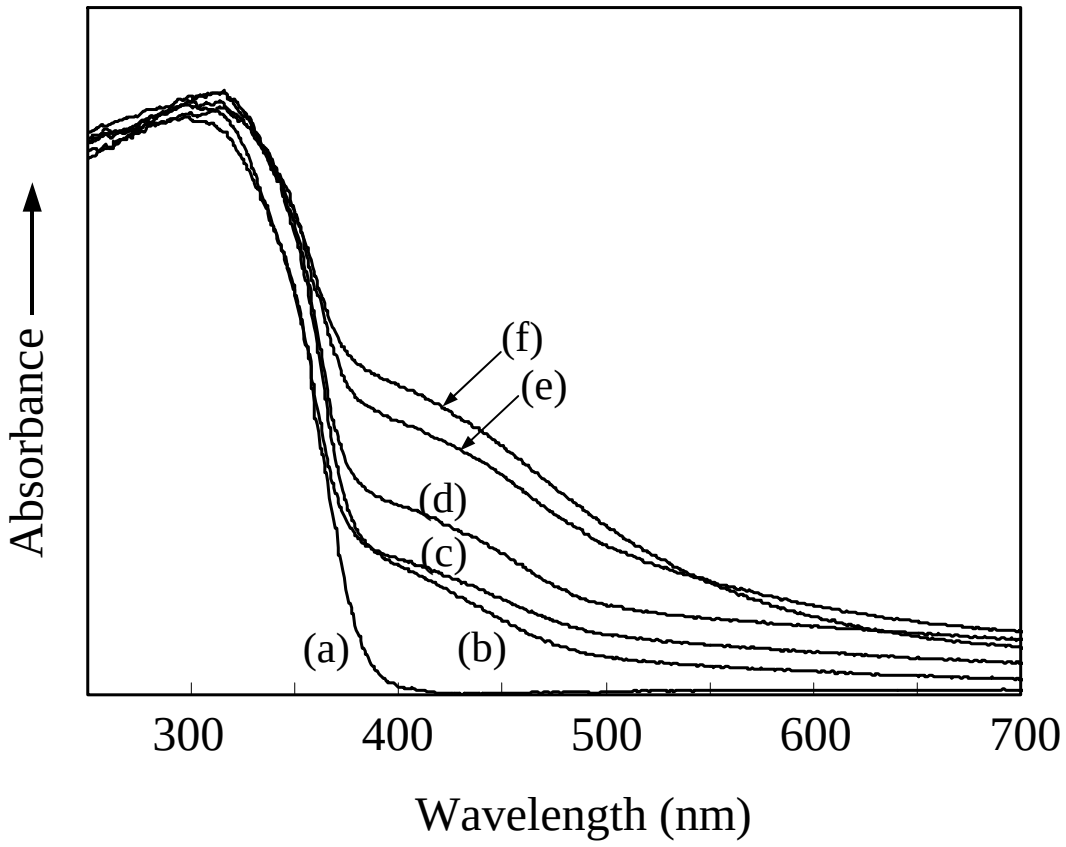

Fig. 2-5 UV-vis spectra of XG(0)'s: (a), without NH_3 treatment; treated in an NH_3 flow at: (b), 500 °C; (c), 550 °C; (d), 600 °C; (e), 650 °C; (f), 700 °C; for 1 h and annealed in air at 400 °C for 30 min.

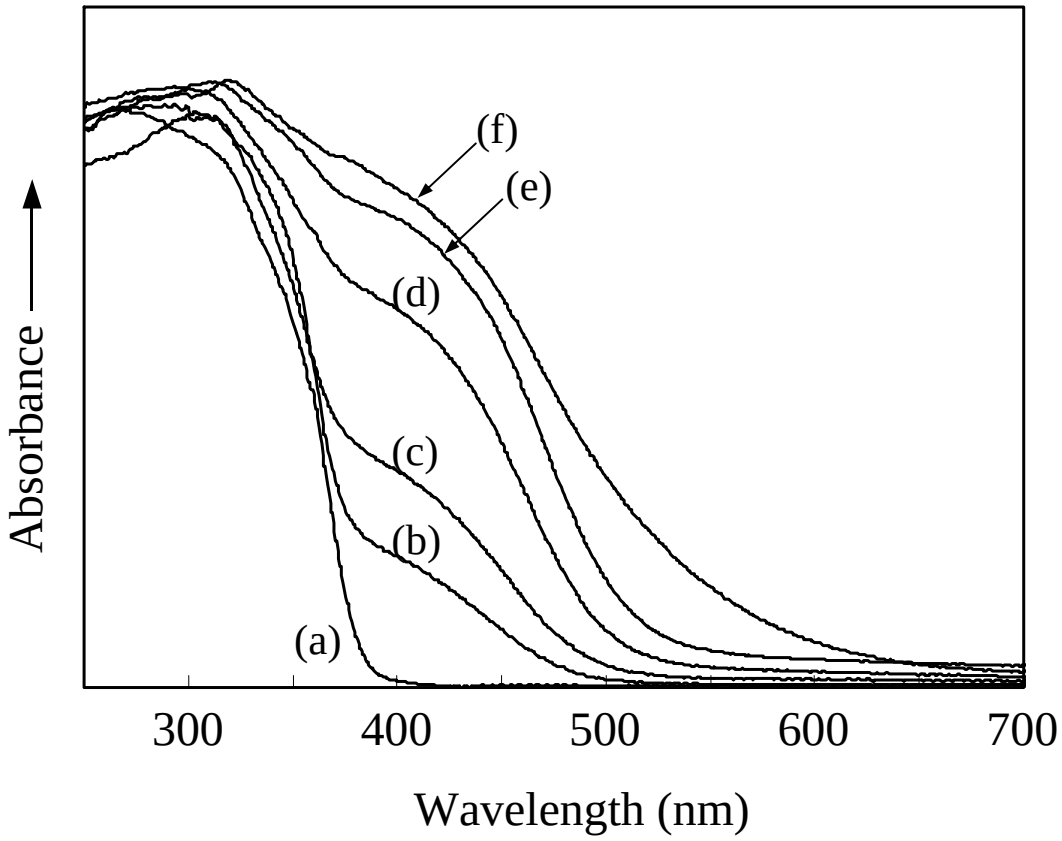

Fig. 2-6 UV-vis spectra of XG(0.1)'s: (a), without NH_3 treatment; treated in an NH_3 flow at: (b), 500 °C; (c), 550 °C; (d), 600 °C; (e), 650 °C; (f), 700 °C; for 1 h and annealed in air at 400 °C for 30 min.

results indicate that the formation of Ti^{3+} was effectively suppressed, while nitrogen was stably doped in the Si-modified titania.

2.3.3 XPS studies of nitrified XG(x)'s

In Fig. 2-7, the N 1s XPS spectra of the samples are depicted. The N 1s XPS spectrum of XG(0) (or XG(0.1); data not shown) without the NH_3 treatment exhibited a peak at 400 eV binding energy (BE), which is due to nitrogen-containing species adsorbed on the surface [21]. After the NH_3 treatment at 600 °C for 1 h, another peak appeared at 396 eV BE, which is assigned to nitrogen doped in TiO_2 [22]. The binding energy of this peak, 396 eV, is much lower than the N 1s BE of nitrogen containing species which are observed at around 400 eV [23], and is close to that of nitrides, 397 eV in TiN [24, 25]. Therefore, the peak at 396 eV is assigned as a nitrogen with a negative charge that substitute oxygen in the lattice position. The intensity of the peak at 396 eV BE in NH_3-treated XG(0.1) was obviously larger than that of NH_3-treated XG(0). Although the intensity of the peak at 396 eV BE decreased in both XG(0) and XG(0.1) after annealing in air at 400 °C for 30 min, the peak at 396 eV BE was clearly observed in the spectrum of XG(0.1). The N/Ti ratios calculated from the intensities of the Ti and $N_{396\ eV}$ peaks are plotted as a function of the NH_3 treatment temperature (Fig. 2-8). The N/Ti ratios increased with an increase in the treatment temperature. The N/Ti ratios of NH_3-treated XG(0.1) were higher than those of NH_3-treated XG(0) at temperature up to 650 °C. However, at 700 °C the N/Ti ratio of NH_3-treated XG(0) abruptly increased and became higher than that of NH_3-treated XG(0.1). This enhancement is due to the formation of TiN_xO_y(rock-salt), as was observed by XRD. After annealing at 400 °C, the N/Ti ratios decreased significantly in both XG(0) and

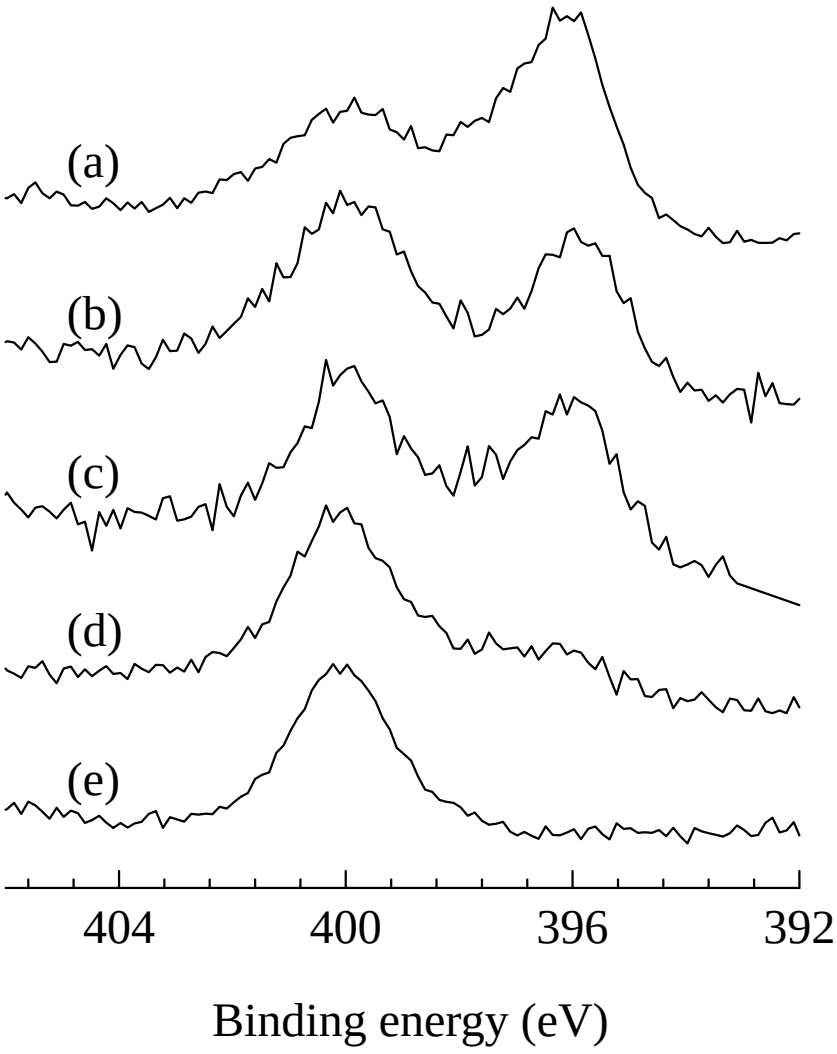

Fig. 2-7 N 1s XPS spectra of: (a), XG(0.1); (c), XG(0); treated in an NH_3 flow at 600 °C for 1 h; (b), XG(0.1); (d), XG(0); after the NH_3 treatment followed by annealing at 400 °C for 30 min; and (e), XG(0) without NH_3 treatment.

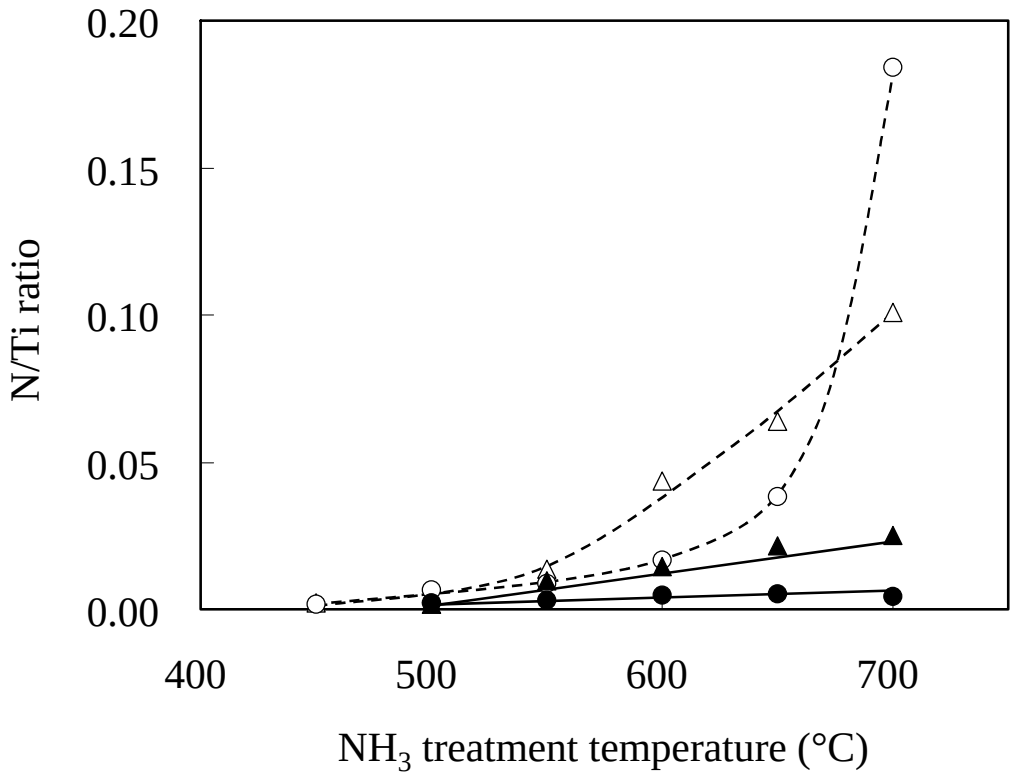

Fig. 2-8 N/Ti ratios of the nitrified samples determined by XPS: (△) and (▲), for XG(0.1); (○) and (●), for XG(0). Open symbols, after NH_3 treatment; solid symbols, after NH_3 treatment followed by annealing at 400 °C in air for 30 min.

XG(0.1). Here, it should be emphasized that the N/Ti ratios of nitrified XG(0.1) were several times higher than those of nitrified XG(0), suggesting that nitrogen atoms were more stably doped in Si-modified titanias than in titania, XG(0). In the Si-modified titanias, silicon atoms are inserted in the distorted octahedral vacant sites in the anatase structure, which caused unbalanced positive charge in the particles [12]. On the other hand, the substitution of O^{2-} with N^{3-} gave excess negative charge. In the case of nitrified Si-modified titanias, the positive charge formed by the Si insertion is compensated by the negative charge by the substitution of O^{2-} with N^{3-}. This explains the more stable doping of nitrogen in the Si-modified titanias than in titanias.

The Ti 2p XPS spectra of the samples are shown in Fig. 2-9. The results for the deconvolution of the Ti 2p peaks are summarized in Table 2-2. The Ti $2p_{1/2}$ and the Ti $2p_{3/2}$ binding energies of XG(x)'s without the NH_3 treatment were about 464.5 eV and 458.8 eV, respectively. After the NH_3 treatment at 600 or 650 °C, the Ti 2p XPS spectra did not change significantly. For XG(x)'s with the NH_3 treatment at 700 °C for 1 h, however, different components were observed at around 461.8 and 456.1 eV for Ti $2p_{1/2}$ and Ti $2p_{3/2}$, respectively. These components are attributed to titanium in TiN_xO_y(rock-salt) [26, 27]. The intensity of the newly observed peak in XG(0.1) treated in NH_3 at 700 °C for 1 h was obviously lower than that in XG(0) treated at 700 °C for 1 h. This result indicates that the formation of TiN_xO_y(rock-salt) was suppressed by Si-modification, which agrees with the results of XRD. There found some discrepancy between XRD and XPS results: The XRD pattern of NH_3-treated XG(0) at 650 °C showed a small diffraction peak due to TiN_xO_y(rock-salt), while XPS result did not show any indication of the presence of this phase in the sample. Since the sample was treated in ambient atmosphere before the XRD and XPS measurements, the surface of

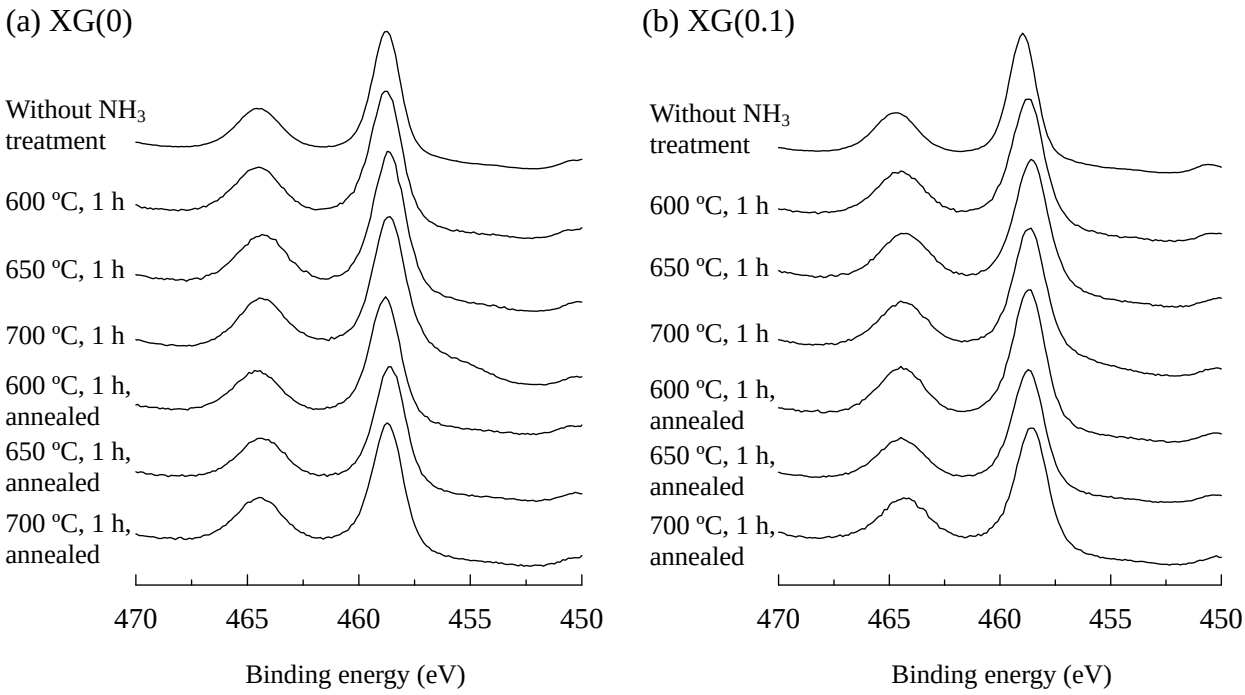

Fig. 2-9 Ti 2p XPS spectra of: (a), XG(0); and (b), XG(0.1).

Table 2-2 Binding energy of core electrons for nitrified XG(x)'s

Sample	NH_3 treatment	Annealing	Ti $2p_{1/2}$ (eV)	Ti $2p_{3/2}$ (eV)
XG(0)	–	–	464.5	458.8
	600 ºC, 1 h	–	464.5	458.8
	650 ºC, 1 h	–	464.3	458.6
	700 ºC, 1 h	–	464.4 (81)[a]	458.6 (82)[a]
			461.8 (19)	456.1 (18)
	600 ºC, 1 h	400 ºC, 30 min	464.5	458.8
	650 ºC, 1 h	400 ºC, 30 min	464.3	458.6
	700 ºC, 1 h	400 ºC, 30 min	464.4	458.7
XG(0.1)	–	–	464.7	458.9
	600 ºC, 1 h	–	464.5	458.7
	650 ºC, 1 h	–	464.3	458.6
	700 ºC, 1 h	–	464.4 (90)	458.7 (90)
			461.7 (10)	456.2 (10)
	600 ºC, 1 h	400 ºC, 30 min	464.4	458.7
	650 ºC, 1 h	400 ºC, 30 min	464.4	458.7
	700 ºC, 1 h	400 ºC, 30 min	464.3	458.6

[a] The number in parentheses indicates the percentage of the band.

the sample seems to be oxidized by air. After annealing in air at 400 °C for 30 min, the Ti 2p spectra were quite similar to those for XG(x)'s without the NH_3 treatment, which indicates that the TiN_xO_y(rock-salt) phase was not included in both XG(0) and XG(0.1). This result also suggests that the proportions of Ti^{3+} in the samples were small although the presence of Ti^{3+} in NH_3-treated XG(x)'s with the annealing was indicated by the UV-vis spectra.

2.3.4 Photocatalytic activities of nitrified XG(x)'s

Figure 2-10 shows the result of photocatalytic degradation of RhB using blue LED as a light source. In this experiment, XG(0) and XG(0.1), both not nitrified, exhibited certain activities; for example, about 30% of RhB was decomposed after irradiation for 10 h. These photocatalytic activities are due to a dye-sensitized photocatalytic reaction, which has been observed in various dye-TiO_2 systems [28, 29]. On the other hand, by using the nitrified samples, the decomposition rate increased significantly. Nitrified XG(0.1) obviously showed a higher photocatalytic activity than nitrified XG(0) and JRC-TIO-4.

For NH_3-treated XG(0.1) or XG(0) without annealing, the photocatalytic activities were much lower than those of the annealed samples (Fig. 2-11). This is probably because of the presence of adsorbed NH_3 and of the increase in the population of oxygen vacancies, which serve as recombination centers and promote the recombination of holes and electrons [30]. The annealing procedure eliminated the adsorbed NH_3 and oxygen vacancies, thus increasing the high photocatalytic activity. However, higher annealing temperature decreases the amount of nitrogen doped and thus reduces the visible light responsibility. Therefore, in this paper, 400 °C was chosen

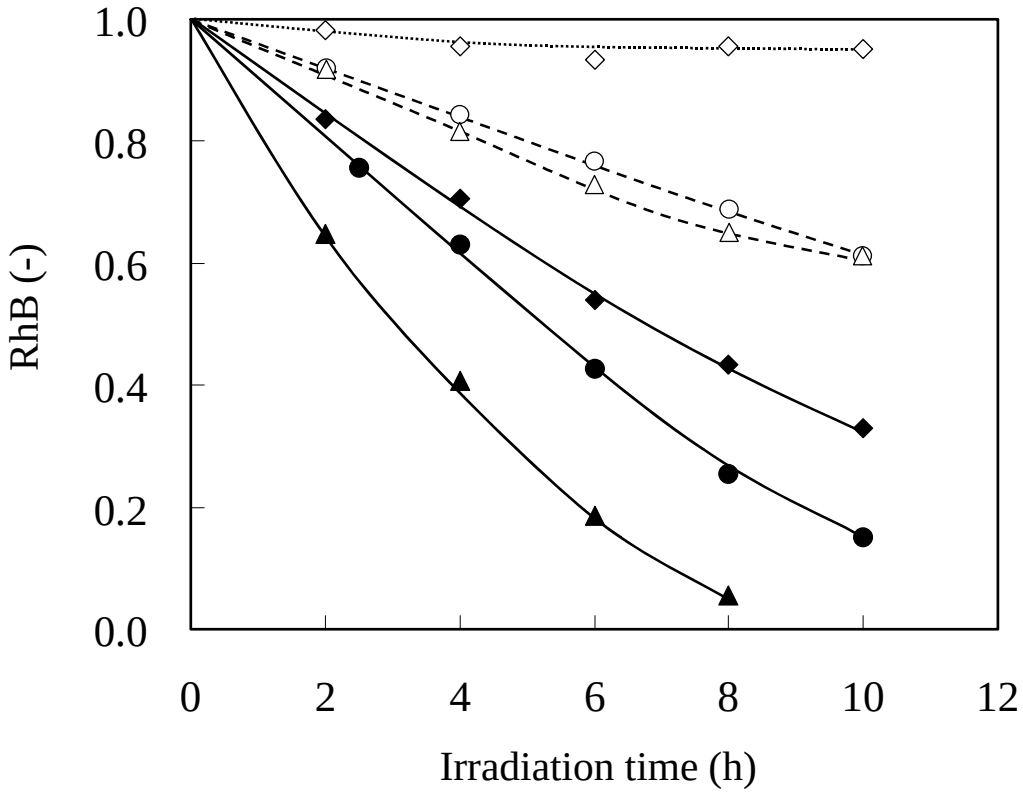

Fig. 2-10 Photocatalytic decomposition of RhB under visible light irradiation: (◇), without catalyst; (○) and (●), XG(0); (△) and (▲), XG(0.1); (◆), JRC-TIO-4. Open symbols, without the NH_3 treatment; solid symbols, after the NH_3 treatment at 600 °C for 1 h and annealing at 400 °C in air for 30 min.

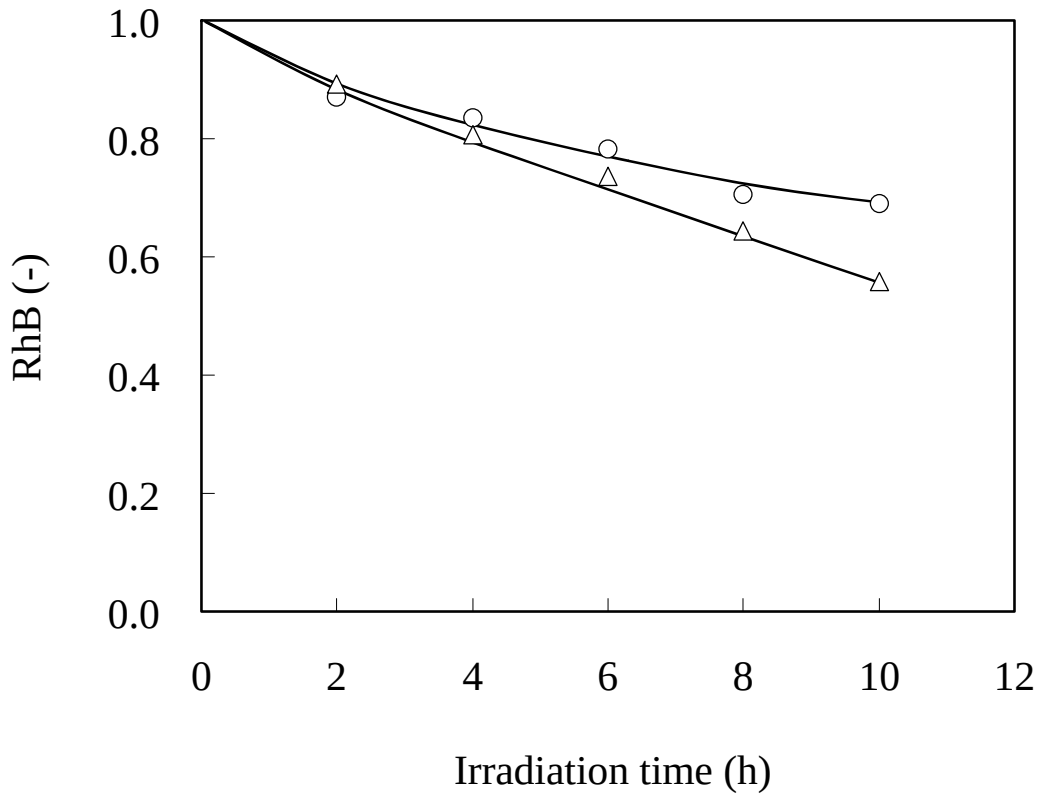

Fig. 2-11 Photocatalytic decomposition of RhB under visible light irradiation: (○), XG(0); and (△), XG(0.1); treated in an NH_3 flow at 600 °C for 1 h and without annealing.

as the annealing temperature.

In order to examine the effect of surface property of the catalysts, zeta potentials of the catalysts were measured and the results are shown in Fig. 2-12. The isoelectric point of XG(0) was 7.1, while that of XG(0.1) was shifted to the lower pH side, 5.8. Since the isoelectric point of pure SiO_2 is ca 2.0, this shift is probably due to a small amount of SiO_2 located on the surface of the Si-modified titanias. Such a change in zeta potential, however, did not affect the equilibrium amount of the adsorbed RhB at pH 5 (Fig. 2-13). Since RhB is a cationic dye, it is preferably adsorbed on the negatively charged surface. In the experiments of RhB photocatalytic decomposition, the pH of the RhB solution was from 4 to 5, and therefore, the surfaces of both XG(0) and XG(0.1) were positively charged. After the NH_3 treatment at 600 °C for 1 h and annealing at 400 °C for 30 min, the isoelectric points for both XG(0) and XG(0.1) did not change significantly. These results indicate that the improved photocatalytic activities of the nitrified samples were not because of the change in the surface property. Therefore, we concluded that the improved visible-light-sensitivity of the nitrified Si-modified titania is due to the increase in the amount of doped nitrogen.

Figure 2-14 shows the result of photocatalytic decomposition of acetaldehyde on the samples. Under visible light irradiation, evolution of CO_2 was not detected for XG(0). On the other hand, using nitrified XG(x)'s, the amount of CO_2 increased with the irradiation time, indicating that photocatalytic decomposition of acetaldehyde proceeded under visible light irradiation. Nitrified XG(0.1) obviously showed a higher photocatalytic activity than nitrified XG(0) and JRC-TIO-4. As shown in Fig. 2-14, the CO_2 concentration increased proportionally, suggesting a pseudo-zero-order kinetics with respect to the acetaldehyde concentration (partial pressure). However, induction

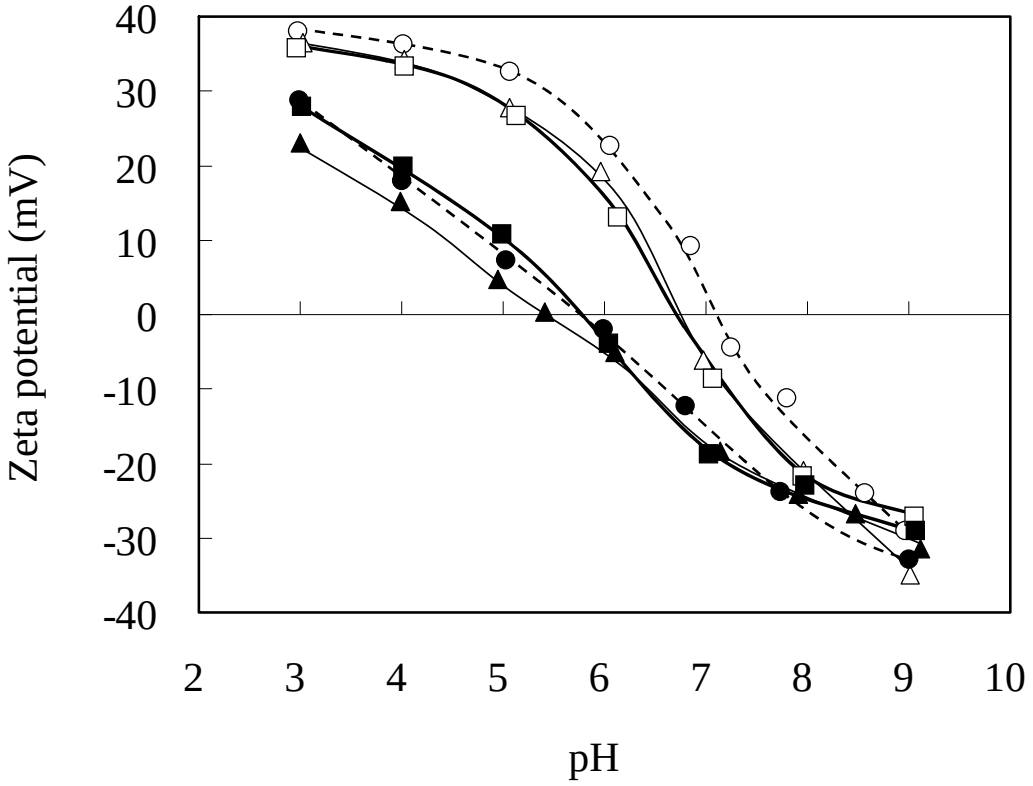

Fig. 2-12 Zeta potential as a function of pH: open symbols, for XG(0); closed symbols, for XG(0.1). Circles, without the NH_3 treatment; triangles, after the NH_3 treatment at 600 °C for 1 h; squares, after the NH_3 treatment and annealing at 400 °C in air for 30 min.

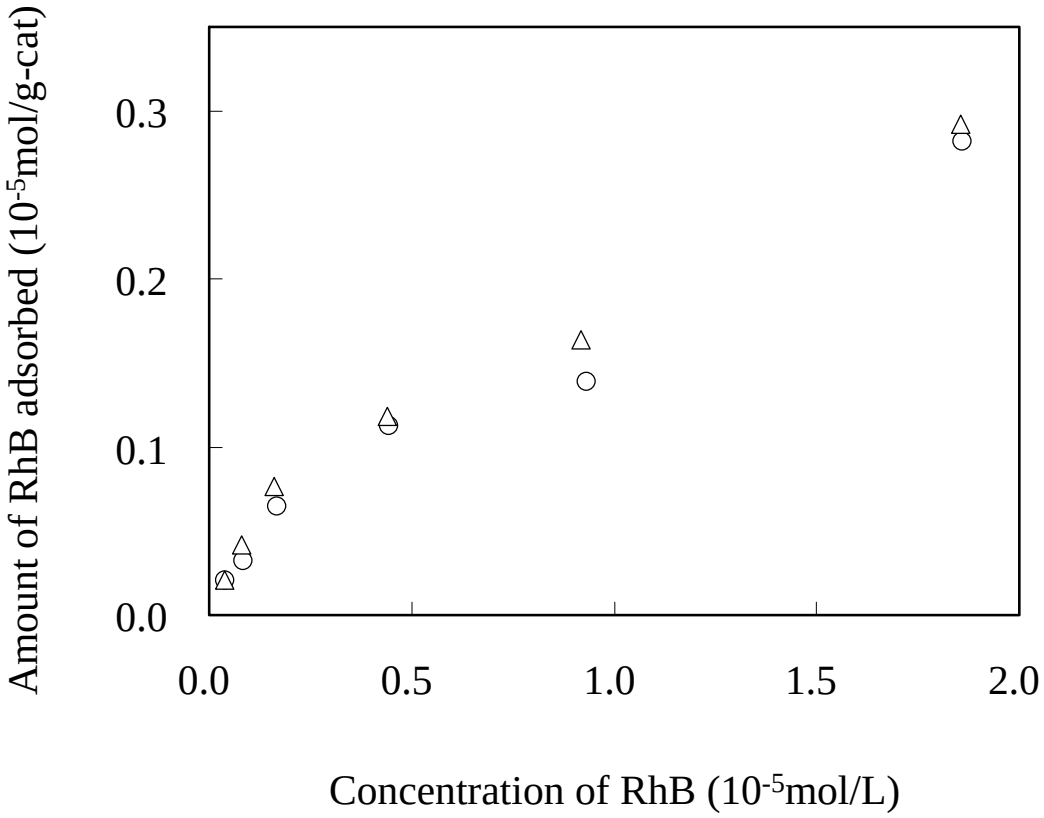

Fig. 2-13 RhB adsorption isotherm of: (○), XG(0); and (△), XG(0.1).

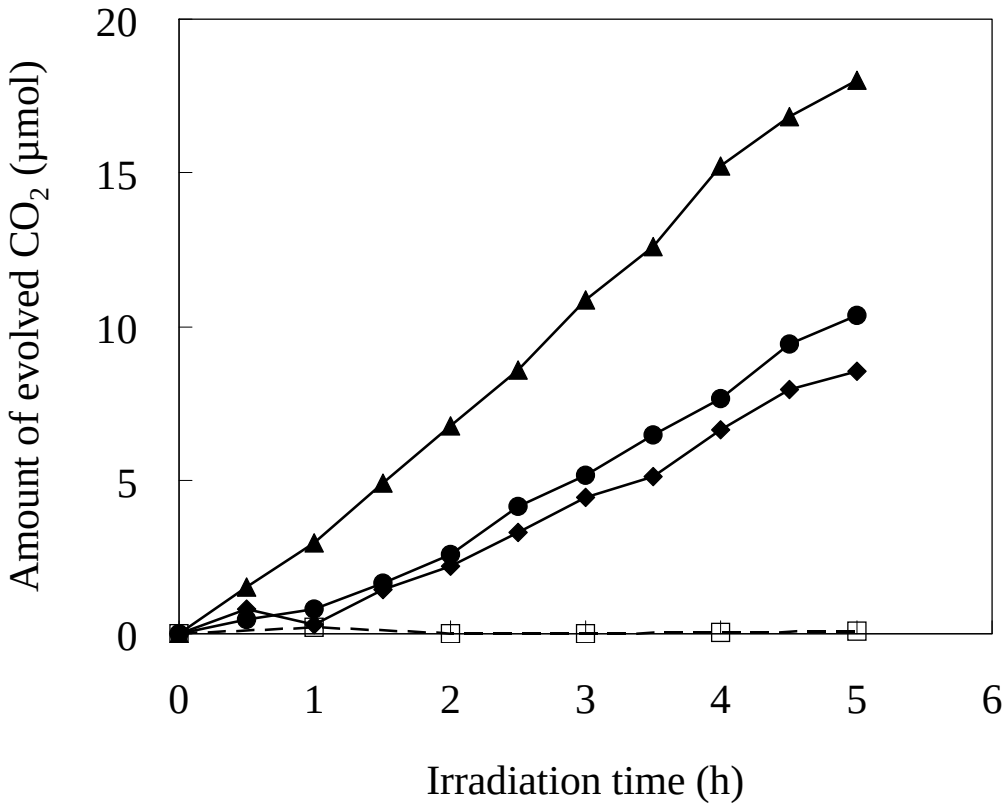

Fig. 2-14 Photocatalytic decomposition of acetaldehyde under visible light irradiation: (▲), XG(0.1); (●), XG(0); (◆), JRC-TIO-4; treated in an NH_3 flow at 600 °C for 1 h and annealed in air at 400 °C for 30 min, and (□), XG(0).

period was clearly observed for nitrified XG(0) and JRC-TIO-4, indicating presence of intermediates [31–34]. The photocatalytic reaction in this paper was carried out using a relatively weak visible light in the presence of a high concentration of acetaldehyde (0.2 mmol of acetaldehyde in 1 L corresponds to 5,000 ppm) and therefore the CO_2 formation rate was not changed when the amount of the acetaldehyde was changed (0.1–0.4 mmol). These results indicate that the reaction rate is not limited by the adsorbability of the reactant on the surface of the catalyst but that the photocatalytic reaction is determined dominantly by the rate of the generation of the photoexcited electron and the positive hole as well as the recombination rate of them.

2.4 Conclusions

By the NH_3 treatment at a high temperature, both of TiO_2 and Si-modified titanias were nitrified. After the NH_3 treatment and the annealing in air, the amount of nitrogen introduced to the Si-modified titanias was higher than that of the pure titania. The nitrified Si-modified titanias showed a strong absorption in the visible region (400–500 nm) and exhibited high photocatalytic activities for degradation of RhB and decomposition of acetaldehyde under visible light irradiation.

References

[1] N. Serpone and D. Lawless, *Langmuir* **1994**, *10*, 643.

[2] M. Anpo, *Catal. Surv. Jpn.* **1997**, *1*, 169.

[3] S. Klosek and D. Raftery, *J. Phys. Chem. B* **2001**, *105*, 2815.

[4] Y. Sakata, T. Yamamoto, T. Okazaki, H. Imamura, and S. Tsuchiya, *Chem. Lett*. **1998**, 1253.

[5] S. Sato, *Chem. Phys. Lett*. **1986**, *123*, 126.

[6] R. Asahi, T. Morikawa, T. Ohwaki, K. Aoki, and Y. Taga, *Science* **2001**, *293*, 269.

[7] T. Lindgren, J. M. Mwabora, E. Avendaño, J. Jonsson, A. Hoel, C.-G. Granqvist and S.-E. Lindquist, *J. Phys. Chem. B* **2003**, *107*, 5709.

[8] H. Irie, Y. Watanabe, and K. Hashimoto, *J. Phys. Chem. B* **2003**, ***107***, 5483.

[9] T. Ohno, T. Mitsui, and M. Matsumura, *Chem. Lett*. **2003**, 364.

[10] H. Luo, T. Takata, Y. Lee, J. Zhao, K. Domen, and Y. Yan, *Chem. Mater*. **2004**, *16*, 846.

[11] A. Hattori and H. Tada, *J. Sol-Gel Sci. Technol.* **2001**, *22*, 47.

[12] S. Iwamoto, W. Tanakulrungsank, M. Inoue, K. Kagawa, and P. Praserthdam, *J. Mater. Sci. Lett.* **2000**, *19*, 1439.

[13] Sh. Iwamoto, Se. Iwamoto, M. Inoue, H. Yoshida, T. Tanaka, and K. Kagawa, *Chem. Mater*. **2005**, *17*, 650.

[14] S. Iwamoto, K. Saito, M. Inoue, and K. Kagawa, *Nano Lett.* **2001**, *1*, 417.

[15] M. Miyauchi, A. Ikezawa, H. Tobimatsu, H. Irie, and K. Hashimoto, *Phys. Chem. Chem. Phys*. **2004**, *6*, 865.

[16] H. Liu and L. Gao, *J. Am. Ceram. Soc.* **2004**, *87*, 1582.

[17] Y. Sakatani, H. Ando, K. Okusako, H. Koike, J. Nunoshige, T. Takata, J. N. Kondo, M. Hara, and K. Domen, *J. Mater. Res.* **2004**, *19*, 2100.

[18] T. Torimoto, R. J. Fox III, and M. A. Fox, *J. Electrochem. Soc.* **1996**, *143*, 3712.

[19] J. Guillot, A. Jouaiti, L. Imhoff, B. Domenichini, O. Heintz, S. Zerkout, A. Mosser, and S. Bourgeois, *Surf. Interface Anal.* **2002**, *33*, 577.

[20] Y. Makino, M. Nose, T. Tanaka, M. Misawa, A. Tanimoto, T. Nakai, K. Kato, and K. Nogi, *Surf. Coat. Technol.* **1998**, *98*, 934.

[21] N. D. Shinn and K. L. Tsang, *J. Vac. Sci. Technol. A* **1991**, *9*, 1558.

[22] N. C. Saha and H. G. Tompkins, *J. Appl. Phys*. **1992**, *72*, 3072.

[23] G. E. Muilenberg, in "Handbook of X-ray Photoelectron Spectroscopy" (Perkin-Elmer Corporation, Minnesota, 1979) p. 40.

[24] H. Höchst, R. D. Bringans, P. Steiner, and Th. Wolf, *Phys. Rev. B* **1982**, *25*, 7183.

[25] M. J. Vasile, A. B. Emerson, and F. A. Baiocchi, *J. Vac. Sci. Technol. A* **1990**, *8*, 99.

[26] A. E. Miller and J. Moulder, *J. Vac. Sci. Technol. A* **1985**, *3*, 2415.

[27] I. Bertóti, M. Mohai, J. L. Sullivan, and S. O. Saied, *Appl. Surf. Sci.* **1995**, *84*, 357.

[28] T. Wu, G. Liu, J. Zhao, H. Hidaka, and N. Serpone, *J. Phys. Chem. B* **1998**, *102*, 5845.

[29] K. Vinodgopal and P. V. Kamat, *J. Phys. Chem.* **1992**, *96*, 5053.

[30] S. Ikeda, N. Sugiyama, S. Murakami, H. Kominami, Y. Kera, H. Noguchi, K. Uosaki, T. Torimoto, and B. Ohtani, *Phys. Chem. Chem. Phys*. **2003**, *5*, 778.

[31] M. L. Sauer and D. F. Ollis, *J. Catal.* **1996**, *158*, 570.

[32] M. R. Nimlos, E. J. Wolfrum, M. L. Brewer, J. A. Fennell, and G. Bintner, *Environ. Sci. Technol.* **1996**, *30*, 3102.

[33] D. S. Muggli, K. H. Lowery, and J. L. Falconer, *J. Catal.* **1998**, *180*, 111.

[34] J.-H. Xu and F. Shiraishi, *J. Chem. Technol. Biotechnol.* **1999**, *74*, 1096.

Chapter 3

Effects of amount of Si addition and annealing treatment on the photocatalytic activities of nitrogen- and silicon-co-doped titanias under visible-light irradiation

3.1 Introduction

Chapter 2 dealt with the nitrification of the Si-modified titanias (Si/Ti=0.1) and it was described that higher concentration of N can be stably incorporated in Si-modified titania than in non-modified titania. The thus-obtained N- and Si-co-doped titania showed a strong absorption in the visible region (400–550 nm) and exhibited high photocatalytic activities for degradation of Rhodamine B and decomposition of acetaldehyde under visible-light irradiation.

In the study presented in this chapter, various N- and Si-co-doped titanias were prepared by changing the amount of Si added and the annealing temperature after the nitrification. The obtained products were characterized by several methods and their photocatalytic activities under visible-light irradiation were examined. It was found that a significant improvement was attained by optimizing the Si/Ti ratio and the preparation conditions.

3.2 Experimental

3.2.1 Preparation of the catalysts

Titania and Si-modified titania were prepared by the glycothermal method and collected as a xerogel form [1]: Titanium tetraisopropoxide (25 g) and an appropriate amount of tetraethyl orthosilicate (Si/Ti atomic ratio of 0–0.5) were added to 100 mL of 1,4-butanediol and this mixture was placed in a 300 mL autoclave. The autoclave had two valves, one of which was for a gas inlet, and the other was connected to a Liebig condenser of stainless tubing for a gas outlet. After the atmosphere inside the autoclave was replaced with nitrogen, the assembly was heated to 300 °C at a rate of 2.3 °C/min and kept at that temperature for 2 h. The outlet valve of the autoclave was, then, slightly opened while keeping the autoclave temperature at 300 °C, and the organic vapor was removed from the autoclave by flash evaporation. After cooling, bulky solid products were directly obtained. The product was calcined in a box furnace in air at 500 °C for 30 min to eliminate the surface organic moieties. The thus-obtained products are designated as XG(x), where x is the Si/Ti charged ratio. XG(x) was placed in a quartz tube reactor, heated to 600 °C at a rate of about 10 °C/min in a 100 mL/min flow of argon, and allowed to react in an NH_3 flow (100 mL/min) for 1 h at that temperature. After the NH_3 treatment, the sample was annealed at a desired temperature (400–700 °C) in air for 30 min in a box furnace. The thus-obtained products are designated as XG(x)-N-A(temp), where temp is the annealing temperature.

For comparison, Si-modified titanias (Si/Ti = 0.3) were prepared by an impregnation method. Two titania samples, XG(0) and JRC-TIO-4 (a reference catalyst supplied from The Catalysis Society of Japan; equivalent to Degussa P-25) were used as the precursors. To a solution of tetraethyl orthosilicate : C_2H_5OH : H_2O : HNO_3 = 1 : 10 : 10 : 0.2, an appropriate amount of the precursor titania was added. The mixture was

dried at 60 °C and then, calcined at 600 °C in air for 30 min. These samples are designated as XG(0.3-imp) and P-25(0.3-imp), respectively. They were nitrified and annealed at 500 °C in the same way as described above, and the nitrified samples are designated as XG(0.3-imp)-N-A(500) and P-25(0.3-imp)-N-A(500), respectively.

3.2.2 Characterization

The UV-vis absorption spectra were recorded on a Shimadzu MPS-2000 spectrophotometer. Powder X-ray diffraction (XRD) patterns were recorded on a Shimadzu XD-D1 diffractometer using CuKα radiation and a carbon-monochromator. The specific surface areas of the samples were calculated by the BET single-point method on the basis of the nitrogen uptake measured at 77 K. X-ray photoelectron spectroscopy (XPS) measurement was performed on an ULVAC-PHI Model 5500 spectrometer with 15 kV - 400 W MgKα emissions as the X-ray source. Electron spin resonance (ESR) spectra were recorded with a JES-SRE2X spectrometer at 123 K. The sample was pretreated by evacuation at 400 °C for 30 min. The *g* factor was determined using Mn^{2+} marker included in MgO.

3.2.3 Photocatalytic reaction

Photocatalytic activity was evaluated by decomposition of acetaldehyde. The decomposition of acetaldehyde was carried out in a closed glass vessel (1.0 L). The catalyst (0.2 g) dispersed on a 90 mmϕ glass filter was placed in the vessel and 0.2 mmol acetaldehyde was injected in it. The vessel was placed in the dark for 1 h and then visible light was irradiated using a 300 W xenon lamp (Optical Modulex SX-UI300XQ, Ushio Inc.) through a UV cut-off filter (L-42, Asahi Technoglass Co. Ltd.) and an

infrared cut-off filter (Super Cold Filter, Ushio Inc.). After a certain period of irradiation, the concentration of the generated CO_2 was measured by a gas chromatograph, Shimadzu GC-8A.

3.3 Results and discussion

3.3.1 Effect of amounts of Si addition

The XRD patterns of XG(x)'s with various Si/Ti ratios are depicted in Figure 3-1, which shows that all the products had the anatase structure. The BET surface areas and crystallite sizes of XG(x)'s without the NH_3 treatment are listed in Table 3-1 together with those for the nitrified samples. The crystallite size of XG(0) was 18 nm, and the addition of only a small amount of Si, for instance, Si/Ti = 0.02, significantly decreased the crystallite size. With further increase in the amount of Si addition, the crystallite size decreased gradually, and for XG(0.5), quite a small crystallite size, 8 nm, was obtained. The BET surface areas increased significantly from 81.6 m^2/g to 152 m^2/g with the increase in the amount of Si modification up to Si/Ti = 0.1; however, it reached a plateau level for Si/Ti = 0.2–0.5.

The XRD patterns of the samples after the NH_3 treatment at 600 °C and annealing at 400 °C, XG(x)-N-A(400), show that all the samples preserved the anatase structure. For XG(0), the surface area decreased from 81.6 m^2/g to 70.2 m^2/g and the crystallite size increased from 18 nm to 21 nm by these treatments. For Si-modified titanias, however, the surface areas and the crystallite sizes were essentially unchanged by the nitrification and annealing, indicating that the Si-modified titanias had high thermal stabilities [2].

Figure 3-2 shows the UV-vis spectra of XG(x)-N-A(400). Whereas XG(0)

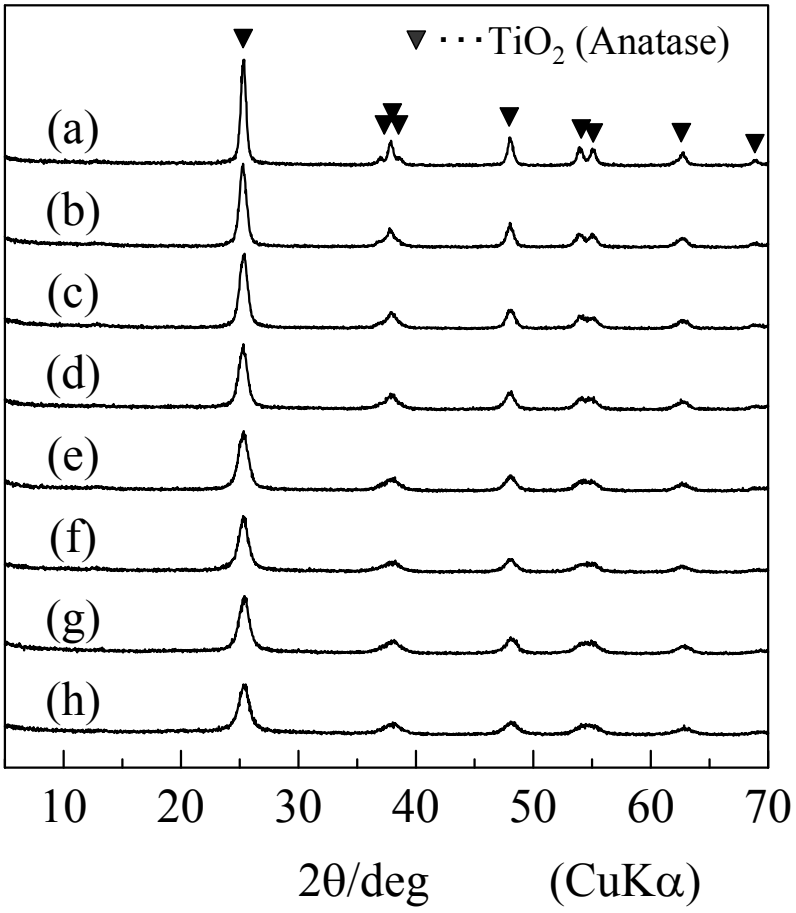

Fig. 3-1 XRD patterns of: XG(x)'s with the Si/Ti charged ratio, x, of: (a), 0; (b), 0.02; (c), 0.06; (d), 0.1; (e), 0.2; (f), 0.3; (g), 0.4, and (h), 0.5.

Table 3-1 Physical properties of XG(x)'s before and after the NH_3 treatment at 600 ºC and annealing in air at 400 ºC

Sample	BET surface area (m^2/g)		Crystallite size (nm)	
	before	after	before	after
XG(0)	81.6	70.2	18.2	21.2
XG(0.02)	113	112	15.6	16.2
XG(0.06)	135	132	12.5	13.0
XG(0.1)	152	149	10.4	10.4
XG(0.2)	164	158	9.9	10.2
XG(0.3)	141	135	8.7	8.8
XG(0.4)	145	145	8.7	8.7
XG(0.5)	161	166	8.2	8.4

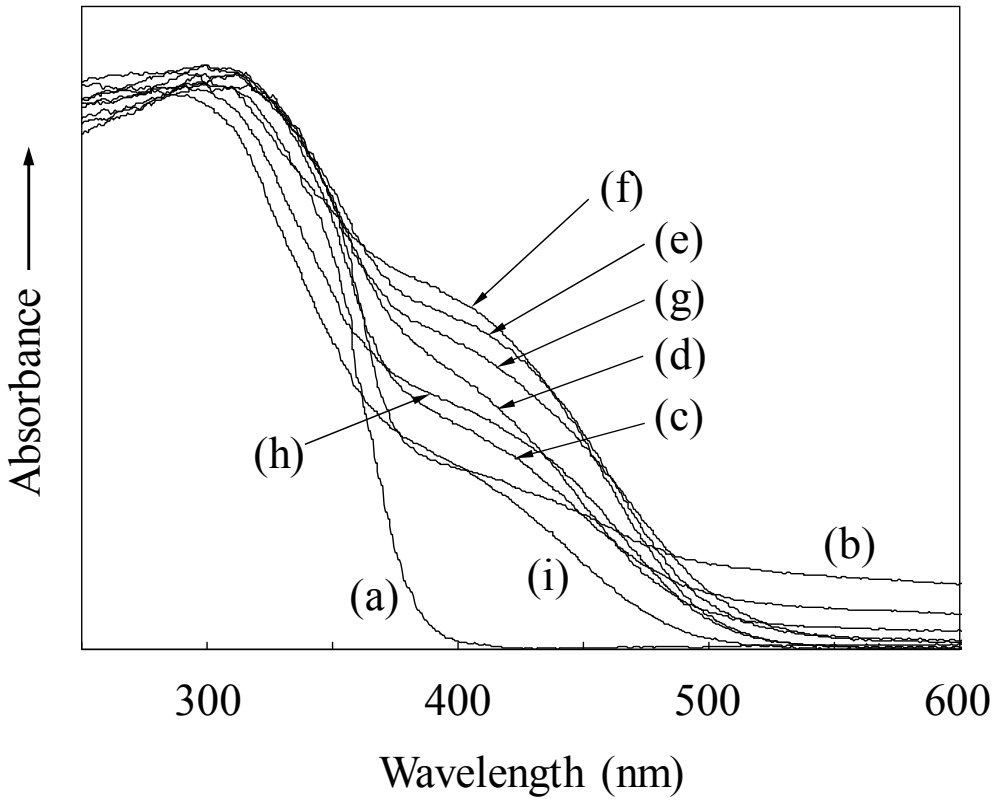

Fig. 3-2 UV-vis spectra of: (a), XG(0) without NH_3 treatment; (b)–(i), XG(x)-N-A(400) with the Si/Ti charged ratio, x, of: (b), 0; (c), 0.02; (d), 0.06; (e), 0.1; (f), 0.2; (g), 0.3; (h), 0.4, and (i), 0.5.

exhibited an absorption only in a UV region (< 400 nm), all the nitrified and annealed samples (XG(x)-N-A(400)) showed absorptions at a visible-light region. The spectrum of XG(0)-N-A(400) had a shoulder absorption band at 400–500 nm and a broad band at higher wavelength (> 500 nm). The former band is attributed to the doped nitrogen into the anatase structure and the latter corresponds to the formation of Ti^{3+} [3]. As compared with the spectra of XG(0)-N-A(400), XG(x)-N-A(400) with $x \geq 0.02$ had a stronger absorption at 400–500 nm, while the absorptions at higher wavelength became very weak. These results indicate that larger amounts of nitrogen were doped in XG(x)'s and that the generation of Ti^{3+} was significantly suppressed by the Si modification.

In the case of unmodified anatase, the negative charges formed by the substitution of O^{2-} with N^{3-} are balanced by formation of oxygen vacancies. In the case of nitrified Si-modified titanias, on the other hand, the negative charge formed by the substitution of O^{2-} with N^{3-} can be compensated by the positive charge formed by the Si insertion, which explains the more stable doping of nitrogen in the Si-modified titanias than in titanias.

The intensity of the absorption band at 400–500 nm increased as the Si/Ti ratio increased to around 0.2 or 0.3, and then it gradually decreased with higher amount of Si modification. S. Iwamoto et al. previously examined the surface properties of Si-modified titania by TPD methods and found that Si-modified titania with the Si/Ti ratio smaller than 0.1 had the surface property similar to that of pure TiO_2 while a part of the surface of Si-modified titania with the Si/Ti ratio higher than 0.2 was covered with SiO_2-based matters [4]. In the case of XG(0.4) and XG(0.5), therefore, it is likely that excess SiO_2-based matters present on the surface of the anatase nanocrystals hinder the perticles from contacting with NH_3 and hence being nitrified.

In order to obtain the information on the surface of the samples, XPS analysis was conducted. In Table 3-2, the binding energies of O1s, Si2p, Ti2p, and Si/Ti ratios for XG(x)-N-A(400) are shown. The Si/Ti ratios of the samples determined by XPS increased with increasing the amount of Si modification, and were somewhat larger than the charged Si/Ti ratios, indicating that Si was enriched in the surface region of the samples. The O1s XPS spectra of XG(x)-N-A(400) are shown in Figure 3-3. In the O1s XPS spectrum of XG(0)-N-A(400), a peak was observed at 530 eV, which corresponds to the oxygen in TiO_2. For the Si-modified titanias, a different O1s component due to the oxygen associated with the Si-O-Ti bridging bond [5,6] was recognized at 532 eV. This component became larger with increasing x; however, the 533 eV component observed in pure SiO_2 [7] was not detected. These results indicate the absence of pure SiO_2 clusters on the surface of the product particles.

The N1s XPS spectra of XG(x)-N-A(400) are shown in Figure 3-4. In the case of XG(x)'s without the NH_3 treatment [8,9], a peak at 400 eV binding energy (BE) due to chemisorbed N_2 on the surface was detected [10–17]. In the spectra of the nitrified samples, another peak at 396 eV BE was observed. Since the binding energy of this peak is close to that of nitrides, 397 eV [18,19], and is much lower than the N1s BE of nitrites and nitrates, which are observed at around 404 and 408 eV [20], respectively, the peak at 396 eV is assigned to nitrogen atoms doped in the TiO_2 lattice; that is, negatively charged nitrogen species that substitute oxygen in the lattice position [10–17,21,22]. The peak at 396 eV for XG(0)-N-A(400) had a very low intensity. For Si-modified titanias, the intensity of this peak significantly increased with the increase in the Si/Ti charged ratio up to 0.2. Figure 3-5 shows the surface composition of XG(x)-N-A(400), as determined by XPS. The concentration of $N_{396\ eV}$ increased with

Table 3-2 Binding energy of core electrons for samples nitrified at 600 ºC and annealed at 400 ºC

Sample	Si/Ti [a]	O 1s (eV)	Si $2p_{1/2}$ (eV)	Ti $2p_{3/2}$ (eV)
XG(0)-N-A(400)		530.1		458.9
XG(0.02)-N-A(400)	0.056	530.2 (83) [b]	102.1	458.9
		532.0 (17)		
XG(0.06)-N-A(400)	0.127	529.9 (74)	102.1	458.7
		531.7 (26)		
XG(0.1)-N-A(400)	0.187	529.9 (69)	102.1	458.6
		531.7 (31)		
XG(0.2)-N-A(400)	0.397	530.1 (62)	102.6	459.0
		532.1 (38)		
XG(0.3)-N-A(400)	0.472	530.1 (56)	102.5	459.0
		532.1 (44)		
XG(0.4)-N-A(400)	0.734	530.2 (47)	102.9	459.0
		532.3 (53)		
XG(0.5)-N-A(400)	1.167	530.2 (37)	102.9	459.0
		532.4 (63)		

[a] Determined by XPS.

[b] The number in parentheses indicates the percentage of the band.

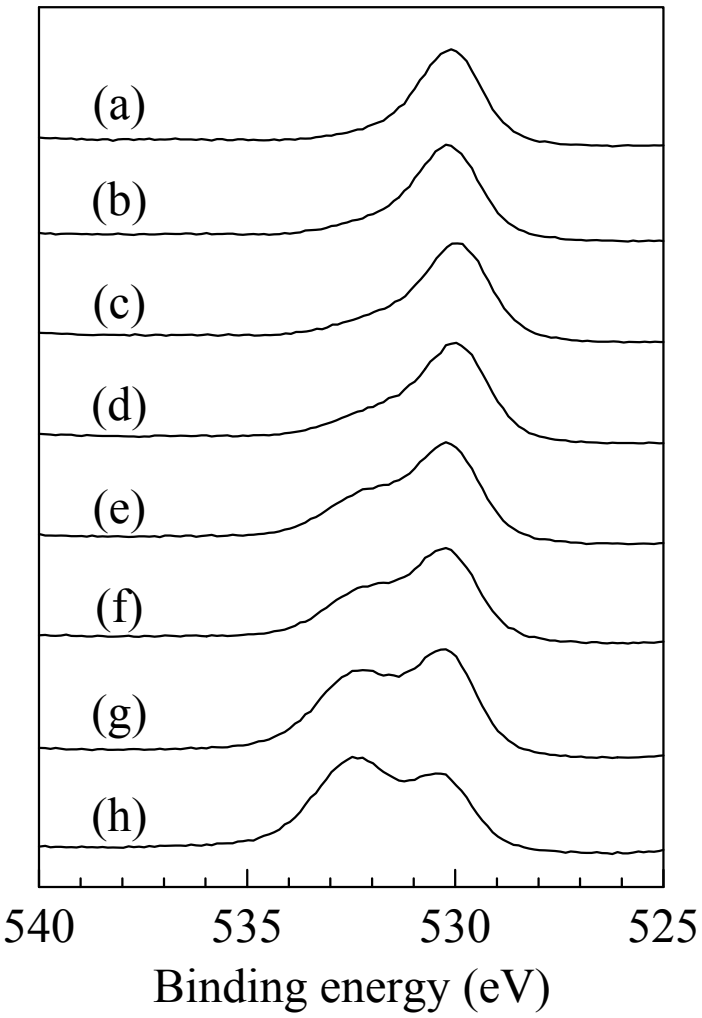

Fig. 3-3 O1s XPS spectra of: XG(x)-N-A(400) with the Si/Ti charged ratio, x, of: (a), 0; (b), 0.02; (c), 0.06; (d), 0.1; (e), 0.2; (f), 0.3; (g), 0.4, and (h), 0.5.

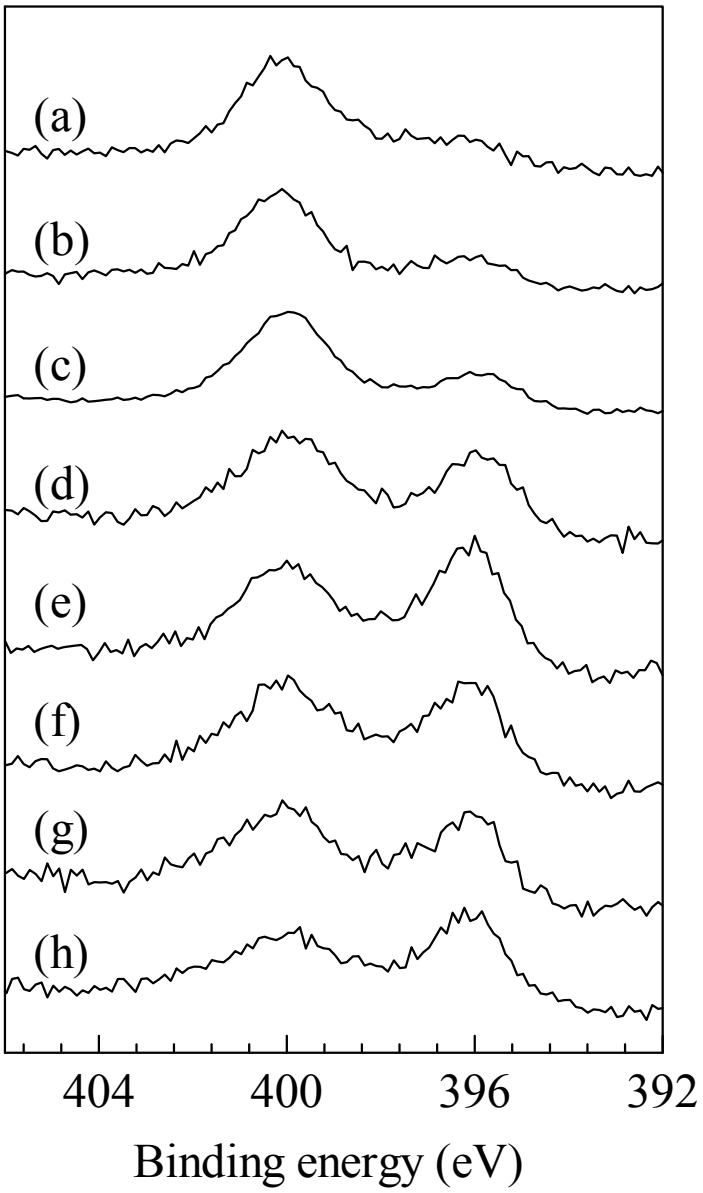

Fig. 3-4 N1s XPS spectra of: XG(x)-N-A(400) with the Si/Ti charged ratio, x, of: (a), 0; (b), 0.02; (c), 0.06; (d), 0.1; (e), 0.2; (f), 0.3; (g), 0.4, and (h), 0.5.

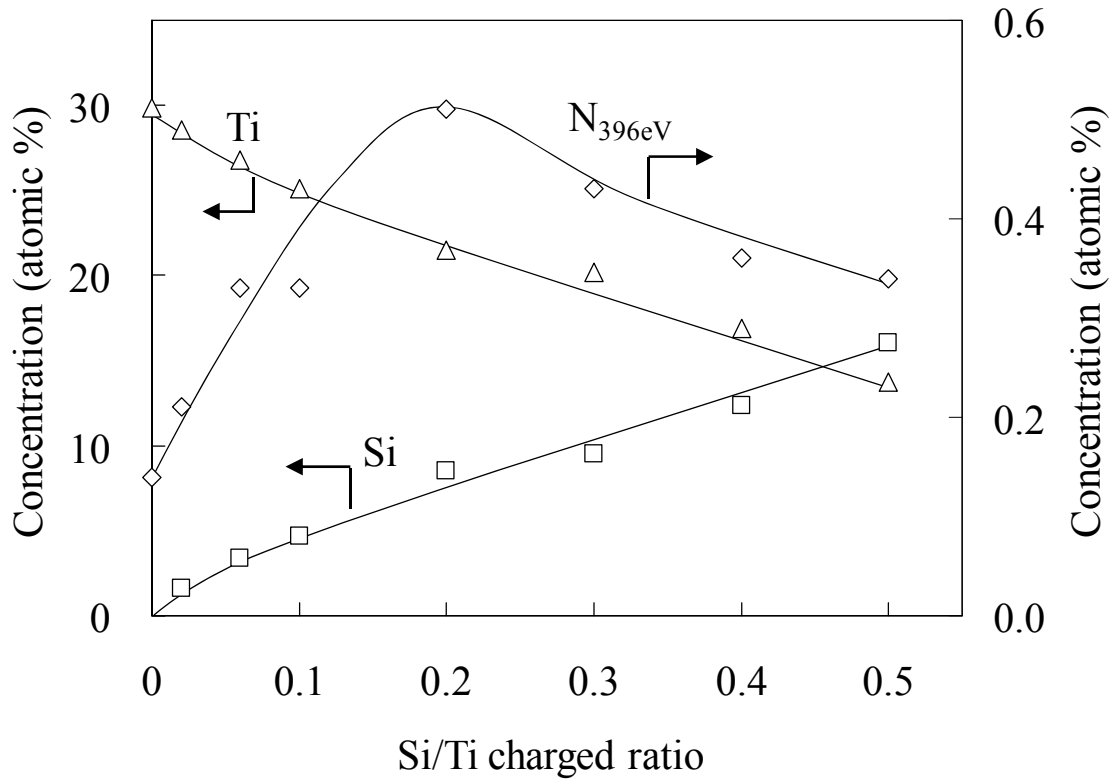

Fig. 3-5 Surface composition of XG(x)-N-A(400), as determined by XPS.

the increase in the Si/Ti charged ratio up to 0.2, but gradually decreased with higher amounts of Si modification. These results are in accordance with those obtained from the UV-vis spectra.

Figure 3-6 shows the results of photocatalytic decomposition of acetaldehyde using XG(x)-N-A(400). The evolution of CO_2 was detected for all the samples, indicating the decomposition of acetaldehyde proceeded on XG(x)-N-A(400) under visible-light irradiation. The photocatalytic activity increased with the increase in the Si/Ti ratio up to 0.4, but further increase in the Si/Ti ratio (XG(0.5)-N-A(400)) resulted in a decrease in the photocatalytic activity.

3.3.2 Effect of annealing temperature

It is well known that photocatalytic activities of TiO_2 under UV-light irradiation is drastically affected by post-calcination treatments because of the changes of physicochemical properties of the catalysts, such as crystal phase, crystallinity, surface area and adsorbability [23,24]. For nitrified TiO_2 photocatalysts, post-calcination causes re-oxidation of nitrified TiO_2 (denitrification), which can affect the photocatalytic activity under visible-light irradiation. Therefore, the effect of the annealing temperature on the photocatalytic activity was examined for the nitrified Si-modified titania catalysts. Since NH_3-TPD analysis carried out for the Si-modified titanias without nitrification showed that the NH_3-desorption started at 100 °C and finished at around 400 °C with the maximum rate of desorption at around 220 °C [2], the annealing was carried out at 400 °C and higher temperatures to exclude the effect of the NH_3 molecules remaining on the surface of the samples after the NH_3 treatment.

XG(0.2) was a white powder and it turned green after the NH_3 treatment at

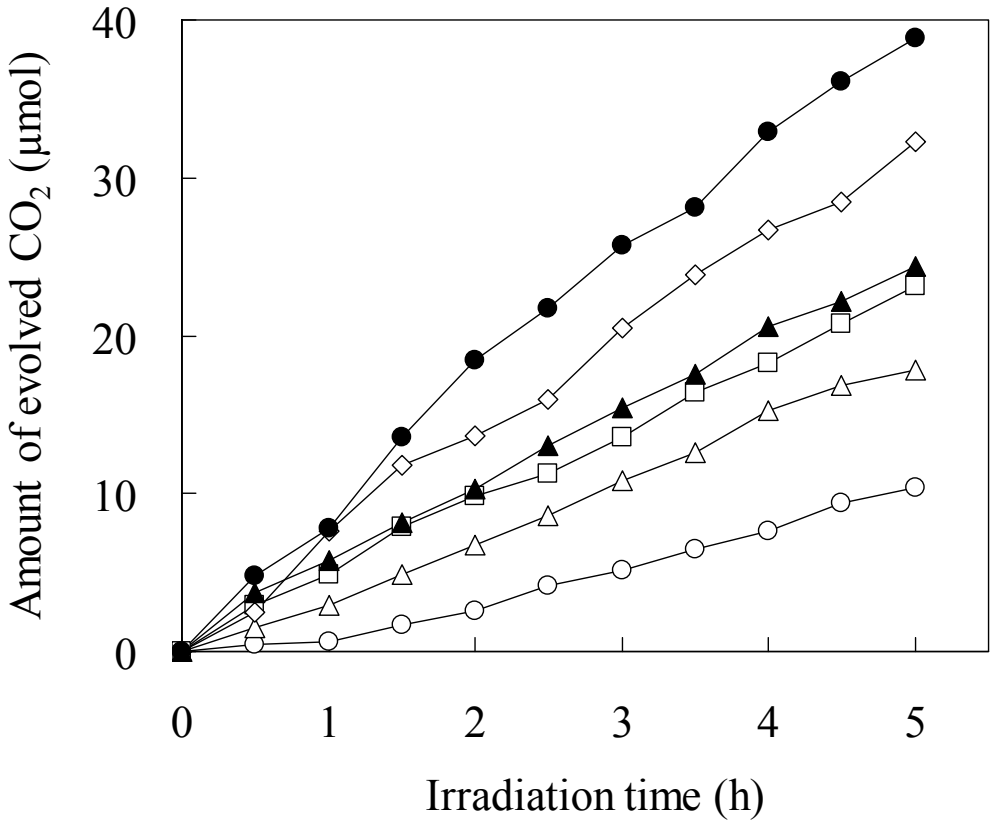

Fig. 3-6 Photocatalytic decomposition of acetaldehyde under visible-light irradiation using XG(x)-N-A(400) with the Si/Ti charged ratio, x, of: ○, 0; △, 0.1; □, 0.2; ◇, 0.3; ●, 0.4, and ▲, 0.5.

600 °C for 1 h. On exposure to air at room temperature, the sample turned yellowish green, which suggests that the nitrified samples were re-oxidized in air even at room temperature. After calcination in air at 400 °C for 1 h, it turned yellow, and further decolorization was observed after annealing at higher temperatures. In Figure 3-7, the UV-vis spectra of NH_3-treated XG(0.2)'s with annealing in air at various temperatures (400–700 °C) are shown. The intensity of the absorption band at 400–500 nm decreased with the increase in the annealing temperature, suggesting that the nitrogen contents in the samples decreased by the annealing. The amount of doped-nitrogen atoms after the annealing treatment was measured by XPS. Figure 3-8 shows the N1s XPS spectra of NH_3-treated XG(0.2)'s with annealing in air at various temperatures (400–650 °C). The intensity of the peak at 396 eV BE, assigned to nitrogen atoms doped in the TiO_2 lattice, decreased with the increase in the annealing temperature.

The photocatalytic activities of NH_3-treated XG(0.2)'s annealed at various temperatures were evaluated and the results are shown in Figure 3-9. Surprisingly, the photocatalytic activity markedly increased by increasing the annealing temperature from 400 °C to 500 °C in spite of the fact that the nitrogen content in the sample decreased. Further increase in the annealing temperature to 650 ºC decreased the photocatalytic activity significantly. This is due to the drastic decrease in the nitrogen contents in the sample as indicated by the UV-vis and XPS analysis (Figures 3-7 and 3-8). After annealing at 700 °C or higher, the sample showed no absorption in visible-light region, nor was photocatalytic activity attained under the visible-light irradiation condition, indicating the sample was re-oxidized completely. These results clearly show that the annealing temperature is also a critical factor for the material to exhibit a high photocatalytic activity under visible-light irradiation.

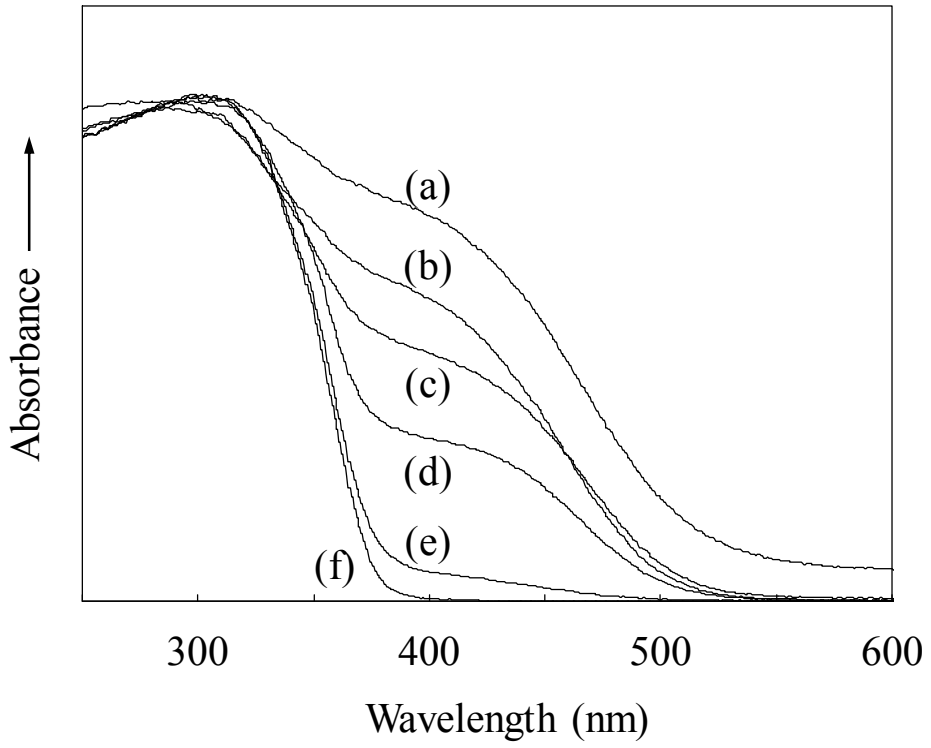

Fig. 3-7 UV-vis spectra of: (a) XG(0.2) treated in an NH_3 flow at 600 °C for 1 h without the annealing treatment; (b), XG(0.2)-N-A(400); (c), XG(0.2)-N-A(500); (d), XG(0.2)-N-A(600); (e), XG(0.2)-N-A(650), and (f), XG(0.2)-N-A(700).

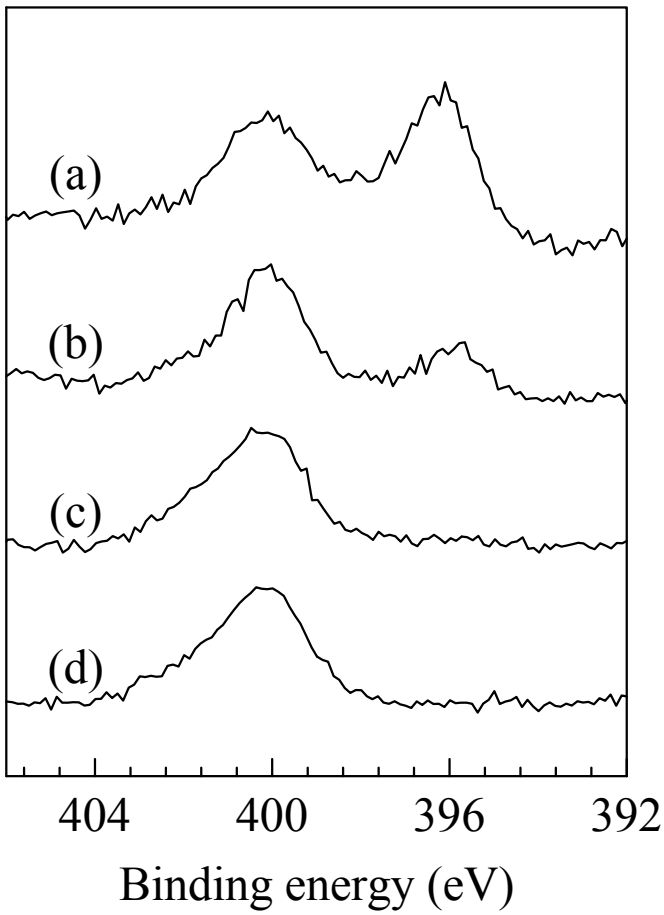

Fig. 3-8 N1s XPS spectra of: (a), XG(0.2)-N-A(400); (b), XG(0.2)-N-A(500); (c), XG(0.2)-N-A(600), and (d), XG(0.2)-N-A(650).

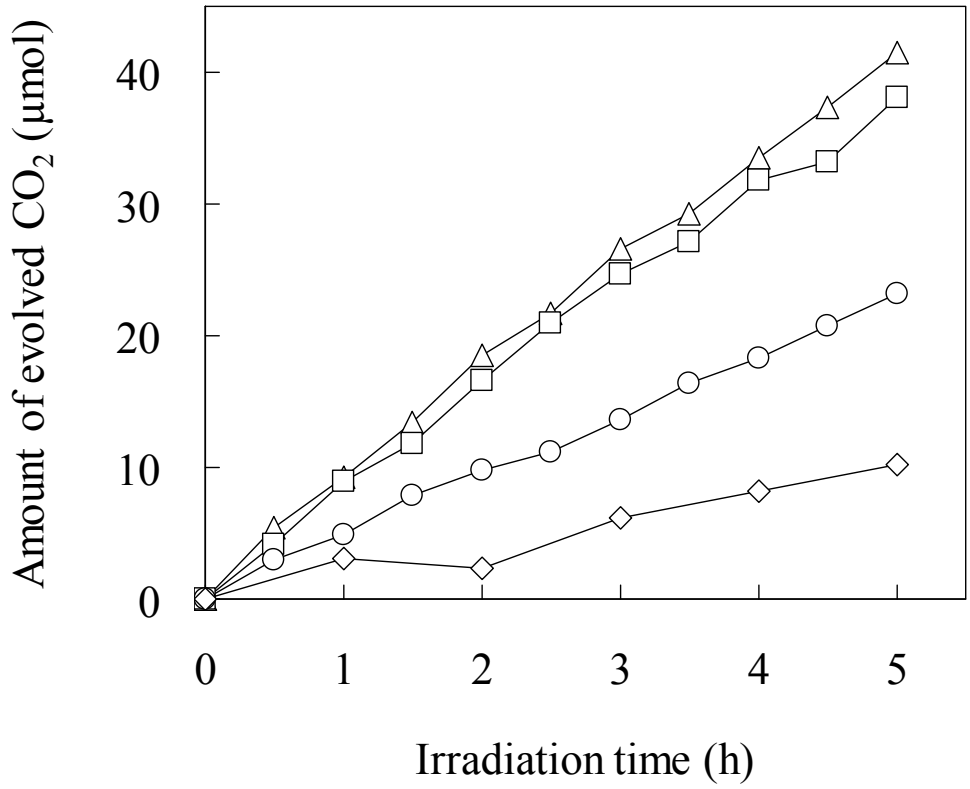

Fig. 3-9 Photocatalytic decomposition of acetaldehyde under visible-light irradiation on: ○, XG(0.2)-N-A(400); △, XG(0.2)-N-A(500); □, XG(0.2)-N-A(600), and ◇, XG(0.2)-N-A(650).

To elucidate the reason why annealing at 500 °C gave a higher photocatalytic activity, ESR spectra of NH_3-treated XG(0.2) annealed at various temperatures were measured in vacuum at 123 K. The spectra taken under a dark condition and under visible-light irradiation are shown in Figures 3-10(I) and 3-10(II), respectively. In the spectrum of XG(0.2)-N-A(400) taken under the dark condition, ESR signals at g = 2.023, 2.006, 2.002 and 1.984 were recognized. The triplet signal at g = 2.023, 2.006 and 1.984 (signal-A) is assigned to paramagnetic N species in N-doped titania [25–31], and the signal at g = 2.002 (signal-B) is due to electrons trapped at anion vacancies [32]. It is likely that the anion (oxygen) vacancy is generated by the substitution of O^{2-} with N^{3-} or simple desorption of the oxygen in the lattice since the thermal treatment in NH_3 gives a severely reductive condition. When the annealing treatment was carried out at 500 °C, the intensity of signal-B decreased drastically, indicating that the oxygen vacancies diminished relatively easily at 500 °C. This result clearly explains the reason for the enhanced photocatalytic activity of the catalyst annealed at 500 °C. The decrease in the population of oxygen vacancies increased the photocatalytic activity because they serve as recombination centers for holes and electrons [33].

Literature survey showed some papers reported that annealing enhanced the performance of N-doped TiO_2. Thus, Ghicov et al. prepared nitrogen-doped TiO_2 nanotubes by ion implantation and reported that the ion implantation process led to amorphization of the TiO_2 structure, while annealing at 450 °C recovered the anatase phase, leading to the enhancement of the photocurrent of the N-doped titania nanotubes [14]. Tesfamichael et al. also prepared N-doped TiO_2 films by ion implantation and reported that annealing in air removed the defects created by the ion implantation thereby increasing the transmittance of the films [34]. In the present work, however, the

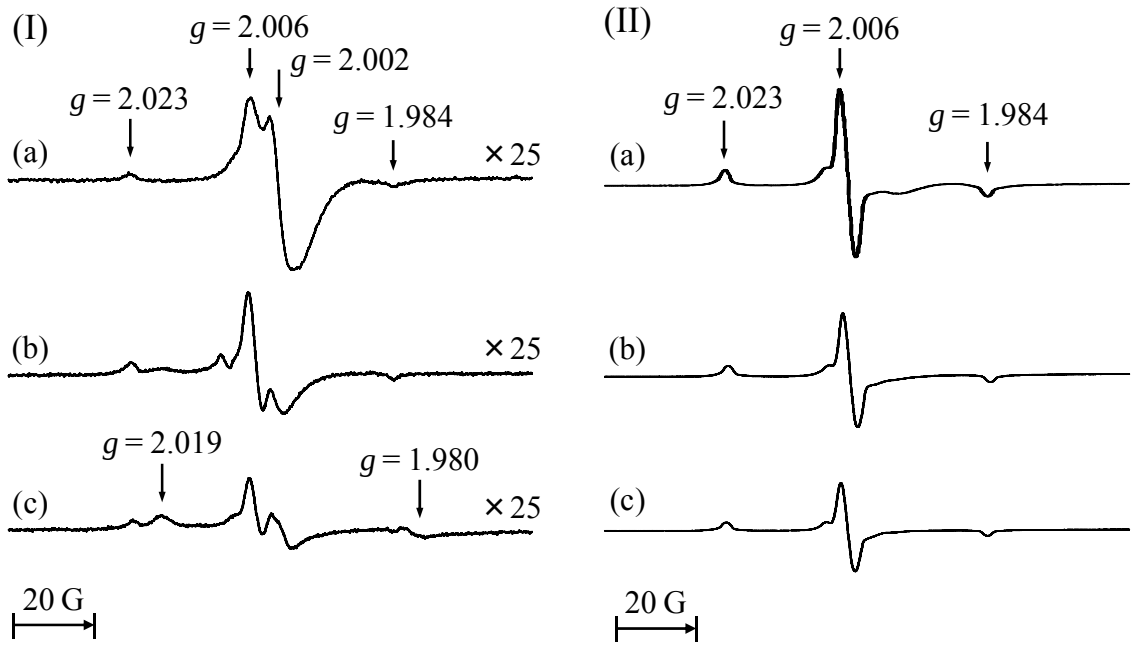

Fig. 3-10 ESR spectra measured in vacuum at 123 K under: (I), a dark condition; (II), visible-light irradiation; for: (a), XG(0.2)-N-A(400); (b), XG(0.2)-N-A(500), and (c), XG(0.2)-N-A(600).

increase in the annealing temperature from 400 °C to 700 °C did not increase the crystallinity (crystallite size) of the catalyst (Figure 3-11). We demonstrate, for the first time, that the annealing at relatively high temperature drastically decreased the population of the oxygen vacancies formed by the NH_3 treatment, and thus enhanced the photocatalytic activity of N-doped TiO_2. However, the population of the oxygen vacancies was too low to be detected by the XRD method.

On visible-light irradiation (Figure 3-10(II)), the intensity of the triplet signal at g = 2.023, 2.006, 1.984 (signal-A) significantly increased, suggesting that the N species which gave the signal-A by visible-light irradiation are closely concerned with the visible-light-induced photocatalytic activity. With the increase in the annealing temperature, the intensity of the triplet signal (signal-A) gradually decreased, indicating that the annealing decreased the amount of the visible-light responsive N species in the sample.

Similar ESR results were previously reported [25–31], and several groups assigned the N species giving signal-A to a NO_2^{2-} species formed from an interstitial NO species trapped in the lattice with a weak interaction with a lattice oxygen atom [25–27,30,31]. However, Valentin et al. denied that the assignment of the paramagnetic N species to NO_2^{2-} since this species was computed to be unstable in bulk TiO_2 [29]. They also characterized the N paramagnetic species by comparing the observed ESR hyperfine coupling constants with computed values for structural models of substitutional and interstitial nitrogen impurities. Since both of the calculated hyperfine coupling constants were close to the experimental values, they concluded that both of the proposed models, substitutionally and interstitially doped nitrogen atoms, can account for the paramagnetic species observed in the N-doped titania [29]. In the

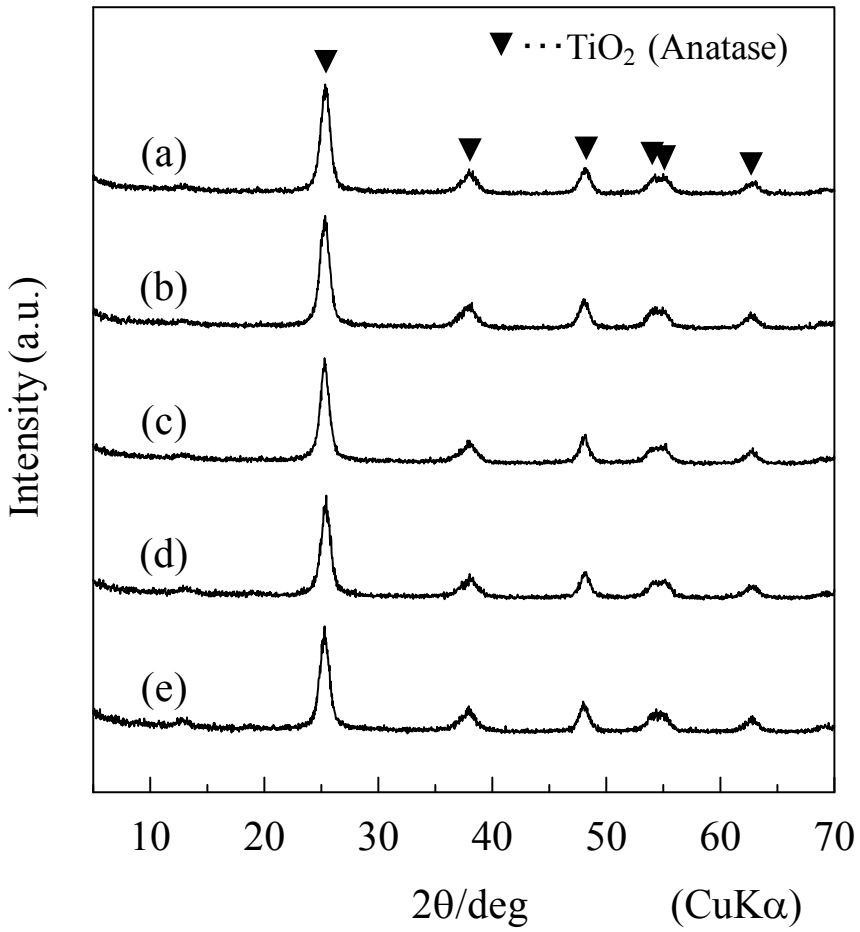

Fig. 3-11 XRD patterns of: (a), XG(0.2); (b), XG(0.2)-N-A(400); (c), XG(0.2)-N-A(500); (d), XG(0.2)-N-A(600), and (e), XG(0.2)-N-A(700). The crystallite sizes are: (a), $9.^{9}$ nm; (b), $10.^{2}$ nm; (c), $10.^{0}$ nm; (d), $9.^{9}$ nm, and (e), $9.^{8}$ nm.

present study, the XPS results shown above suggested that nitrogen doped in the titania is negatively charged. Therefore, the signal-A was assigned to the substitutionally doped nitrogen although further study is needed to discuss the chemical state of doped nitrogen more detail.

After the annealing at 600 °C, new ESR signals appeared at g = 2.019, 2.002 and 1.980 (signal-C) in the spectrum measured under the dark condition. This triplet signal is assigned to the paramagnetic N species in nitrogen oxides adsorbed on the surface [25–31], which are probably generated by oxidation of doped nitrogen. The intensity of signal-C was not changed by the visible-light irradiation (Figure 3-12), suggesting that the N species giving signal-C are not involved in the visible-light-induced photocatalytic reaction.

3.3.3 Optimization of preparation conditions for N- and Si-co-doped titania photocatalysts

In order to attain the highest photocatalytic activity, N- and Si-co-doped titania catalysts with various Si/Ti ratio (0.1–0.5), annealed at 400, 500, and 600 °C were prepared. Figure 3-13 shows the photocatalytic activities of these nitrified XG(x) catalysts. With the increase in the Si/Ti charged ratio up to 0.2–0.4, the photocatalytic activity increased significantly. However, the catalyst with Si/Ti of 0.5 showed apparently lower activities.

The increase in the annealing temperature up to 500 °C increased the photocatalytic activity regardless of the Si/Ti ratio. Further increase in the annealing temperature up to 600 °C resulted in a decrease in the photocatalytic activity except for XG(0.5). Among the catalysts examined in this study, the highest photocatalytic activity

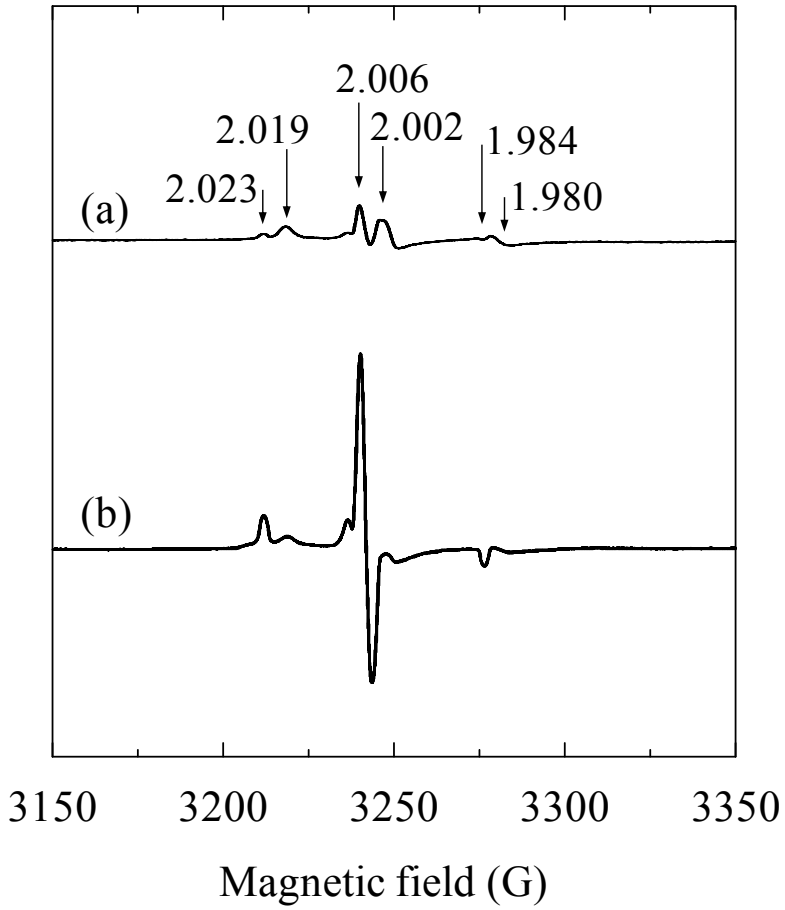

Fig. 3-12 ESR spectra of XG(0.2)-N-A(650) measured in air at 123 K under: (a), a dark condition and (b), visible-light irradiation.

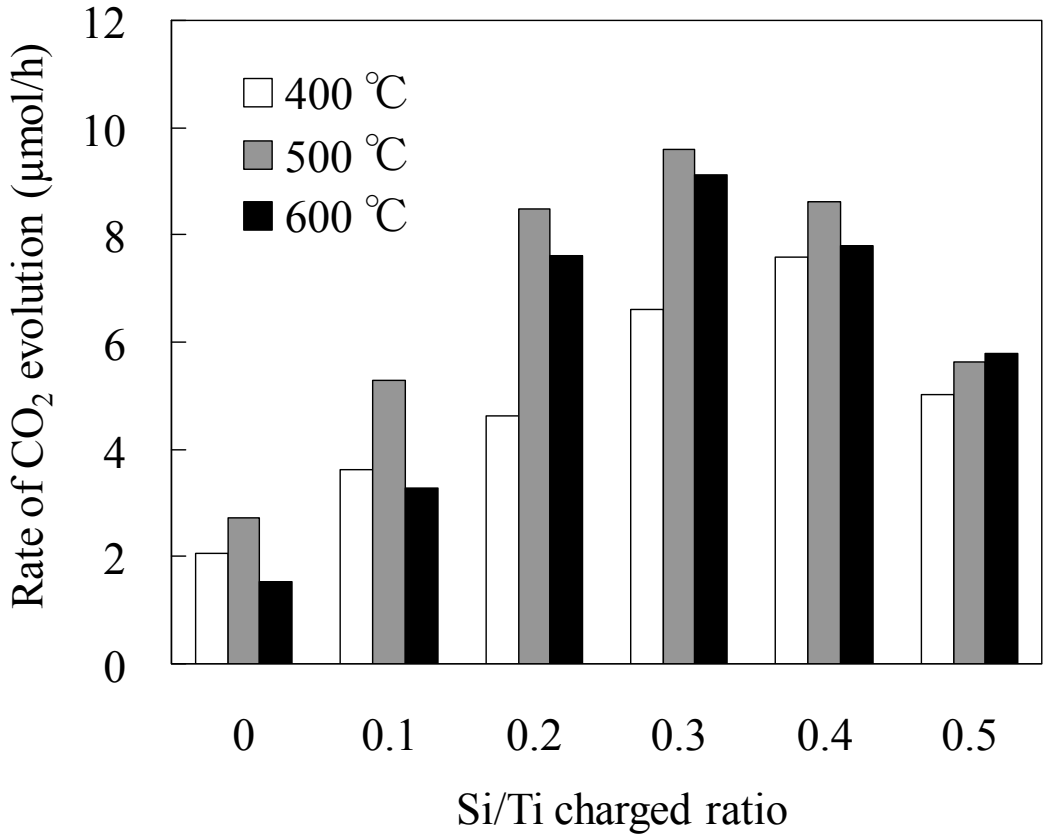

Fig. 3-13 Photocatalytic activity of XG(x)'s treated in an NH_3 flow at 600 ºC for 1 h and annealed at various temperatures for 30 min.

was attained by the Si-modified titania with Si/Ti ratio of 0.3 annealed at 500 °C.

In order to confirm the advantages of XG(x) samples, we examined the photocatalytic activities of the nitrified catalysts prepared from the Si-impregnated titanias. The results are shown in Figure 3-14. With the Si-loading (Si/Ti = 0.3) by the impregnation method, the photocatalytic activities for both XG(0) and P-25 increased slightly. However, they were much lower than that of XG(0.3)-N-A(500), and hence the superiority of the catalysts made from the glycothermally-prepared Si-modified titanias is apparent. The Si-modified samples, P-25(0.3-imp)-N-A(500) and XG(0.3-imp)-N-A(500) showed a slightly stronger absorption in the visible region (400–550 nm) than the corresponding unmodified samples, P-25-N-A(500) and XG(0)-N-A(500) (Figure 3-15), suggesting that the addition of Si by the impregnation method contributes to a slight increase in the amount of doped nitrogen. However, compared with XG(0.3)-N-A(500), these absorptions are apparently weaker. These differences are due to the higher dispersion of the silicon atoms in the glycothermal products as compared with those prepared by the impregnation method [35]. For the former products, Si atoms in the anatase lattice allow N atoms to accommodate in the lattice and suppress the generation of Ti^{3+} significantly. These unique features contribute to their higher photocatalytic activities under visible-light irradiation.

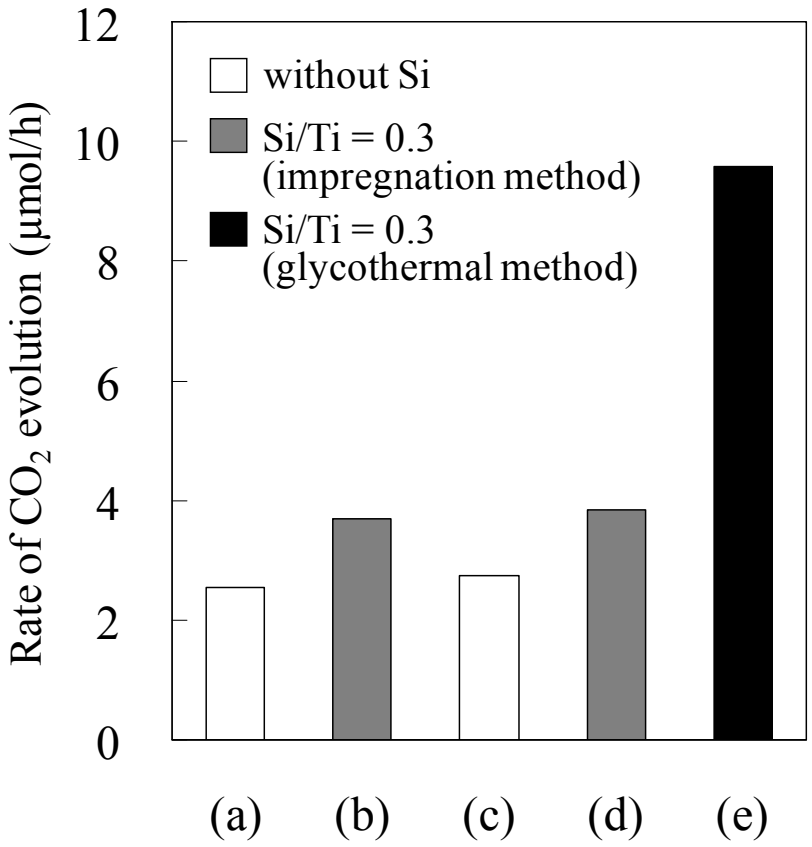

Fig. 3-14 Photocatalytic activity of: (a), P-25-N-A(500); (b), P-25(0.3-imp)-N-A(500); (c), XG(0)-N-A(500); (d), XG(0.3-imp)-N-A(500), and (e), XG(0.3)-N-A(500).

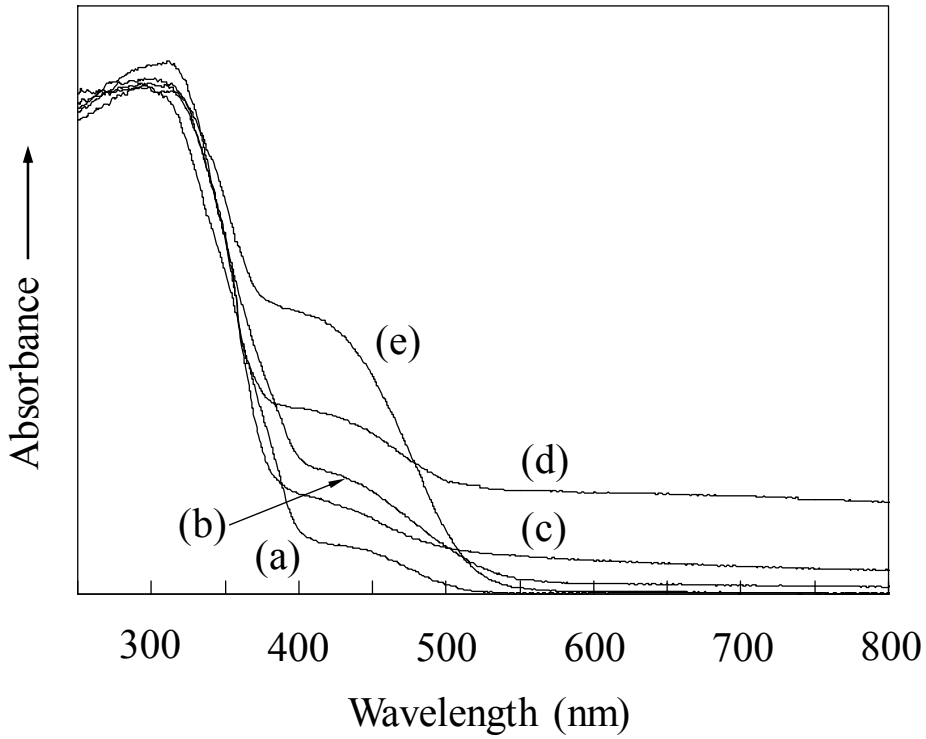

Fig. 3-15 UV-vis spectra of: (a), P-25-N-A(500); (b), P-25(0.3-imp)-N-A(500); (c), XG(0)-N-A(500); (d), XG(0.3-imp)-N-A(500), and (e), XG(0.3)-N-A(500).

3.4 Conclusions

The Si-modified titanias nitrified by the NH_3 treatment and annealed in air at high temperatures showed photocatalytic activities for the decomposition of acetaldehyde under visible-light irradiation. With increasing the Si/Ti ratio, the amounts of nitrogen doped in the titania lattice gradually increased and the photocatalytic activities were enhanced. An excess Si modification resulted in a decrease in the activity, and hence high photocatalytic activities were obtained for the catalysts with the Si/Ti ratio = 0.2–0.4. The annealing treatment after the NH_3 treatment greatly affected the photocatalytic activities. The amount of nitrogen doped in the samples tended to decrease gradually by increasing the annealing temperature. However, the population of oxygen vacancies produced by the NH_3 treatment drastically decreased by the annealing procedure at 500 °C. Consequently, the optimized photocatalytic activity was attained with the catalyst of Si/Ti = 0.3 annealed at this temperature.

References

[1] S. Iwamoto, K. Saito, M. Inoue, and K. Kagawa, *Nano Lett.* **2001**, *1*, 417.

[2] S. Iwamoto, W. Tanakulrungsank, M. Inoue, K. Kagawa, and P. Praserthdam, *J. Mater. Sci. Lett.* **2000**, *19*, 1439.

[3] T. Torimoto, R. J. Fox III, and M. A. Fox, *J. Electrochem. Soc.* **1996**, *143*, 3712.

[4] Sh. Iwamoto, Se. Iwamoto, M. Inoue, S. Uemura, K. Kagawa, W. Tanakulrungsank, and P. Praserthdam, *Ceram. Trans.* **2000**, *115*, 643.

[5] C. U. I. Odenbrand, S. L. T. Andersson, L. A. H. Andersson, J. G. M. Brandin, and G. Busca, *J. Catal.* **1990**, *125*, 541.

[6] A. Y. Stakheev, E. S. Shpiro, and J. Apijok, *J. Phys. Chem.* **1993**, *97*, 5668.

[7] Handbook of X-ray Photoelectron Spectroscopy; G. E. Muilenberg, Ed. Perkin-Elmer Corporation, Minnesota, 1979; p. 45.

[8] H. Ozaki, S. Iwamoto, and M. Inoue, *Chem. Lett.* **2005**, *34*, 1082.

[9] H. Ozaki, S. Iwamoto, and M. Inoue, *J. Mater. Sci.* **2007**, *42*, 4009.

[10] R. Asahi, T. Morikawa, T. Ohwaki, K. Aoki, and Y. Taga, *Science* **2001**, *293*, 269.

[11] H. Irie, Y. Watanabe, and K. Hashimoto, *J. Phys. Chem. B* **2003**, *107*, 5483.

[12] S.-Z. Chen, P.-Y. Zhang, D.-M. Zhuang, and W.-P. Zhu, *Catal. Commun.* **2004**, *5*, 677.

[13] M.-C. Yang, T.-S. Yang, and M.-S. Wong, *Thin Solid Films* **2004**, *469–470*, 1.

[14] A. Ghicov, J. M. Macak, H. Tsuchiya, J. Kunze, V. Haeublein, L. Frey, and P. Schmuki, *Nano Lett.* **2006**, *6*, 1080.

[15] Z. Wang, W. Cai, X. Hong, X. Zhao, F. Xu, and C. Cai, *Appl. Catal., B.* **2005**, *57*, 223.

[16] J. Yuan, M. Chen, J. Shi, and W. Shangguan, *Internat. J. Hydrogen Energy* **2006**, *31*, 1326.

[17] N. C. Saha and H. G. Tompkins, *J. Appl. Phys*. **1992**, *72*, 3072.

[18] H. Höchst, R. D. Bringans, P. Steiner, and Th. Wolf, *Phys. Rev. B* **1982**, *25*, 7183.

[19] M. J. Vasile, A. B. Emerson, and F. A. Baiocchi, *J. Vac. Sci. Technol. A* **1990**, *8*, 99.

[20] Handbook of X-ray Photoelectron Spectroscopy; G. E. Muilenberg, Ed. Perkin-Elmer Corporation, Minnesota, 1979; p. 43.

[21] K. Kobayakawa, Y. Murakami, and Y. Sato, *J. Photochem. Photobiol., A* **2005**, *170*, 177.

[22] Y. Suda, H. Kawasaki, T. Ueda, and T. Ohshima, *Thin Solid Films* **2004**, *453-454*, 162.

[23] H. Kominami, S. Murakami, J. Kato, Y. Kera, and B. Ohtani, *J. Phys. Chem. B* **2002**, *106*, 10501.

[24] K. Hashimoto, K. Wasada, N. Toukai, H. Kominami, and Y. Kera, *J. Photochem. Photobiol., A* **2000**, *136*, 103.

[25] M. Che and C. Naccache, *Chem. Phys. Lett.* **1971**, *8*, 45.

[26] R. D. Iyengar and R. Kellerman, *J. Colloid Interface Sci.* **1971**, *35*, 424.

[27] S. Livraghi, A. Votta, M. C. Paganini, and E. Giamello, *Chem. Commun.* **2005**, 498.

[28] S. Livraghi, M. C. Paganini, E. Giamello, A. Selloni, C. D. Valentin, and G. Pacchioni, *J. Am. Chem. Soc.* **2006**, *128*, 15666.

[29] C. D. Valentin, G. Pacchioni, A. Selloni, S. Livraghi, and E. Giamello, *J. Phys. Chem. B* **2005**, *119*, 11414.

[30] Y. Sakatani, J. Nunoshige, H. Ando, K. Okusako, H. Koike, T. Takata, J. N. Kondo, M. Hara, and K. Domen, *Chem. Lett.* **2003**, *32*, 1156.

[31] Y. Yamamoto, S. Moribe, T. Ikoma, K. Akiyama, Q. Zhang, F. Saito, and S. Tero-Kubota, *Mol. Phys.* **2006**, *104*, 1733.

[32] M. Okumura, J. M. Coronado, J. Soria, M. Haruta, and J. C. Conesa, *J. Catal.* **2001**, *203*, 168.

[33] S. Ikeda, N. Sugiyama, S. Murakami, H. Kominami, Y. Kera, H. Noguchi, K. Uosaki, T. Torimoto, and B. Ohtani, *Phys. Chem. Chem. Phys*. **2003**, *5*, 778.

[34] T. Tesfamichael, G. Will, and J. Bell, *Appl. Surf. Sci.* **2005**, *245*, 172.

[35] Sh. Iwamoto, Se. Iwamoto, M. Inoue, H. Yoshida, T. Tanaka, and K. Kagawa, *Chem. Mater*. **2005**, *17*, 650.

Chapter 4

Nitrification of P-modified titanias prepared by the glycothermal method and their visible-light responsive photocatalytic activities

4.1 Introduction

In chapter 2 and 3, it was described that the titanias co-doped with N and Si showed a strong absorption in the visible region (400–550 nm) and exhibited high photocatalytic activities for degradation of RhB and decomposition of acetaldehyde under visible-light irradiation.

Co-doping of nitrogen and other elements into TiO_2 has been also examined to improve photocatalytic activity under visible light irradiation by several groups. [1–4]. Sakatani et al. prepared metal ion-and-nitrogen co-doped titanias by a polymerized complex method and found that the photocatalyst prepared with Sr^{2+} exhibited high activity for decomposition of acetaldehyde under visible-light irradiation [2]. They reported that Sr^{2+} is distributed uniformly in the TiO_2 lattice and that the formations of Ti^{3+} and lattice defects were suppressed by the optimum dosage of Sr^{2+} [2]. Wei et al. investigated the preparation and photocatalysis of TiO_2 powder co-doped with La^{3+} and N [4] and found that the 0.5 % La^{3+}-doped TiO_2 treated in an NH_3 flow exhibited superior catalytic activity for degradation of methyl orange under visible light irradiation. They reported that the recombination of the carriers could be prevented by

co-doping [4]. However, these co-doped titanias showed a weak absorption in the visible region (400–500 nm), indicating that only small amounts of nitrogen atoms were introduced into the TiO_2 lattice.

In the study presented in this chapter, the titanias modified with other elements (B, Mg, Al, P, Zn, Ga) were prepared by the glycothermal method and the nitrification of the products was investigated. The photocatalytic decomposition of acetaldehyde by using the obtained co-doped titanias under visible-light irradiation was also examined.

4.2 Experimental

4.2.1 Preparation of the catalysts

Titania and modified titania samples were prepared by the glycothermal method and the products were collected as a xerogel form [5]: TIP (25 g) and one of the modifiers were added to 100 mL of 1,4-butanediol (1,4-BG). As the modifiers, trimethyl borate, magnesium acetate tetrahydrate, aluminum triisopropoxide, triethyl phosphate, zinc diacetylacetonate, and gallium triacetylacetonate were used for B, Mg, Al, P, Zn, and Ga, respectively. This mixture was placed in a 300 mL autoclave equipped with two valves, one of which was used as a gas inlet and the other was connected to a Liebig condenser of stainless steel tubing. After the atmosphere inside the autoclave was replaced with nitrogen, the assembly was heated to 300 °C at a rate of 2.3 °C/min and kept at that temperature for 2 h. After the glycothermal reaction, the valve of the autoclave was slightly opened in order to remove the organic vapor from the autoclave by flash evaporation while keeping the autoclave temperature at 300 °C. After cooling, bulky solid product was directly obtained. The product was calcined in a box furnace in air at 500 °C for 30 min to remove the surface organic moieties. The thus-obtained

products are designated as M-XG(x), where M represents the element used for the modification and x is the M/Ti charged ratio. The product without any modifiers is designated as XG(0).

The nitrification was carried out as follows: A portion of XG(0) or M-XG(x)'s was placed in a quartz tube and the atmosphere inside was purged with an Ar flow (100 mL/min). The sample was heated to 600 °C at a rate of about 10 °C/min in the same flow of argon, and then the gas flow was replaced by an NH_3 flow (100 mL/min). The sample was kept at 600 °C for 1 h and then cooled. After the NH_3 treatment, the sample was annealed at 500 °C in air for 30 min using a box furnace. The thus-obtained nitrified and annealed products are designated as N-XG(0) or N-M-XG(x). As a reference TiO_2, JRC-TIO-4 (equivalent to Degussa P-25; rutile/anatase=3/7; BET surface area=49 m^2/g) was used. The JRC-TIO-4 nitrified in the same way is designated as N-JRC-TIO-4.

4.2.2 Characterization

The UV-vis absorption spectra of the samples were recorded on a Shimadzu MPS-2000 spectrophotometer. Powder X-ray diffraction (XRD) patterns were recorded on a Shimadzu XD-D1 diffractometer using CuKα radiation and a carbon-monochromator. The specific surface areas of the samples were calculated by the BET single-point method on the basis of the nitrogen uptake measured at 77 K using a Micromeritics Flowsorb II 2300. X-ray photoelectron spectroscopy (XPS) measurement was performed on an ULVAC-PHI Model 5500 spectrometer with 15 kV - 400 W MgKα emission as the X-ray source.

4.2.3 Photocatalytic reaction

Decomposition of acetaldehyde was carried out to evaluate the photocatalytic activities of the samples. The catalyst (0.2 g) dispersed on a 90 mmϕ glass filter was placed in a closed glass vessel (1.0 L) and 0.2 mmol acetaldehyde was injected in the vessel. The vessel was placed in the dark for 1 h, and then visible light was irradiated using a 300 W xenon lamp (Optical Modulex SX-UI300XQ, Ushio Inc.) through a UV cut-off filter (L-42, Asahi Technoglass Co. Ltd.) and an infrared cut-off filter (Super Cold Filter, Ushio Inc.). After a certain period of irradiation time, the concentration of generated CO_2 was measured by a gas chromatograph, Shimadzu GC-8A.

4.3 Results and discussion

4.3.1 Physical properties and photocatalytic activities of N-M-XG(0.1)

In Fig. 4-1, XRD patterns of M-XG(0.1) as well as TiO_2 without modification, XG(0), are depicted, which show that the products with the anatase structure formed. After nitrification, the XRD patterns of the samples did not change significantly, and no other crystalline phases were observed for N-XG(0), N-B-XG(0.1), N-Ga-XG(0.1), N-Al-XG(0.1), and N-P-XG(0.1). However, small peaks due to $MgTiO_3$ and $Zn_2Ti_3O_8$ were detected for N-Zn-XG(0.1) and N-Mg-XG(0.1). The physical properties of the nitrified samples are summarized in Table 4-1. All the nitrified samples had large surface areas; especially, N-Al-XG(0.1) and N-P-XG(0.1) had quite large surface areas, 106 and 102 m^2/g, and small crystallite sizes, 10 and 14 nm, respectively. The surface areas of N-Zn-XG(0.1) and N-Ga-XG(0.1) were smaller than those expected from the crystallite sizes, which may be due to the presence of an amorphous phase on the surface of the nanocrystals of anatase.

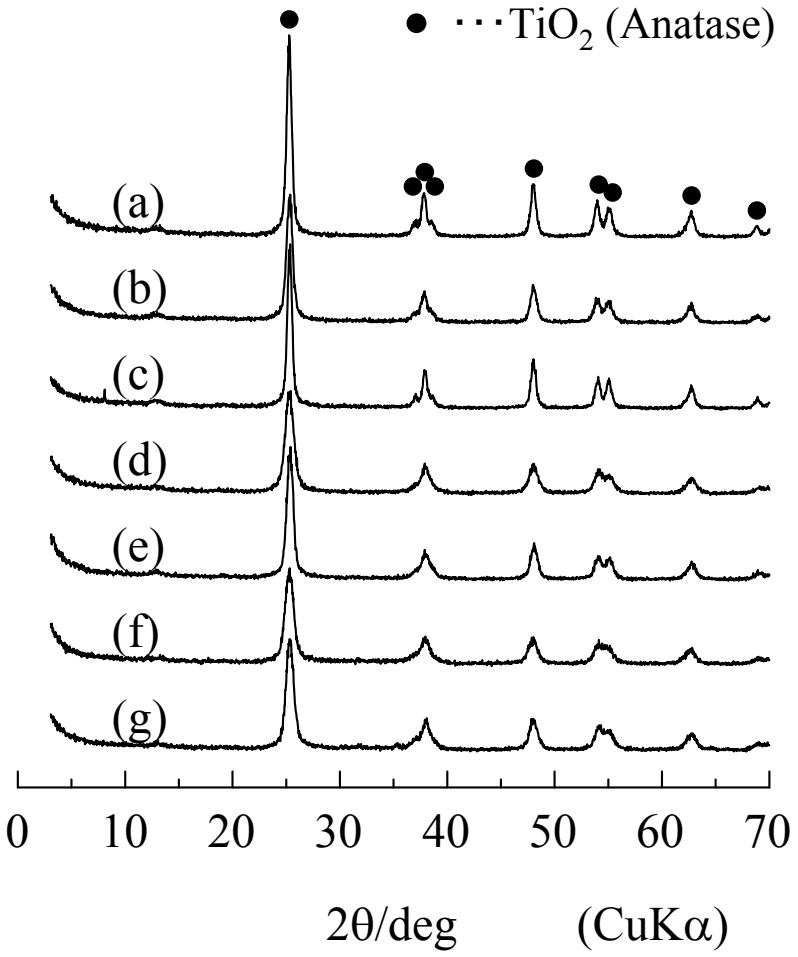

Fig. 4-1 XRD patterns of: (a) XG(0), (b) B-XG(0.1), (c) Mg-XG(0.1), (d) Al-XG(0.1), (e) P-XG(0.1), (f) Zn-XG(0.1), and (g) Ga-XG(0.1).

Table 4-1 Physical properties of N-M-XG(x).

Sample	BET surface area (m^2/g)	Crystallite size (nm)	Color
N-XG(0)	70	20	Gray
N-B-XG(0.1)	94	16	Greenish gray
N-Mg-XG(0.1)	66	22	Gray
N-Al-XG(0.1)	106	10	Pale yellow
N-P-XG(0.1)	102	14	Yellow
N-Zn-XG(0.1)	58	12	Yellow
N-Ga-XG(0.1)	75	13	Pale yellow
N-JRC-TIO-4	49	–	Pale yellow

N-M-XG(0.1) had various colors depending on the modifier: N-XG(0) and N-Mg-XG(0.1) were gray; N-B-XG(0.1), greenish-gray; N-Al-XG(0.1) and N-Ga-XG(0.1), pale yellow; N-P-XG(0.1) and N-Zn-XG(0.1), yellow. Figure 4-2 shows the UV-vis absorption spectra of N-M-XG(0.1). Whereas XG(0) (Fig. 4-2a) exhibited an absorption only in the UV region (<400 nm), the nitrified samples showed absorption bands at the visible light region (>400 nm). The spectra of N-XG(0), N-Mg-XG(0.1), and N-B-XG(0.1), shown in Fig 4-2b, 4-2e, and 4-2g, respectively, have a broad absorption at higher wavelength (>500 nm), indicating the presence of Ti^{3+} [6]. On the other hand, N-Al-XG(0.1), N-Ga-XG(0.1), N-Zn-XG(0.1), and N-P-XG(0.1) did not exhibit the absorption at higher wavelength but showed a shoulder absorption at wavelengths lower than 550 nm. This shoulder absorption band is attributed to the electronic transition from the N 2p level, formed by incorporation of nitrogen atoms into the TiO_2 lattice, to the conduction band [7]. Of all the samples examined, N-P-XG(0.1) showed the strongest absorption at 400–550 nm, which clearly indicates that larger amount of nitrogen was doped in N-P-XG(0.1).

Figure 4-3 shows the result of photocatalytic decomposition of acetaldehyde. Under visible light irradiation, evolution of CO_2 was not detected for XG(0) and JRC-TIO-4. On the other hand, for the nitrified samples, the amount of CO_2 proportionally increased with the irradiation time, indicating that photocatalytic decomposition of acetaldehyde proceeded under visible light irradiation. N-P-XG(0.1) exhibited high photocatalytic activity, which was about 2 times higher than those of N-XG(0) and N-JRC-TIO-4 and was as high as that of nitrified Si-modified titania with Si/Ti = 0.1, which was reported in our previous paper [8,9]. The high photocatalytic activity of N-P-XG(0.1) as well as N-Si-XG(0.1) is mainly because of the strong

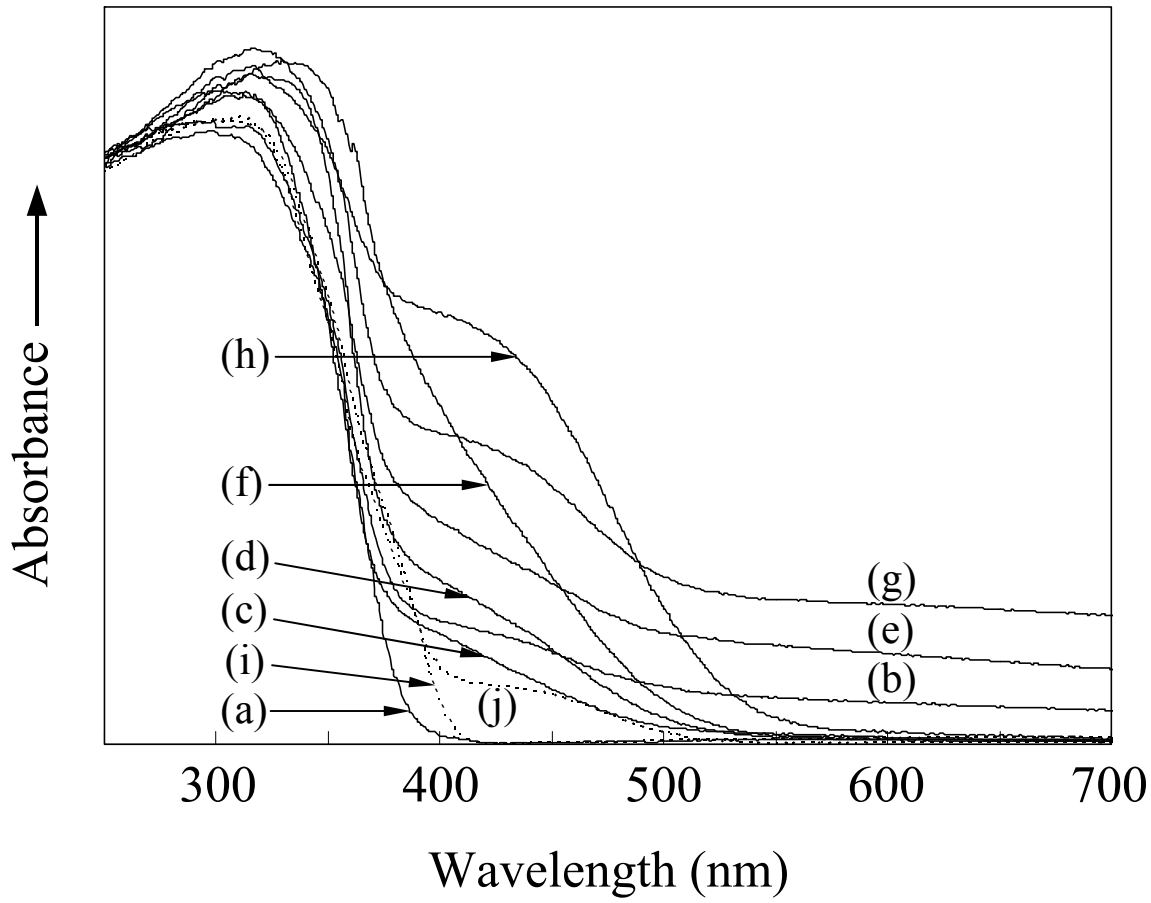

Fig. 4-2 UV-vis spectra of: (a) XG(0), (b) N-XG(0), (c) N-Al-XG(0.1), (d) N-Ga-XG(0.1), (e) N-Mg-XG(0.1), (f) N-Zn-XG(0.1), (g) N-B-XG(0.1), (h) N-P-XG(0.1), (i) JRC-TIO-4 and (j) N-JRC-TIO-4.

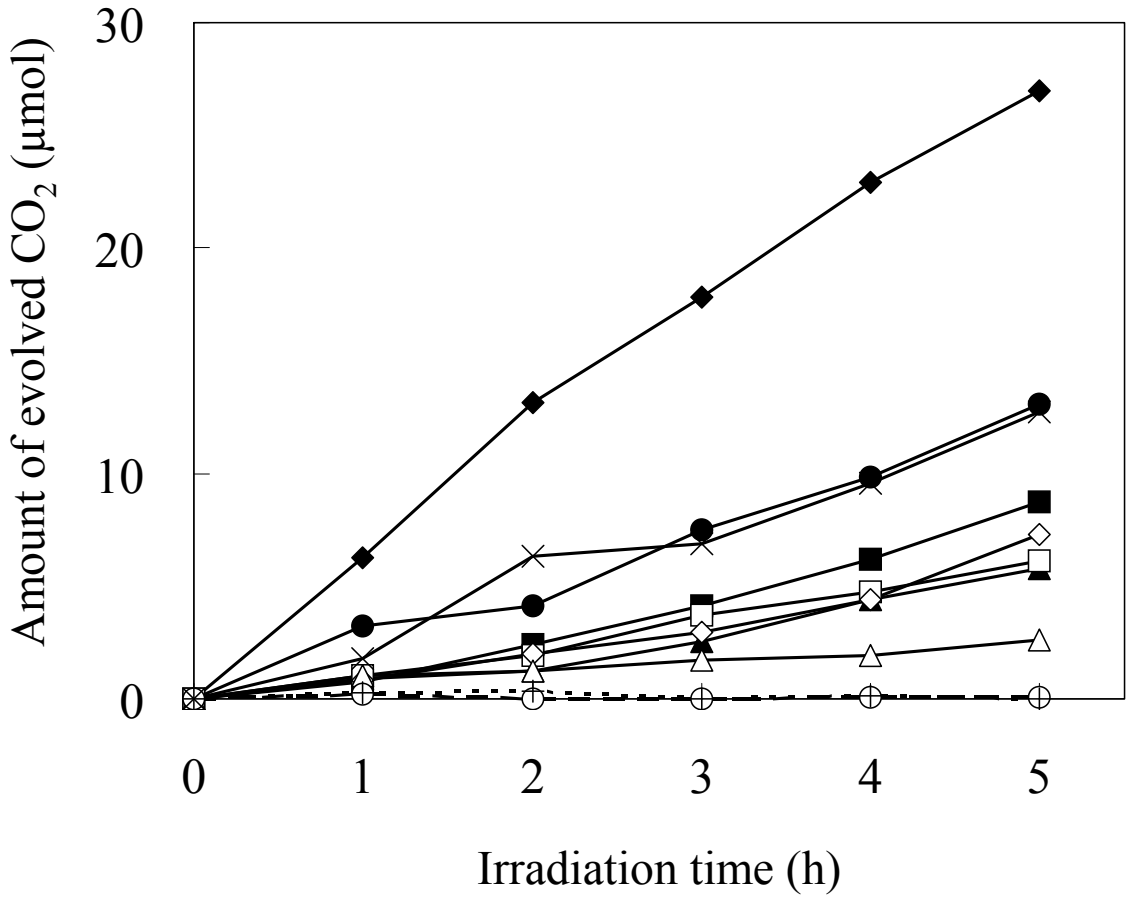

Fig. 4-3 Photocatalytic decomposition of acetaldehyde under visible light irradiation: (○) XG(0), (●) N-XG(0), (△) N-Ga-XG(0.1), (□) N-Al-XG(0.1), (◇) N-Zn-XG(0.1), (▲) N-Mg-XG(0.1), (■) N-B-XG(0.1), (◆) N-P-XG(0.1), (+) JRC-TIO-4, and (×) N-JRC-TIO-4.

absorption in the visible region (400–550 nm) [8,9]. On the other hand, the activities of the other N-M-XG(0.1) (M = B, Mg, Al, Zn, Ga) were lower than that of N-XG(0). The low activities of N-B-XG(0.1) and N-Mg-XG(0.1) can be explained by formation of Ti^{3+}, which accelerates the recombination of holes and electrons [10]. The absorption of N-Al-XG(0.1) in the visible light region was much weaker than those of the others, and therefore this catalyst showed a low activity. In the case of Zn and Ga modification, the presence of by-products in the catalysts, as suggested by the XRD patterns, and their lower surface areas would be the reason for the lower activities. Since N-P-XG(0.1) exhibited the highest photocatalytic activity among N-M-XG(0.1), P-modified titanias were examined further.

4.3.2 Physical properties of N-P-XG(x)

Figure 4-4 shows the XRD patterns of P-modified titanias with various P/Ti ratios. Although the anatase structure was observed in P-XG(x)'s with $x \leq 0.8$, the peak intensity decreased with increasing the P/Ti ratio. In the XRD patterns of P-XG(0.2), P-XG(0.4), and P-XG(0.6), diffraction peaks assigned to $Ti(OH)PO_4$ were observed in addition to the peaks due to anatase. With further increase in the P/Ti ratio, the content of amorphous phases increased and P-XG(1.0) was completely amorphous.

The properties of the samples are summarized in Table 4-2. P-XG(x)'s with $x \leq 0.4$ had smaller crystallite sizes and larger surface areas than XG(0). When P/Ti is larger than 0.6, the surface area decreased gradually.

After the NH_3 treatment and the annealing, diffraction peaks due to anatase did not change significantly; however the peaks due to $Ti(OH)PO_4$ at 26.9 ° and 28.2 °, observed in P-XG(x)'s with x = 0.2, 0.4, 0.6 disappeared and new peaks were

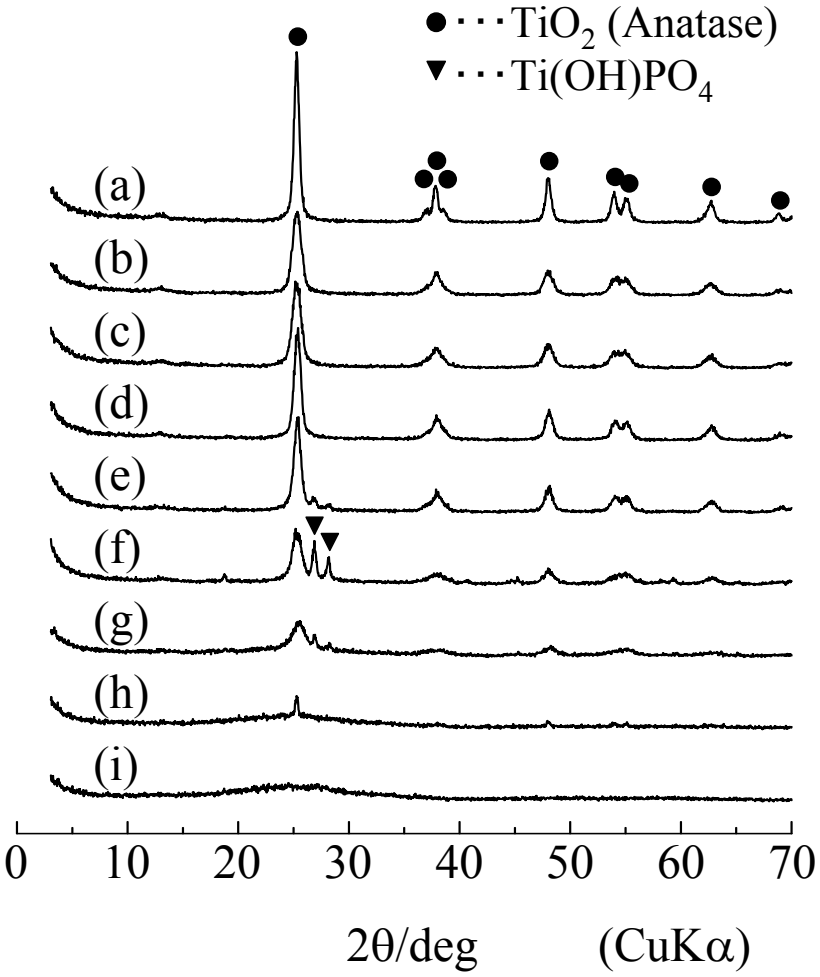

Fig. 4-4 XRD patterns of P-XG(x)'s, with the P/Ti charged ratio, x, of: (a) 0, (b) 0.02, (c) 0.06, (d) 0.1, (e) 0.2, (f) 0.4, (g) 0.6, (h) 0.8, and (i) 1.0.

Table 4-2 Physical properties of P-XG(x) and N-P-XG(x).

P/Ti ratio	BET surface area (m^2/g)		Crystallite size (nm)		Color
	P-XG(x)	N-P-XG(x)	P-XG(x)	N-P-XG(x)	
0	81	70	18	20	Gray
0.02	121	116	11	11	Pale yellow
0.06	117	111	10	10	Yellow
0.1	108	102	14	14	Yellow
0.2	115	117	13	13	Green
0.4	126	98	8	9	Gray
0.6	82	75	8	8	Greenish gray
0.8	56	53	–	–	Dark yellow
1.0	52	52	–	–	Dark yellow

recognized at 27.1 ° and 27.8 °, indicating that another product derived from the titanium hydroxide phosphate was generated by the NH_3 treatment at the high temperature.

Figure 4-5 shows the UV-vis absorption spectra of N-P-XG(x)'s. With an increase in P/Ti ratio up to 0.1, the shoulder absorption at 400–550 nm became stronger, while the absorption at higher wavelength became weaker. The spectrum of N-P-XG(0.2) exhibited a broad absorption band at higher wavelength. This absorption band became larger in the spectrum of N-P-XG(0.4) and then decreased in intensity as the P/Ti ratio further increased. This absorption band is probably related to the nitrification of the $Ti(OH)PO_4$ phase, because the precursor of N-P-XG(0.4), which exhibited the strongest absorption, showed the strongest diffraction peaks due to $Ti(OH)PO_4$ as shown in Fig. 4-4.

In Fig. 4-6, N 1s XPS spectra of XG(0), N-XG(0), and N-P-XG(x)'s are shown. The N 1s XPS spectrum of XG(0) without the NH_3 treatment exhibited a peak at 400 eV binding energy (BE), which is due to nitrogen-containing species adsorbed on the surface [11]. The nitrified samples had another peak at 396 eV BE, which is assigned to nitrogen atoms doped in the TiO_2 lattice [12]. The intensity of the peak at 396 eV BE in N-P-XG(x) increased with an increase in the P/Ti ratio up to 0.1, indicating that higher amounts of nitrogen atoms were introduced into the P-modified titanias than that introduced into pure titania. For N-P-XG(x)'s with $x \geq 0.2$, the N 1s XPS spectra were quite different from those of N-P-XG(x)'s with $x \leq 0.1$. Deconvolution of N 1s spectra was carried out for N-P-XG(x)'s and some of the results are shown in Fig. 4-7. The spectrum of N-P-XG(0.06) was deconvoluted into three components at 396, 400, and 402 eV. As for N-P-XG(0.1), another small component was found at 397.8 eV in

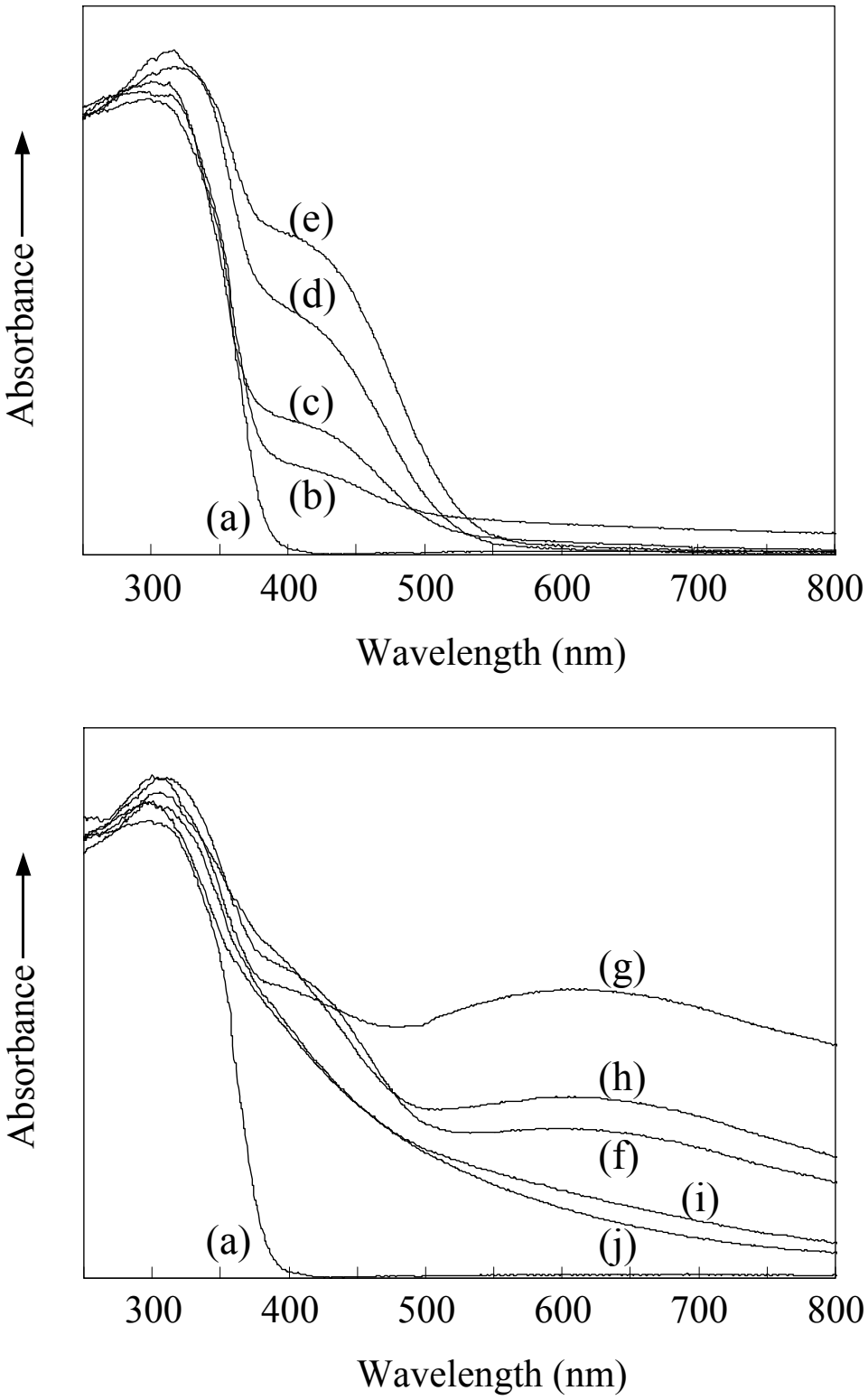

Fig. 4-5 UV-vis spectra of: (a) XG(0), (b) N-XG(0), (c) N-P-XG(0.0.2), (d) N-P-XG(0.06), (e) N-P-XG(0.1), (f) N-P-XG(0.2), (g) N-P-XG(0.4), (h) N-P-XG(0.6), (i) N-P-XG(0.8), and (j) N-P-XG(1.0).

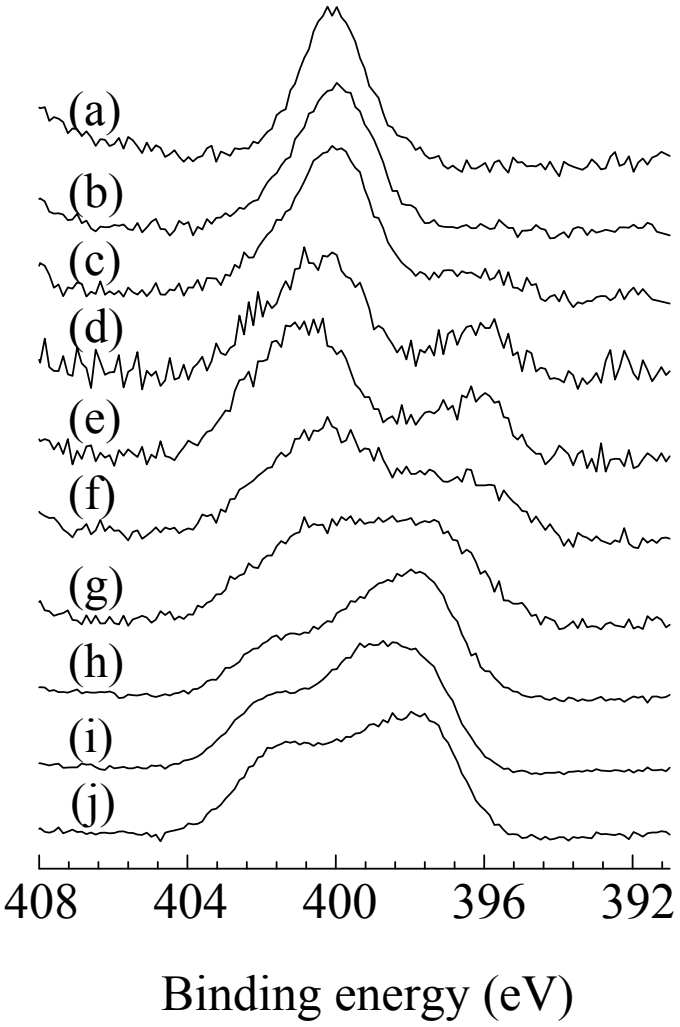

Fig. 4-6 N 1s XPS spectra of: (a) XG(0) and N-P-XG(x) with the P/Ti charged ratio, x, of: (b) 0, (c) 0.02, (d) 0.06, (e) 0.1, (f) 0.2, (g) 0.4, (h) 0.6, (i) 0.8, and (j) 1.0.

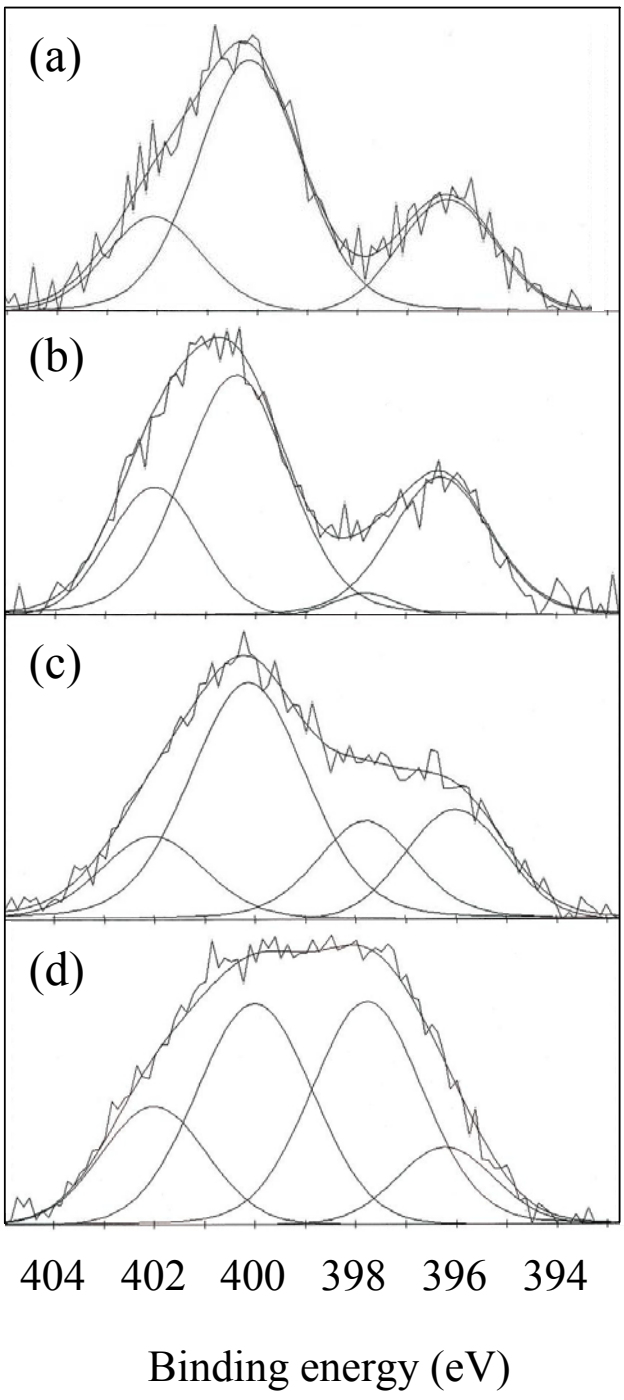

Fig. 4-7 Deconvolution of N 1s XPS spectra of: (a) N-P-XG(0.06), (b) N-P-XG(0.1), (c) N-P-XG(0.2), and (d) N-P-XG(0.4).

addition to the three components. The intensity of the component at 397.8 eV increased with the further increase in the P/Ti ratio. Marchand et al. examined the XPS spectra of phosphorus oxynitride glasses and attributed the peak at 397.8 eV BE to nitrogen doubly bonded to phosphorus [13]. Quan et al. measured XPS of PON and identified the N 1s XPS peak at 397.6 eV to nitrogen atoms in P–N=P segments [14]. Therefore, the component observed at 397.8 eV was assigned to nitrogens in the phosphorous oxynitride species formed by the nitrification of $Ti(OH)PO_4$. The two components at 400 and 402 eV are attributed to nitroxide species in the surface regions of the powders which formed by the oxidation of NH_3 or nitrified compounds [15].

The N/Ti ratios calculated from the intensity of each N 1s component are plotted as a function of the P/Ti charged ratio (Fig. 4-8). The $N_{396\ eV}$/Ti ratio was significantly increased with increasing x value in N-P-XG(x) up to 0.1, indicating the larger amount of nitrogen atoms was stably doped in P-modified titanias as compared to XG(0). However, the excess amount of P atoms incorporated in the sample resulted in the decrease in the $N_{396\ eV}$/Ti ratio. This is because of the decrease in the content of the anatase phase in N-P-XG(x) as indicated by XRD. On the contrary, the ratios of $N_{397.8\ eV}$, $N_{400\ eV}$, and $N_{402\ eV}$ to Ti increased with the increase in the P/Ti ratio, which is attributed to the nitrification of $Ti(OH)PO_4$ and amorphous phosphorous species in the catalysts.

4.3.3 Photocatalytic activity of N-P-XG(x)

Figure 4-9 shows the rate of CO_2 evolution as a function of the P/Ti charged ratio. The CO_2 evolution rate increased with increasing the P/Ti ratio to 0.1. Further increase in the P/Ti charged ratio resulted in a decrease in the photocatalytic activity. This tendency resembled the $N_{396\ eV}$/Ti ratio determined by XPS shown in Fig. 4-8,

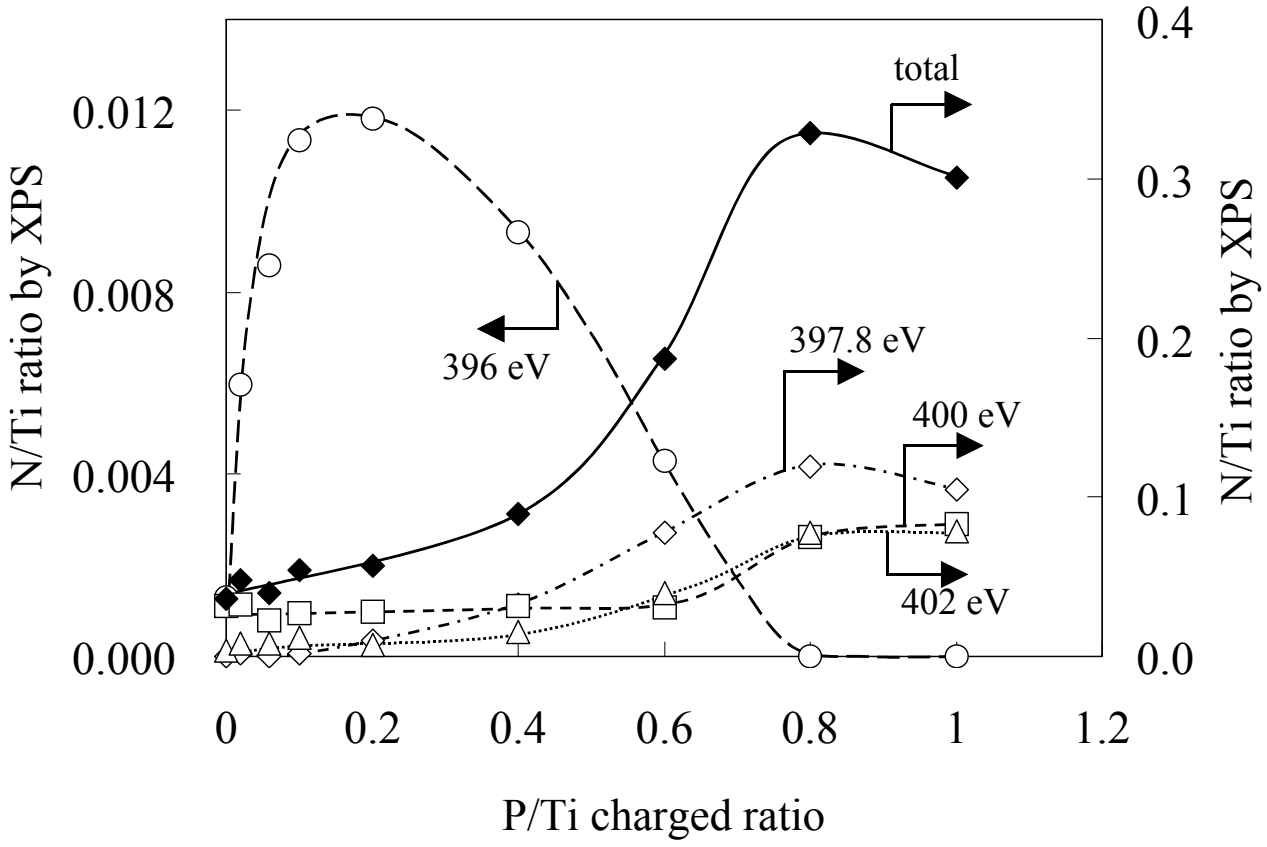

Fig. 4-8 N/Ti ratios of each N 1s component as a function of the P/Ti charged ratio, calculated from the intensities of N 1s XPS peaks at (○) 396 eV, (◇) 397.8 eV, (□) 400 eV, and (△) 402 eV. The closed symbol represents the ratio of the total amount of N to Ti.

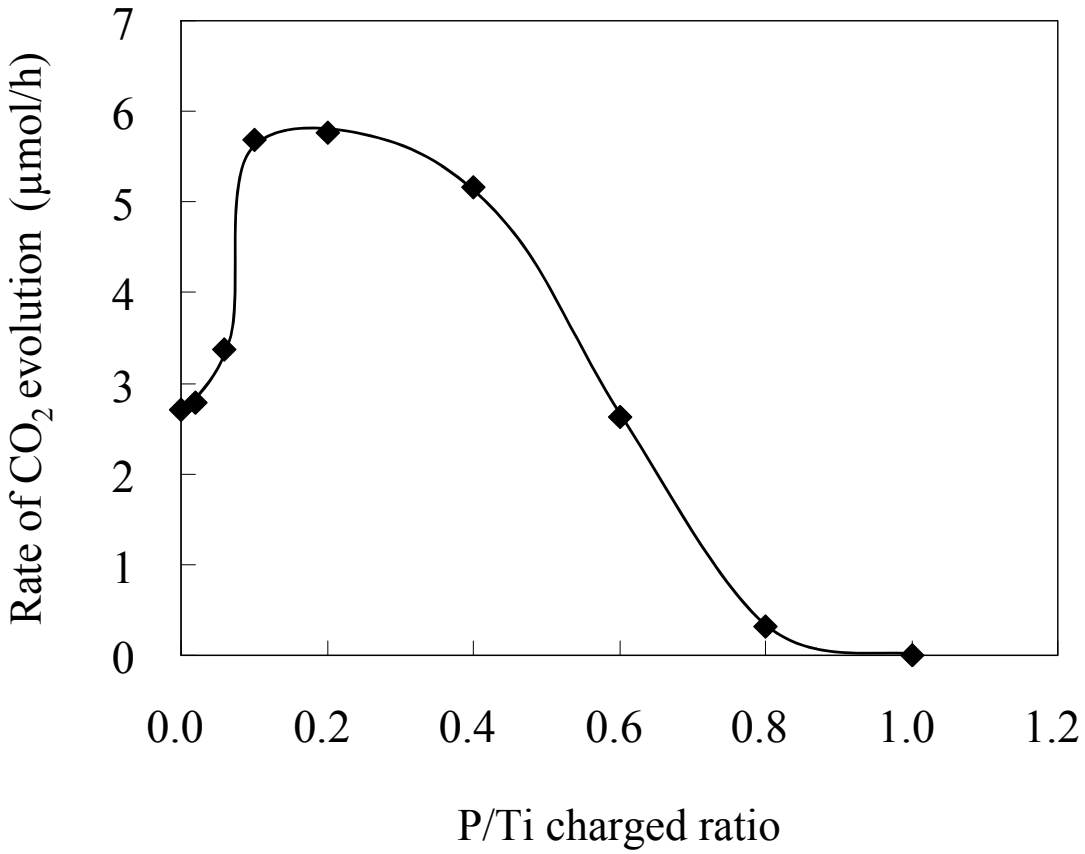

Fig. 4-9 Photocatalytic activity of N-P-XG(x) under visible light irradiation.

indicating that the amount of nitrogen atoms introduced into the TiO_2 lattice is related to the photocatalytic activity under visible light irradiation.

Surface area is one of the important factors which affect photocatalytic activity, but the high surface area of N-P-XG(x) is not the reason for the improved photocatalytic activity under the visible light irradiation. As mentioned above, the surface area was highest for N-P-XG(0.02) and it rather decreased as the P/Ti charged ratio increased. Therefore, we concluded that the enhanced photocatalytic activity is due to the increase in the amount of the nitrogen atoms doped in the TiO_2 lattice by P-modification.

4.4 Conclusions

Among the nitrified titanias modified with B, Mg, Al, P, Zn, and Ga, the titanias modified with P and N exhibited high photocatalytic activities for decomposition of acetaldehyde under visible light irradiation. The N- and P-co-doped TiO_2 showed a stronger absorption in the visible region (400–550 nm) and had a larger peak at 396 eV in the N 1s XPS spectrum. The photocatalytic activity of N-P-XG(x) was related to the amount of the nitrogen atoms introduced into the TiO_2 lattice.

References

[1] K. Nukumizu, J. Nunoshige, T. Takata, J. N. Kondo, M. Hara, H. Kobayashi, and K. Domen, *Chem. Lett.* **2003**, 196.

[2] Y. Sakatani, H. Ando, K. Okusako, H. Koike, J. Nunoshige, T. Takata, J. N. Kondo, M. Hara, and K. Domen, *J. Mater. Res.* **2004**, *19*, 2100.

[3] Y. Sakatani, J. Nunoshige, H. Ando, K. Okusako, H. Koike, T. Takata, J. N. Kondo, M. Hara, and K. Domen, *Chem. Lett.* **2003**, 1156.

[4] H. Wei, Y. Wu, N. Lun, and F. Zhao, *J. Mater. Sci.* **2004**, *39*, 1305.

[5] S. Iwamoto, K. Saito, M. Inoue, and K. Kagawa, *Nano Lett.* **2001**, *1*, 417.

[6] T. Torimoto, R.J. Fox, III, and M. A. Fox, *J. Electrochem. Soc.* **1996**, *143*, 3712.

[7] Y. Suda, H. Kawasaki, T. Ueda, and T. Ohshima, *Thin Solid Films* **2004**, *453-454*, 162.

[8] H. Ozaki, S. Iwamoto, and M. Inoue, *Chem. Lett.* **2005**, *34*, 1082.

[9] H. Ozaki, S. Iwamoto, and M. Inoue, *J. Mater. Sci.* **2007**, *42*, 4009.

[10] S. Ikeda, N. Sugiyama, S. Murakami, H. Kominami, Y. Kera, H. Noguchi, K. Uosaki, T. Torimoto, and B. Ohtani, *Phys. Chem. Chem. Phys.* **2003**, *5*, 778.

[11] N. D. Shinn and K. L. Tsang, *J. Vac. Sci. Technol. A* **1991**, *9*, 1558.

[12] N. C. Saha and H. G. Tompkins, *J. Appl. Phys.* **1992**, *72*, 3072.

[13] R. Marchand, D. Agliz, L. Boukbir, and A. Quemerais, *J. Non-Cryst. Solids* **1988**, *103*, 35.

[14] D. T. Quan, A. Le Bloa, H. Hbib, O. Bonnaud, J. Meinnel, A. Quemerais, and R. Marchand, *Rev. Phys. Appl.* **1989**, *24*, 545.

[15] T. Jirsak, J. Dvorak, and J. A. Rodriguez, *Surf. Sci.* **1999**, *436*, L683.

Chapter 5

Effect of the addition of a small amount of vanadium on the photocatalytic activities of nitrogen- and silicon-co-doped titanias under visible-light irradiation

5.1 Introduction

The physical properties and the visible-light-induced photocatalytic activities of N- and Si-co-doped titanias were discussed in chapter 2 and 3. The nitrification of the Si-modified titanias in an NH_3 flow at high temperatures was examined and it was found that the thus-obtained N- and Si-co-doped titanias had higher nitrogen contents and exhibited higher photocatalytic activities for decomposition of acetaldehyde under visible-light irradiation.

Several transition-metal-ion dopants in TiO_2 have been investigated previously with regard to the photocatalytic activity under UV light irradiation [1–3]. However, studies on the effect of transition metal modification for N-doped TiO_2, which exhibits visible-light sensitivity, are relatively few [4,5].

In the study presented in this chapter, N- and Si-co-doped titanias were further modified with vanadium by an impregnation method using an ammonium vanadate solution, and the obtained catalysts were characterized by XRD, BET surface area measurement, UV-vis, and ESR. Photocatalytic decomposition of acetaldehyde using

the V-loaded N- and Si-co-doped titanias was also examined.

5.2 Experimental

5.2.1 Preparation of the catalysts

Si-modified titania with a Si/Ti charged ratio of 0.2 was prepared by the glycothermal method and collected as a xerogel form [6]. The as-synthesized product was calcined in a box furnace in air at 500 °C for 30 min to remove the surface organic moieties. The thus-obtained sample was designated as Si(0.2)-TiO_2. Si(0.2)-TiO_2 was heated in a 100 mL/min flow of argon up to 600 °C at a rate of about 10 °C/min and then exposed to NH_3 (100 mL/min) for 1 h, followed by annealing at 500 °C in air for 30 min (designated as N-Si(0.2)-TiO_2). Vanadium loading onto Si(0.2)-TiO_2 and N-Si(0.2)-TiO_2 was carried out by an impregnation method: Si(0.2)-TiO_2 or N-Si(0.2)-TiO_2 was added to an aqueous solution of ammonium vanadate (NH_4VO_3). Then, the samples were dried and calcined at 500 °C for 30 min. The thus-obtained V-modified catalysts are designated as V(x)-Si(0.2)-TiO_2 or V(x)-N-Si(0.2)-TiO_2, where x is V/Ti charged atomic ratio, $0 \leq x \leq 0.10$.

5.2.2 Characterization

The UV-vis absorption spectra were recorded on a Shimadzu MPS-2000 spectrophotometer. Powder X-ray diffraction (XRD) patterns were recorded on a Shimadzu XD-D1 diffractometer using CuKα radiation and a carbon-monochromator. The specific surface areas of the samples were determined by the BET single-point method on the basis of the nitrogen uptake measured at 77 K. X-band ESR spectra were recorded at 123 K under an aerated condition with a JEOL JES-SRE2X spectrometer

equipped with a 500 W mercury lamp.

5.2.3 Photocatalytic reaction

Photocatalytic activity was evaluated by decomposition of acetaldehyde. The reaction was carried out in a closed glass vessel (1.0 L). The catalyst (0.2 g) dispersed on a 90 mmϕ glass filter was placed in the vessel and 0.2 mmol acetaldehyde was injected in it. The vessel was placed in the dark for 1 h and then visible light was irradiated using a 300 W xenon lamp (Optical Modulex SX-UI300XQ, Ushio Inc.) through a UV cut-off filter (L-42, Asahi Technoglass Co. Ltd.) and an infrared cut-off filter (Super Cold Filter, Ushio Inc.). After a certain period of irradiation, the CO_2 concentration was measured by a gas chromatograph, Shimadzu GC-8A. The amount of CO_2 formed was calculated by subtracting the initial amount of CO_2 in the vessel.

5.3 Results and discussion

The XRD patterns of Si(0.2)-TiO_2 and N-Si(0.2)-TiO_2 showed diffraction peaks due to the anatase structure. Crystallite sizes of these two samples were identical (10 nm) and their BET surface areas were 164 and 158 m^2/g, respectively, indicating the obtained products were well-dispersed nanocrystals. After the V loading, XRD patterns as well as BET surface areas did not change significantly; for example, crystallite size and BET surface area of V(0.001)-N-Si(.2)-TiO_2 were 10 nm and 161 m^2/g, respectively.

Si(0.2)-TiO_2 is a white powder and the color turned into vivid yellow after the NH_3 treatment and annealing. In the case of low vanadium loading with x in V(x)-N-Si(0.2)-TiO_2 less than 0.01, the color of the sample did not change significantly

after the loading of vanadium. With the increase in the amount of V-loading (x > 0.01), the color became orange or brownish. The UV-vis absorption spectra of V(x)-Si(0.2)-TiO_2 and V(x)-N-Si(0.2)-TiO_2 are shown in Figures 5-1(a) and 5-1(b), respectively. Si(0.2)-TiO_2 exhibited absorption only in the UV region. With the vanadium modification, however, an expansion of the absorption into the visible region was recognized. It was reported that V_2O_5 which includes square-pyramidal VO_5 polymers or highly distorted octahedral VO_6 polymers shows an absorption at lower than 570 nm and that V^{4+} has an absorption band centered at 770 nm due to the d-d transition [7,8]. Therefore, the spectra suggest the presence both of V^{5+} and V^{4+} in the samples. As for N-Si(0.2)-TiO_2 (i.e., x = 0), the catalyst had a stronger absorption band at 400–550 nm, which is attributed to the doped nitrogen into the anatase structure. The UV-vis spectra of V(x)-N-Si(0.2)-TiO_2 with x lower than 0.01 were almost same as that of the mother material, N-Si(0.2)-TiO_2. For V(x)-N-Si(0.2)-TiO_2 with higher x, an broad absorption at visible light region (>400 nm) was also observed.

Figure 5-2 shows the CO_2 generation due to the photocatalytic oxidation of acetaldehyde under visible light irradiation using V(0.01)-N-Si(0.2)-TiO_2 and N-Si(0.2)-TiO_2. In the previous study, we found that N-Si(0.1)-TiO_2 exhibited about two times higher photocatalytic activity than that of nitrified-TiO_2 without Si modification [10], and that the photocatalytic activity was further improved, by about three times, using N-Si(0.2)-TiO_2. Compared with N-Si(0.2)-TiO_2, the V-loaded catalyst showed an apparently higher photocatalytic activity.

The photocatalytic activities of V(x)-N-Si(0.2)-TiO_2 and V(x)-Si(0.2)-TiO_2 with varied amounts of V-loading are shown in Figure 5-3. For Si(0.2)-TiO_2 without N-doping, the addition of V resulted in an appearance of a certain degree of

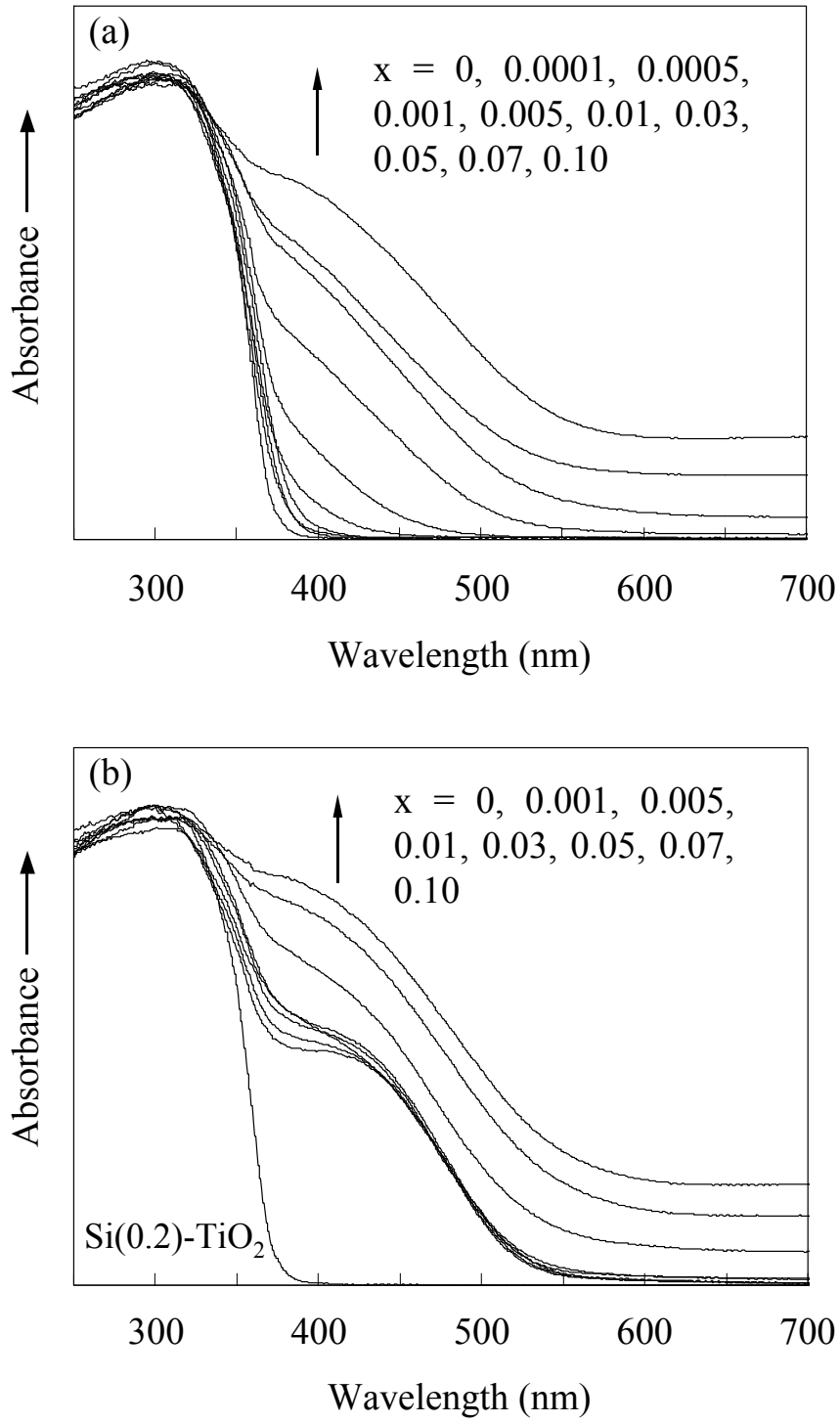

Fig. 5-1 UV-vis spectra of: (a) V(x)-Si(0.2)-TiO_2 and (b) V(x)-N-Si(0.2)-TiO_2.

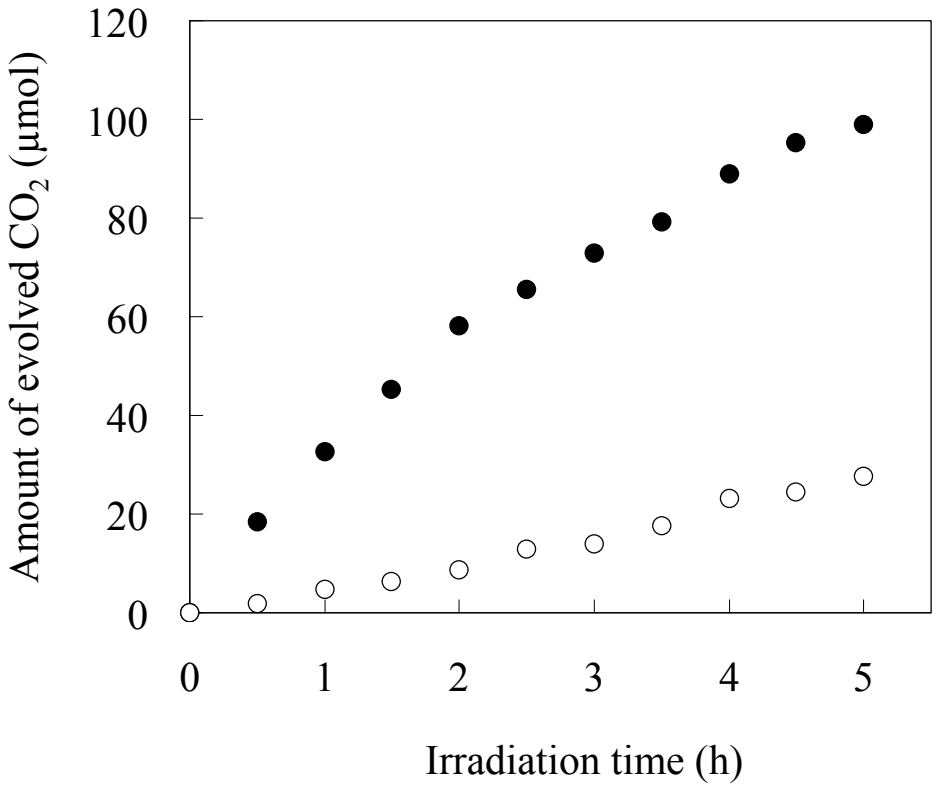

Fig. 5-2 Photocatalytic decomposition of acetaldehyde under visible-light irradiation on: (●), V(0.01)-N-Si(0.2)-TiO_2 and (○), N-Si(0.2)-TiO_2.

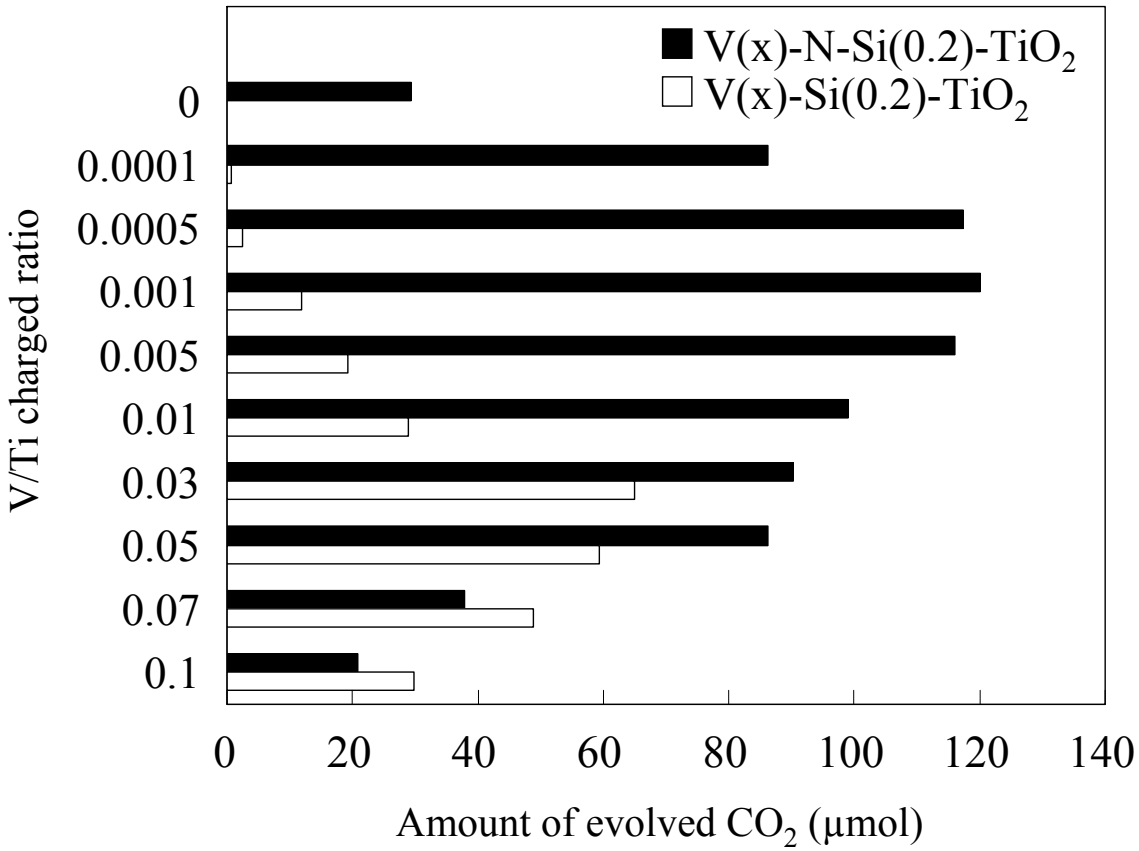

Fig. 5-3 Amounts of the CO_2 generated with V(x)-N-Si(0.2)-TiO_2 and V(x)-Si(0.2)-TiO_2 after 5 h of visible-light irradiation.

photocatalytic activity as shown in Figure 5-3 (white bars). When the amount of V-loading was small, for example, V(0.0001)-Si(0.2)-TiO_2 and V(0.0005)-Si(0.2)-TiO_2, the catalysts had little absorption in the visible light region as shown in Figure 5-1(a), and exhibited quite low photocatalytic activities. The photocatalytic activity increased, however, gradually with the increase in the amount of V loading and reached a maximum at the V/Ti ratio of 0.03. Anpo et al. reported that the V-modified TiO_2 obtained by an ion-implantation method exhibited the visible light absorption and a photocatalytic activity for the degradation of propanol diluted in water under visible-light irradiation [9]. Appearance of visible-light responsibility of V-doped TiO_2 prepared by an impregnation method [10] and by sol-gel methods [11,12] was also reported. Therefore, the observed visible-light sensitivity of V(x)-Si(0.2)-TiO_2 is due to the vanadium species loaded on the catalyst. On the contrary, a very small amount of V loading (V/Ti ratio = 0.0001–0.005) significantly improved the photocatalytic activity for V(x)-N-Si(0.2)-TiO_2 as shown in Figure 5-3 with black bars, suggesting that presence of highly dispersed vanadium species has a critical role in enhancement of the photocatalytic activity. The highest photocatalytic activity was obtained with V(0.001)-N-Si(0.2)-TiO_2 which was 4 times higher than that of N-Si(0.2)-TiO_2. Since these catalysts contained quite small amounts of V, they showed similar UV-vis spectra as that of the material without the V-loading. When V/Ti ratio was increased to 0.005, the photocatalytic activity decreased slightly and further increase in the amount of V loading drastically lowered the photocatalytic activity. These results are completely different from those for V(x)-Si(0.2)-TiO_2 and suggested that the enhanced photocatalytic activity is not due to the increase in the absorption of the light in the visible region. Choi et al. examined the role of various metal ion dopants in

quantum-sized TiO_2 and reported that the quantum yield for TiO_2 was significantly improved by the V modification. Considering the energy diagram of TiO_2 and the transition metal oxides, they insisted on an ability of V-dopant as effective electron/hole traps [1]. Therefore, it is likely that the small amount of V species loaded on N- and Si-co-doped titanias functioned as effective electron/hole traps and inhibited the electron-hole recombination.

In order to observe an electron transfer behavior on irradiation, ESR measurement was performed (Fig. 5-4). For the non-doped sample, Si(0.2)-TiO_2, a ESR signal at g = 2.003 was observed under a dark condition. This signal is assigned to free electrons in TiO_2. Under UV light illumination, signals at g = 1.990 and 1.959 were recognized, which were assigned to trapped electrons on Ti (Ti^{3+}) [13,14]. When the ESR measurement under UV light illumination was carried out on V(0.0001)-Si(0.2)-TiO_2, the intensity of Ti^{3+} signals decreased apparently. Increase in the amount of loaded V up to V/Ti = 0.001 resulted in the drastic decrease in the intensity of the Ti^{3+} signals, while there appeared other signals due to V^{4+}. These results suggested that photoexcited electrons in TiO_2 conduction band are transferred to V trap sites [15]. Although these ESR signals were not observed clearly in the case of the N-doped samples because of the overlapping of strong ESR signals due to paramagnetic nitrogen species in the same region, it is likely that similar electron transfer takes place and causes effective separation of the photogenerated electron–hole, consequently resulting in the improvement in the photocatalytic activity.

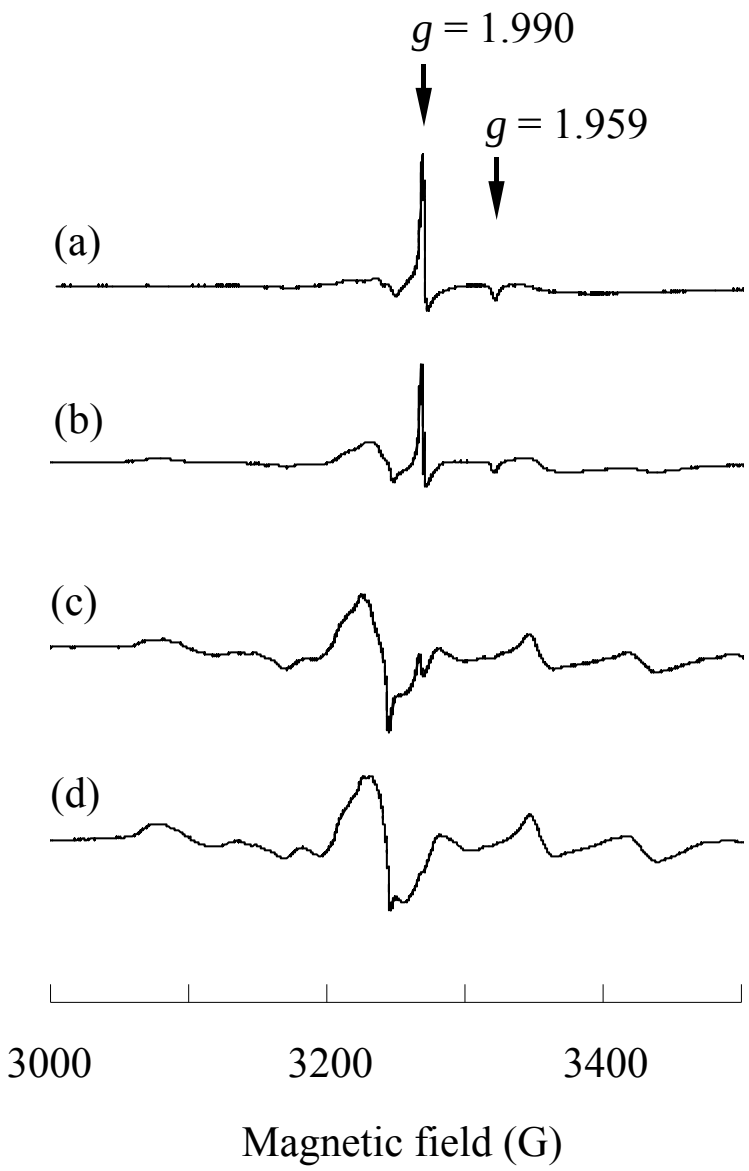

Fig. 5-4 ESR spectra of: (a) Si(0.2)-TiO_2, (b) V(0.0001)-Si(0.2)-TiO_2, (c) V(0.0005)-Si(0.2)-TiO_2 and (d) V(0.001)-Si(0.2)-TiO_2; under UV light illumination at 123 K.

5.4 Conclusions

Photocatalytic activity for decomposition of acetaldehyde under visible-light irradiation was examined using N-Si(0.2)-TiO_2 modified with V by an impregnation method. It was demonstrated that the photocatalytic activity was enhanced drastically by the addition of a very small amount of vanadium, V/Ti = 0.0001–0.01. V(0.001)-N-Si(0.2)-TiO_2 showed the highest photocatalytic activity, which was 4 times higher than that of N-Si(0.2)-TiO_2. Higher V-loadings, however, resulted in a decrease in the photocatalytic activity. The results suggest that highly dispersed vanadium species located on the surface of the N- and Si-co-doped titanias play a critical role as the electron trap sites. These trap sites contribute an effective separation of photoinduced electrons and holes and consequently bring about the improvement in photocatalytic activity under visible-light irradiation.

References

[1] W. Choi, A. Termin, and M. R. Hoffman, *J. Phys. Chem.* **1994**, *98*, 13669.

[2] M. I. Litter and J. A. Navio, *J. Photochem. Photobiol. A: Chem.* **1996**, *98*, 171.

[3] K. Nagaveni, M. S. Hegde, and G. Madras, *J. Phys. Chem. B* **2004**, *108*, 20204.

[4] T. Ohno, Z. Miyamoto, K. Nishijima, H. Kanemitsu, and F. Xueyuan, *Appl. Catal. A: Gen.* **2006**, *302*, 62.

[5] B. Gao, Y. Ma, Y. Cao, W. Yang, and J. Yao, *J. Phys. Chem. B* **2006**, *110*, 14391.

[6] S. Iwamoto, K. Saito, M. Inoue, and K. Kagawa, *Nano Lett.* **2001**, *1*, 417.

[7] F. Amano, T. Yamaguchi, and T. Tanaka, *J. Phys. Chem. B* **2006**, *110*, 281.

[8] X. Gao and I. E. Wachs, *J. Phys .Chem. B* **2000**, *104*, 1261.

[9] H. Yamashita, M. Harada, J. Misaka, M. Takeuchi, K. Ikeue, and M. Anpo, *J. Photochem. Photobiol. A: Chem.* **2002**, *148*, 257.

[10] S. Klosek and D. Raftery, *J. Phys. Chem. B* **2001**, *105*, 2815.

[11] J. C.-S. Wu and C-H. Chen, *J. Photochem. Photobiol. A: Chem.* **2004**, *163*, 509.

[12] K. Iketani, R. Sun, M. Toki, K. Hirota, and O. Yamaguchi, *Mater. Sci. Eng. B* **2004**, *108*, 187.

[13] Y. Nakaoka and Y. Nosaka, *J. Photochem. Photobiol. A: Chem.* **1997**, *110*, 299.

[14] R. F. Howe and M. Grätzel, *J. Phys. Chem.* **1987**, *91*, 3906.

[15] M. Grätzel and R. F. Howe, *J. Phys. Chem.* **1990**, *94*, 2566.

Chapter 6

Effect of iron on visible-light-induced photocatalytic activities of nitrogen- and silicon-co-doped titanias

6.1 Introduction

Fe^{3+} is one of the most frequently examined dopants because it is assumed that Fe^{3+} cations can act as effective traps of photogenerated electrons. Some paper reported that photocatalytic activity was increased by Fe-doping[1,2,3–5], while others reported that the presence of foreign metal species is generally detrimental for photocatalytic degradation of organic species [6–8], and the effects of the introduction of Fe^{3+} cations still remains controversial. On the other hand, only a few papers have reported the effects of transition metal modification on the visible-light-induced photocatalytic activities of N-doped TiO_2 [9–11]. Ohno et al. recently examined the effect of loading of Fe^{3+} cations on N-doped or S-doped titanias upon their photocatalytic activities and found that their activities were about twice as high as those without the Fe-loading [9]. This chapter describes more than 10 times enhancement of the visible-light-induced photocatalytic activity by the addition of a small amount of Fe to N- and Si-co-doped titanias. The prepared catalysts were characterized by XRD, BET surface area, XPS, UV-vis, ESR, and the mechanism of the promotive effect of Fe^{3+} cations was discussed.

6.2 Experimental

6.2.1 Preparation of the catalysts

Nanocrystalline Si-modified titania with a Si/Ti charged ratio of 0.2 was prepared by the glycothermal method and collected as a xerogel form as described in the previous report [12]: Titanium tetraisopropoxide (25 g) and tetraethyl orthosilicate (3.7 g) were added to 100 mL of 1,4-butanediol and this mixture was placed in a 300 mL autoclave. After the atmosphere inside the autoclave was replaced with nitrogen, the assembly was heated to 300 °C at a rate of 2.3 °C/min and kept at that temperature for 2 h. After the glycothermal reaction, one of the valves of the autoclave was slightly opened to remove the organic matter in the autoclave by flash evaporation while keeping the autoclave temperature at 300 °C. After cooling, bulky solid products were directly obtained. The as-synthesized product was calcined in a box furnace in air at 500 °C for 30 min to remove the surface organic moieties. The thus-obtained Si-modified titania was designated as Si(0.2)-TiO_2. Nanocrystalline titania powder without Si-modification was synthesized in the same way as mentioned above except for the addition of tetraethyl orthosilicate (designated as TiO_2(GT)). Nitrification of TiO_2(GT) and Si(0.2)-TiO_2 was carried out as follows: First, the samples were heated in a 100 mL/min flow of argon up to 600 °C at a rate of about 10 °C/min, and then, they were contacted to an NH_3 flow (100 mL/min) for 1 h. The samples were finally annealed at 500 °C in air for 30 min in a box furnace. The thus-obtained nitrified and annealed samples are designated as N-TiO_2(GT) and N-Si(0.2)-TiO_2. A reference TiO_2 sample, JRC-TIO-4 (a reference catalyst supplied from The Catalysis Society of Japan; equivalent to Degussa P-25) and a commercially available TiO_2, ST-01 (Ishihara Sangyo Ltd.), were also treated in the same manner and they were designated as N-P-25 and

N-ST-01, respectively. Fe-loading was carried out by an impregnation method: A portion of the samples was added to an aqueous solution of iron nitrate ($Fe(NO_3)_3$), and dried, followed by calcination at 500 °C for 30 min. The Fe-loaded catalysts are designated by adding "Fe(x)-", where x is the Fe/Ti charged atomic ratio ($0 \leq x \leq 0.10$); for example, Fe-loaded N-Si(0.2)-TiO_2 with Fe/Ti = 0.01 is expressed as Fe(0.01)-N-Si(0.2)-TiO_2.

6.2.2 Characterization

The UV-vis absorption spectra were recorded on a Shimadzu MPS-2000 spectrophotometer. Powder X-ray diffraction (XRD) patterns were recorded on a Shimadzu XD-D1 diffractometer using CuKα radiation and a carbon-monochromator. The specific surface areas of the samples were calculated by the BET single-point method on the basis of the nitrogen uptake measured at 77 K using a Micromeritics Flowsorb II 2300. X-ray photoelectron spectroscopy (XPS) measurement was performed on an ULVAC-PHI Model 5500 spectrometer with 15 kV-400 W MgKα emission as the X-ray source. The X-band ESR spectra were recorded with a JEOL JES-SRE2X spectrometer. The measurement was carried out at 123 K under both aerated and evacuated conditions. For nitrified samples, the sample was kept in the dark for 10 h at 298 K, and cooled to 123 K prior to the measurement. A 500 W mercury lamp and a UV cut-off filter (L-42, Asahi Technoglass Co. Ltd.) were used to measure the ESR signals under irradiated conditions.

6.2.3 Photocatalytic reaction

Photocatalytic activity was evaluated by decomposition of acetaldehyde. The

reaction was carried out in a closed glass vessel (1.0 L). The catalyst (0.2 g) dispersed on a 90 mmϕ glass filter was placed in the vessel and 0.2 mmol acetaldehyde was injected in it. The vessel was placed in the dark for 1 h and then visible-light was irradiated using a 300 W xenon lamp (Optical Modulex SX-UI300XQ, Ushio Inc.) through a UV cut-off filter (L-42, Asahi Technoglass Co. Ltd.) and an infrared cut-off filter (Super Cold Filter, Ushio Inc.). After a certain period of irradiation, the CO_2 concentration was measured by a gas chromatograph, Shimadzu GC-8A. The amount of CO_2 formed was calculated by subtracting the initial amount of CO_2 in the vessel.

6.3 Results and discussion

6.3.1 Characterization of the catalysts

The XRD patterns of TiO_2(GT), Si(0.2)-TiO_2 and ST-01 showed diffraction peaks due to the anatase structure. After the NH_3 treatment at 600 °C and annealing in air at 500 °C, the samples preserved the anatase structure. The XRD pattern of P-25 shows diffraction peaks due to anatase and rutile structures, and it did not change significantly after the nitrification. The BET surface areas and crystallite sizes of the samples are listed in Table 6-1. ST-01 had quite a large surface area, 304 m^2/g; however, after the NH_3 treatment and annealing, the surface area decreased significantly. A small crystallite sizes, 8 nm, was increased to 23 nm after the treatment. For P-25 and TiO_2(GT), slight decreases in the BET surface area and increases in the crystallite size were also observed. On the other hand, Si(0.2)-TiO_2 maintained its original crystallite size and BET surface area after the nitrification because of high thermal stability of the sample [13,14].

Figure 6-1 shows the UV-vis spectra of N-P-25, N-TiO_2(GT), N-ST-01, and

Table 6-1 Physical properties of the non-nitrified samples without Fe-loading and the nitrified samples before and after Fe-loading.

Sample	BET surface area (m^2/g)	Crystallite size (nm) [a]	Color
P-25	49	31	White
ST-01	304	8	White
TiO_2(GT)	81	18	White
Si(0.2)-TiO_2	164	10	White
N-P-25	41	34	Pale yellow
N-ST-01	72	23	Pale yellow
N-TiO_2(GT)	70	20	Gray
N-Si(0.2)-TiO_2	158	10	Yellow
Fe(0.01) -N-P-25	42	35	Pale yellow
Fe(0.01)-N-ST-01	71	23	Pale yellow
Fe(0.01)-N-TiO_2(GT)	72	20	Gray
Fe(0.01)-N-Si(0.2)-TiO_2	159	10	Yellow

[a] calculated from the XRD peak broadening of the anatase phase.

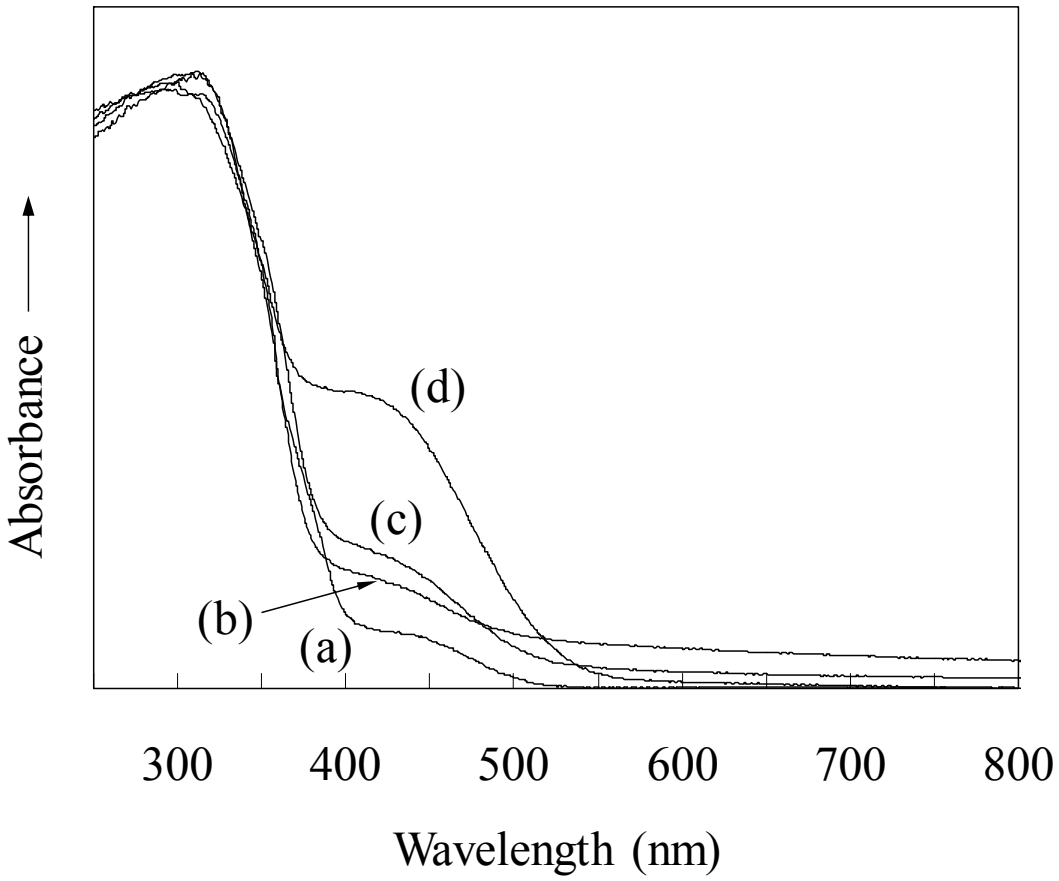

Fig. 6-1 UV-vis spectra of: (a) N-P-25, (b) N-TiO_2(GT), (c) N-ST-01, and (d) N-Si(0.2)-TiO_2.

N-Si(0.2)-TiO_2. The spectra of the nitrified samples had a shoulder absorption band at 400–550 nm, which is due to the doped nitrogen in the sample. Among the three nitrified titanias without Si modification (N-P-25, N-TiO_2(GT), and N-ST-01), N-ST-01 had the most intense absorption at 400–550 nm, suggesting that a larger amount of nitrogen was incorporated in this sample. Nosaka et al. prepared N-doped titanias from nine commercially available TiO_2 samples with different particle sizes and crystalline components and found that the largest amount of nitrogen was incorporated in ST-01 having the smallest particle size [15]. They also found that N-doped ST-01 showed the highest activity for decomposition of 2-propanol under visible-light irradiation [15]. Here, it should be noted that compared with N-ST-01, N- and Si-co-doped titanias showed a much stronger absorption in the visible region and exhibited higher photocatalytic activity as will be described later.

In Figure 6-2, the N 1s XPS spectra of the nitrified samples are depicted. The spectra had two peaks at around 400 and 396 eV. The former peak is attributed to nitrogen-containing species adsorbed on the surface [16], and the latter is assigned to nitrogen doped in TiO_2 [17]. For N-P-25, the peak at 396 eV could be hardly detected, and for N-TiO_2(GT) and N-ST-01, only a small peak was recognized. On the contrary, the peak at 396 eV was clearly observed in the spectrum of N-Si(0.2)-TiO_2. The N/Ti ratios calculated from the intensities of Ti and $N_{396\ eV}$ peaks were 0.0006, 0.0016, 0.0021, and 0.0066 for N-P-25, N-TiO_2(GT), N-ST-01, and N-Si(0.2)-TiO_2, respectively, which clearly indicated that a larger amount of nitrogen was incorporated in N-Si(0.2)-TiO_2.

The Fe-loading with Fe/Ti = 0.01 did not alter the BET surface areas of the samples significantly as shown in Table 6-1, nor modify the XRD patterns. In Figure

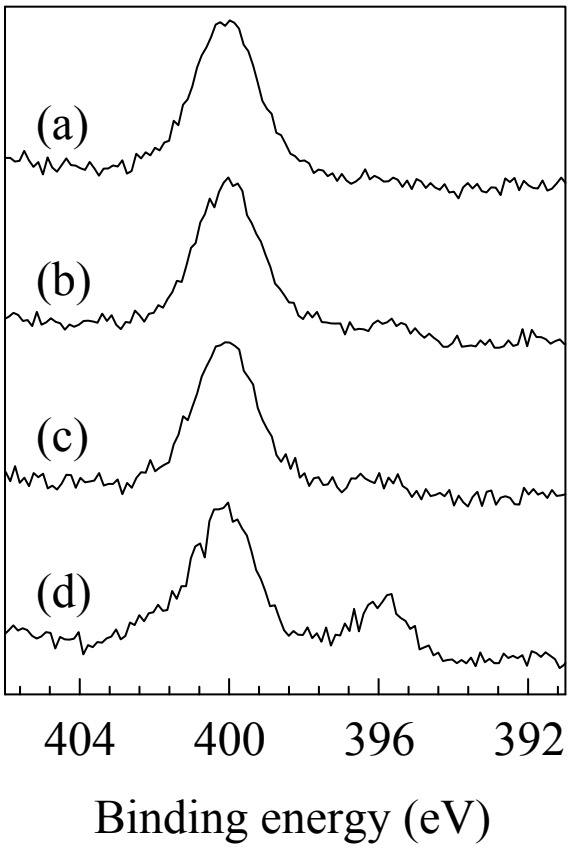

Fig. 6-2 N1s XPS spectra of: (a) N-P-25, (b) N-TiO_2(GT), (c) N-ST-01, and (d) N-Si(0.2)-TiO_2.

6-3, the UV-vis spectra of Fe(x)-Si(0.2)-TiO_2 and Fe(x)-N-Si(0.2)-TiO_2 are depicted. Si(0.2)-TiO_2 exhibited absorption at the wavelength shorter than 390 nm, due to the intrinsic band gap of TiO_2. By the introduction of small amounts of Fe, absorption in the visible region around 400 nm was observed. With increasing the amount of Fe loaded, this absorption band at the visible region became more apparent, which is consistent with the change in color from white, to yellow, and then to brown. For the samples with higher Fe contents, another broad band centered at around 500 nm was recognized. These absorption bands can be ascribed to charge-transfer transition ($O^{2-} \rightarrow Fe^{3+}$) due to the Fe^{3+} species loaded on the sample [2,18,19]. For Fe(x)-N-Si(0.2)-TiO_2, the change in color by the Fe addition was not so clear since the mother material, N-Si(0.2)-TiO_2, is yellow having a significant absorption at a visible region lower than 550 nm. As shown in Figure 3(b), however, an increase in the absorption at around 400 nm was recognized with low contents of Fe, and a broad absorption at higher wavelength was observed for the samples with increased Fe-loadings. These changes are similar to the case of Fe-Si(0.2)-TiO_2 as mentioned above.

6.3.2 Photocatalytic activities of the nitrified samples with and without Fe loading

Figure 6-4 shows the CO_2 generation due to the photocatalytic oxidation of acetaldehyde under visible-light irradiation using Fe(0.01)-N-Si(0.2)-TiO_2 and N-Si(0.2)-TiO_2. The latter catalyst exhibited about three times higher photocatalytic activity than that of nitrified TiO_2(GT) without Si modification (see Figure 6-5 (white bar)). The Fe-loading onto N-Si(0.2)-TiO_2 resulted in a significant enhancement in the photocatalytic activity under visible-light irradiation.

In Figure 6-5, the photocatalytic activities of N-P-25, N-TiO_2(GT), N-ST-01, and

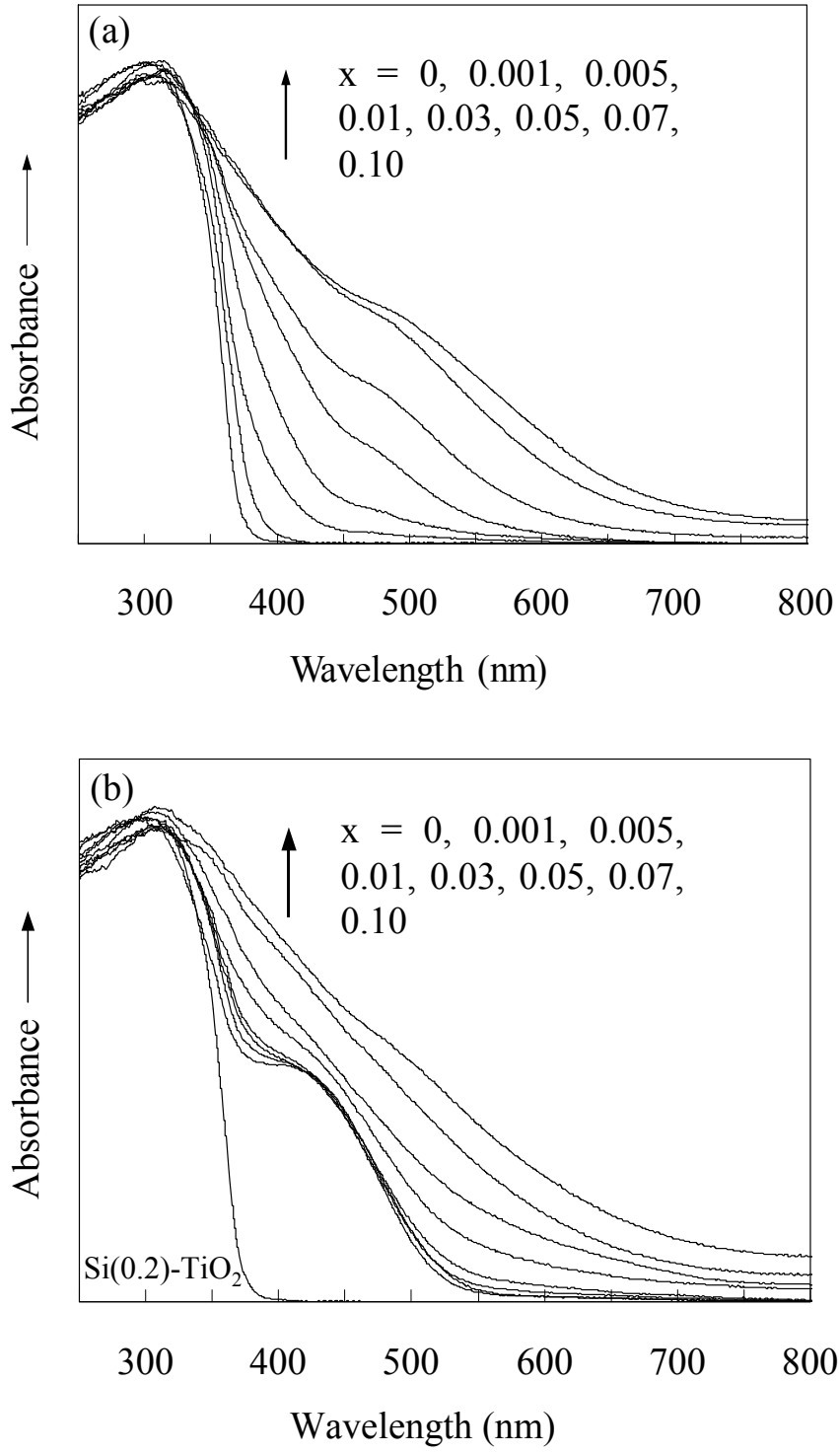

Fig. 6-3 UV-vis spectra of: (a) Fe(x)-Si(0.2)-TiO_2 and (b) Fe(x)-N-Si(0.2)-TiO_2.

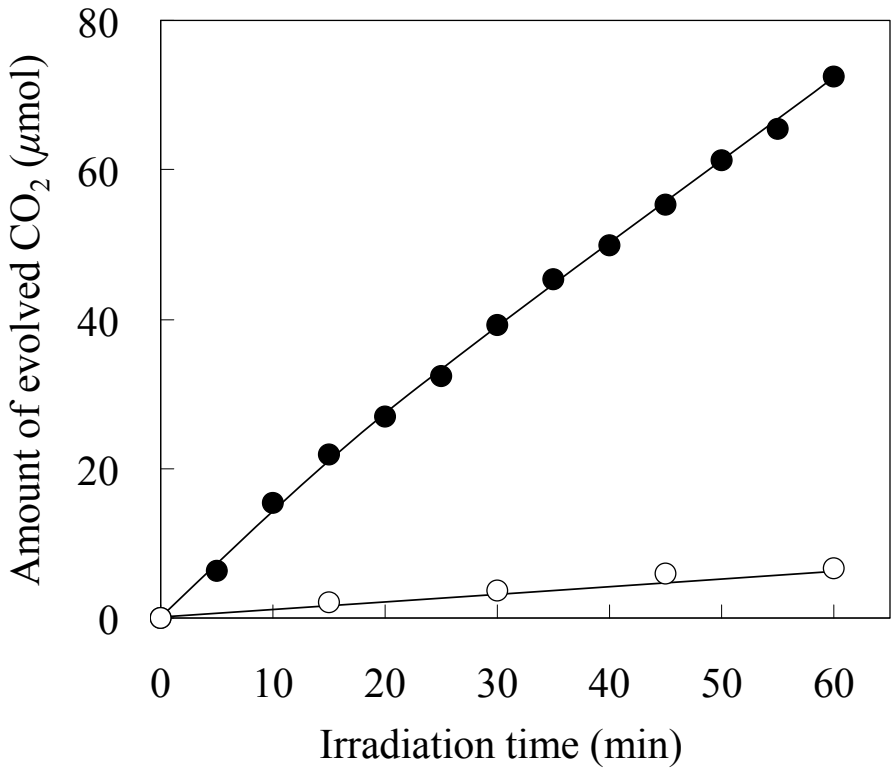

Fig. 6-4 Photocatalytic decomposition of acetaldehyde under visible-light irradiation on: (●), Fe(0.01)-N-Si(0.2)-TiO_2 and (○), N-Si(0.2)-TiO_2. Reaction conditions: Acetaldehyde, 0.2 mmol; catalyst, 0.2 g.

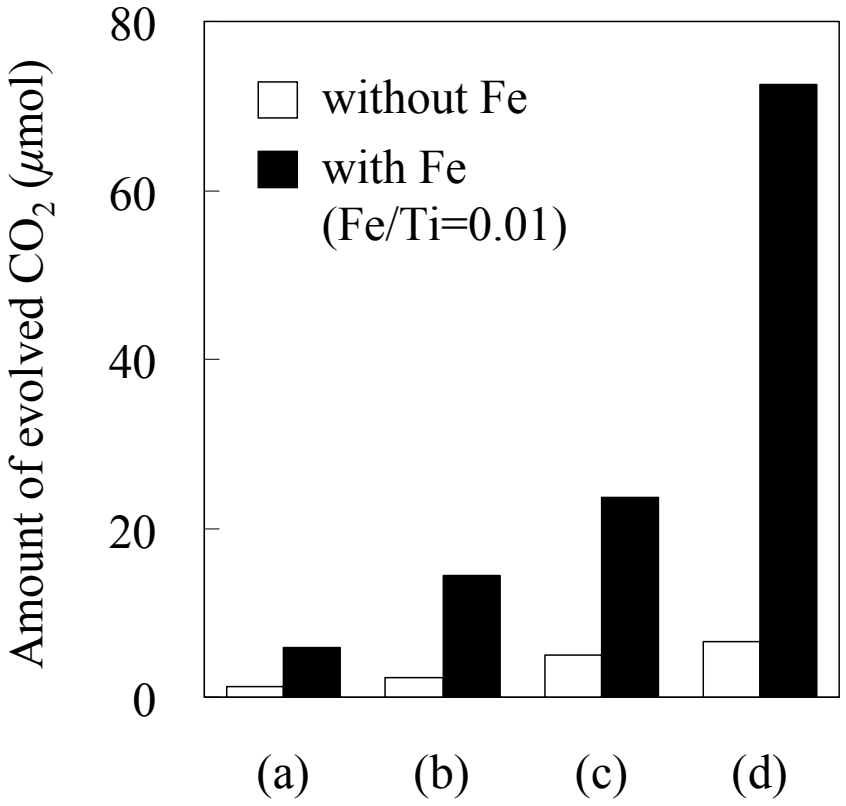

Fig. 6-5 Amounts of CO_2 generated after 1 h of visible-light irradiation: (a) N-P-25, (b) N-TiO_2(GT), (c) N-ST-01, and (d) N-Si(0.2)-TiO_2; with and without the Fe loading. Reaction conditions: Acetaldehyde, 0.2 mmol; catalyst, 0.2 g.

N-Si(0.2)-TiO_2 with and without the Fe-loading are compared. The activities increased in the order of: N-P-25 < N-TiO_2(GT) < N-ST-01 < N-Si(0.2)-TiO_2 both with and without the Fe loading. This order corresponds to the amount of nitrogen doped in the samples measured by XPS, indicating that the amount of doped nitrogen is one of the critical factors affecting the photocatalytic activity under visible-light irradiation. For all the N-doped samples, the addition of Fe caused a marked promotive effect on the photocatalytic activity. Ohno et al. previously reported that the photocatalytic activity of N-doped TiO_2 (ST-01) was improved about two-fold by the loading of Fe^{3+} cations [9]. Among the samples examined here, Fe(0.01)-N-Si(0.2)-TiO_2 showed the highest photocatalytic activity.

The photocatalytic activities of Fe(x)-N-Si(0.2)-TiO_2, Fe(x)-Si(0.2)-TiO_2 and Fe(x)-TiO_2(GT) with varied amounts of Fe-loading are shown in Figure 6-6. For TiO_2(GT) and Si(0.2)-TiO_2 both with and without Fe addition, no visible-light-induced photocatalytic activity was recognized. On the contrary, the addition of a small amount of Fe drastically improved the photocatalytic activity for Fe(x)-N-Si(0.2)-TiO_2. Since the UV-vis spectra of Fe(x)-N-Si(0.2)-TiO_2 of x less than 0.01 were similar to that of the mother material without the Fe-loading, the enhanced photocatalytic activity is not due to the increase in the absorption of visible-light by the modification of Fe. It is noteworthy that high activities were obtained for a wide range of Fe/Ti from 0.005 to 0.07. The highest photocatalytic activity, 12 times as high as that of N-Si(0.2)-TiO_2, was attained for Fe(0.03)-N-Si(0.2)-TiO_2. Further increase in the Fe-loading lowered the photocatalytic activity. This is probably because a part of the titania surface was covered with large excess of iron species which had no photocatalytic activity.

Generation of photocatalytic activities *under visible-light irradiation* by Fe

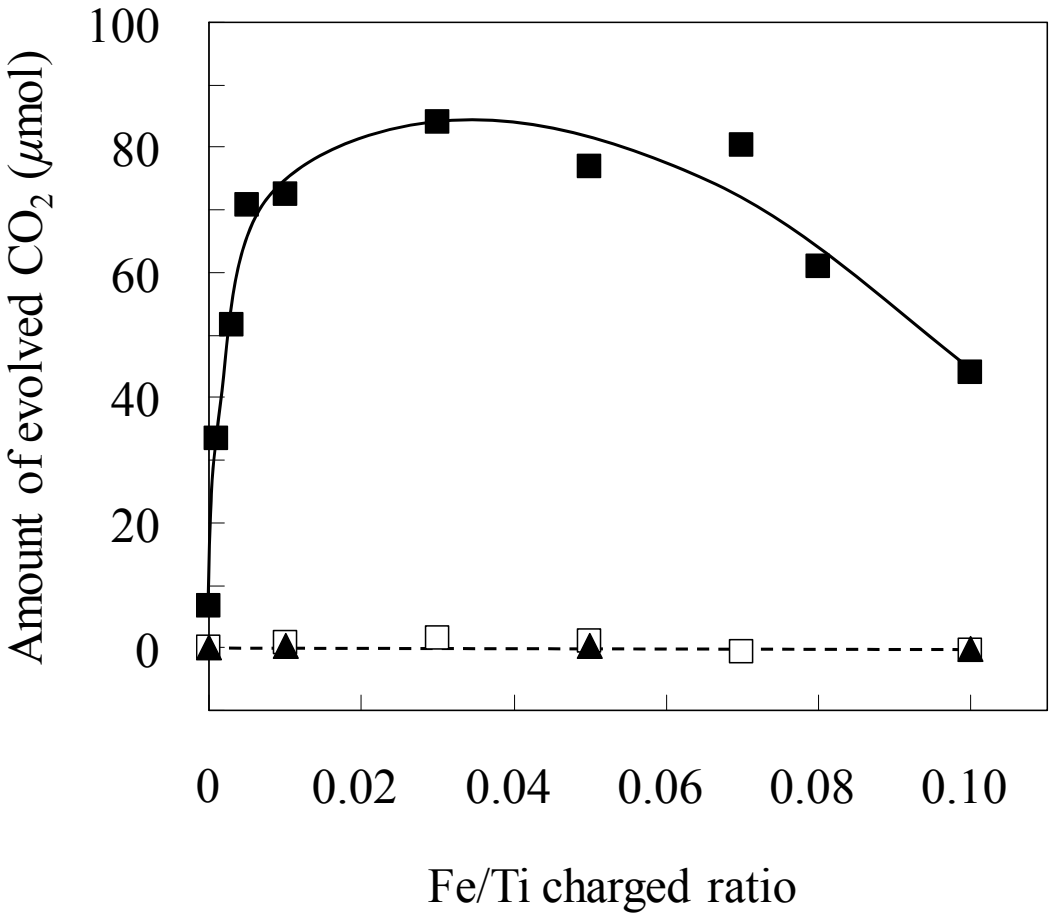

Fig. 6-6 Amounts of the CO_2 generated after 1 h of visible-light irradiation over: (■) Fe(x)-N-Si(0.2)-TiO_2, (□) Fe(x)-Si(0.2)-TiO_2, and (▲) Fe(x)-TiO_2(GT) with various Fe-loading. Reaction conditions: Acetaldehyde, 0.2 mmol; catalyst, 0.2 g.

addition was reported by some papers [20–23]. On the other hand, as shown in Figure 6-6, no visible-light-induced photocatalytic activity was observed over Fe-impregnated TiO_2(GT) and Si(0.2)-TiO_2. This discrepancy is due to the preparation method as well as the structure of Fe species. The visible-light-induced activities are obtained for Fe-doped TiO_2 catalysts, in which Fe ions are doped in the anatase structure [20–23]. For the Fe-loaded TiO_2(GT) and Si(0.2)-TiO_2 examined in this study, Fe species are located on the surface of the catalysts, and therefore, no visible-light-induced photocatalytic activity was recognized.

Several authors previously reported that the enhanced photocatalytic activity of the iron-modified TiO_2 samples *under UV-light irradiation* was due to the effective electron-hole charge separation by the addition of Fe^{3+} [1,2,24]. Choi et al. examined the role of various metal ion dopants in quantum-sized TiO_2 and reported that the quantum yield for TiO_2 was significantly improved by the Fe^{3+} doping [1]. They emphasized an ability of Fe^{3+} dopant as effective electron/hole traps by considering the energy diagrams of TiO_2 and the transition metal oxides. In the present study we demonstrate that the iron species loaded on N- and Si- co-doped titanias functioned as an effective electron transporter from the conduction band to oxygen molecules and inhibited the electron-hole recombination (vide infra).

6.3.3 ESR studies of Fe-loaded N-Si(0.2)-TiO_2

In order to explore the effect of Fe-loading on electron transfer behavior under an irradiation condition, the ESR spectra of Fe(x)-Si(0.2)-TiO_2 without N-doping are discussed first. The ESR spectra of Si(0.2)-TiO_2 under a dark and a UV-light irradiation conditions are depicted in Figures 6-7(a) and 6-7(b), respectively, and those of

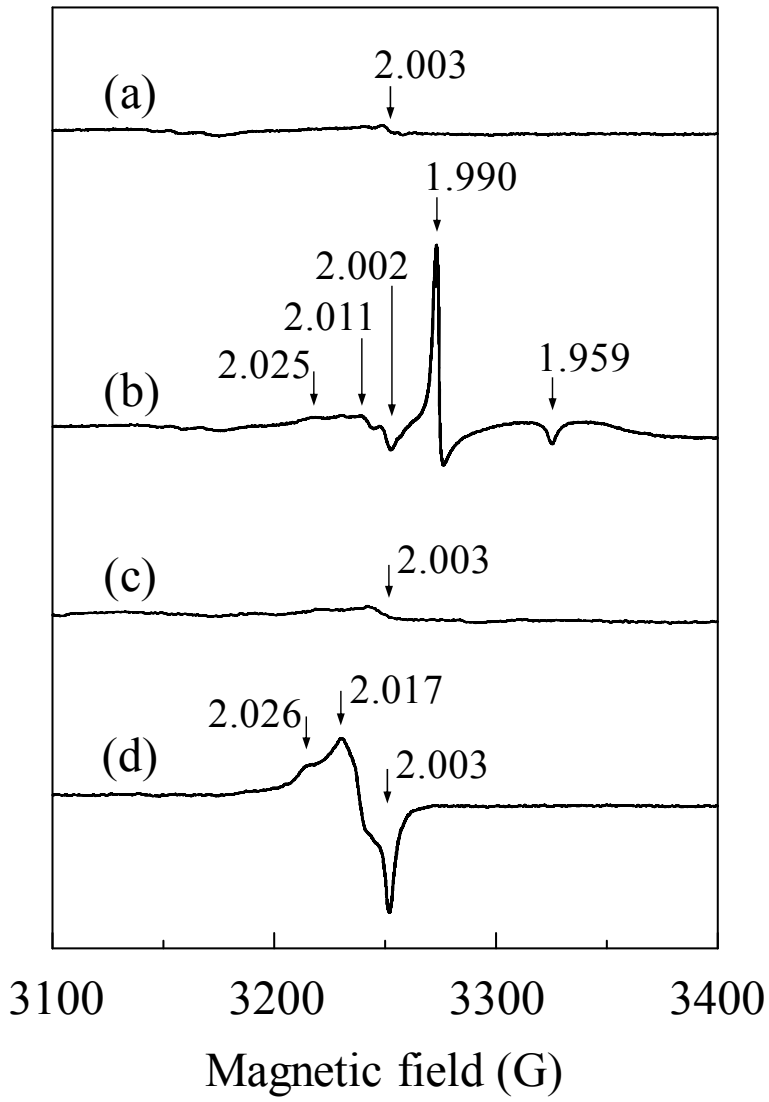

Fig. 6-7 ESR spectra of: (a) and (b), Si(0.2)-TiO_2; (c) and (d), Fe(0.001)-Si(0.2)-TiO_2; measured at 123 K in air under: (a) and (c), a dark condition; (b) and (d), UV-light irradiation.

Fe(0.001)-Si(0.2)-TiO_2 are shown in Figures 6-7(c) and 6-7(d). For the non-nitrified sample, Si(0.2)-TiO_2, under a dark condition, only a weak ESR signal was observed at g = 2.003, which is assigned to free electrons in TiO_2 [25]. On UV-light illumination, however, several ESR signals appeared. The signals at g = 1.990 and 1.959 were assigned to trapped electrons on Ti (Ti^{3+}) [26,27] and some other weak signals at $g \approx$ 2.025–2.002 were assigned to O_2^- (g_1 = 2.025, g_2 = 2.009, g_3 = 2.003) and trapped holes (g_1 = 2.016, g_2 = 2.012, g_3 = 2.002) [27].

As for Fe(0.001)-Si(0.2)-TiO_2, the ESR spectrum measured under a dark condition was essentially identical with that of Si(0.2)-TiO_2. On the contrary, in the ESR spectrum of Fe(0.001)-Si(0.2)-TiO_2 measured under UV-light illumination, no signals due to Ti^{3+} were observed. A similar result, disappearance of the Ti^{3+} signal by the Fe-loading, was previously reported under evacuated conditions [4,28]. The present study clearly demonstrates that a similar phenomenon occurs under the aerated conditions. Moreover, the signals at $g \approx$ 2.025–2.002 assigned to O_2^- and trapped holes became significant. These results indicate that the Fe species promote the transfer of the photoexcited electrons from the conduction band of TiO_2 to oxygen molecules.

When ESR of evacuated Fe(0.001)-Si(0.2)-TiO_2 was measured under a dark condition, an ESR signal at g = 4.3 assigned to Fe^{3+} species was observed in the magnetic field from 1000 to 2000 G, as shown in Figure 6-8(I)(a). After UV-light irradiation for 5 min (Figure 6-8(I)(b)), the intensity of the signal apparently decreased, suggesting that Fe^{3+} was reduced to Fe^{2+} by trapping the photoexcited electrons in the conduction band of TiO_2. As the irradiation time was prolonged, the intensity of the Fe^{3+} signal further decreased. On the other hand, under an aerated condition, as shown in Figure 6-8(II), the intensity of the Fe^{3+} signal did not change significantly even after

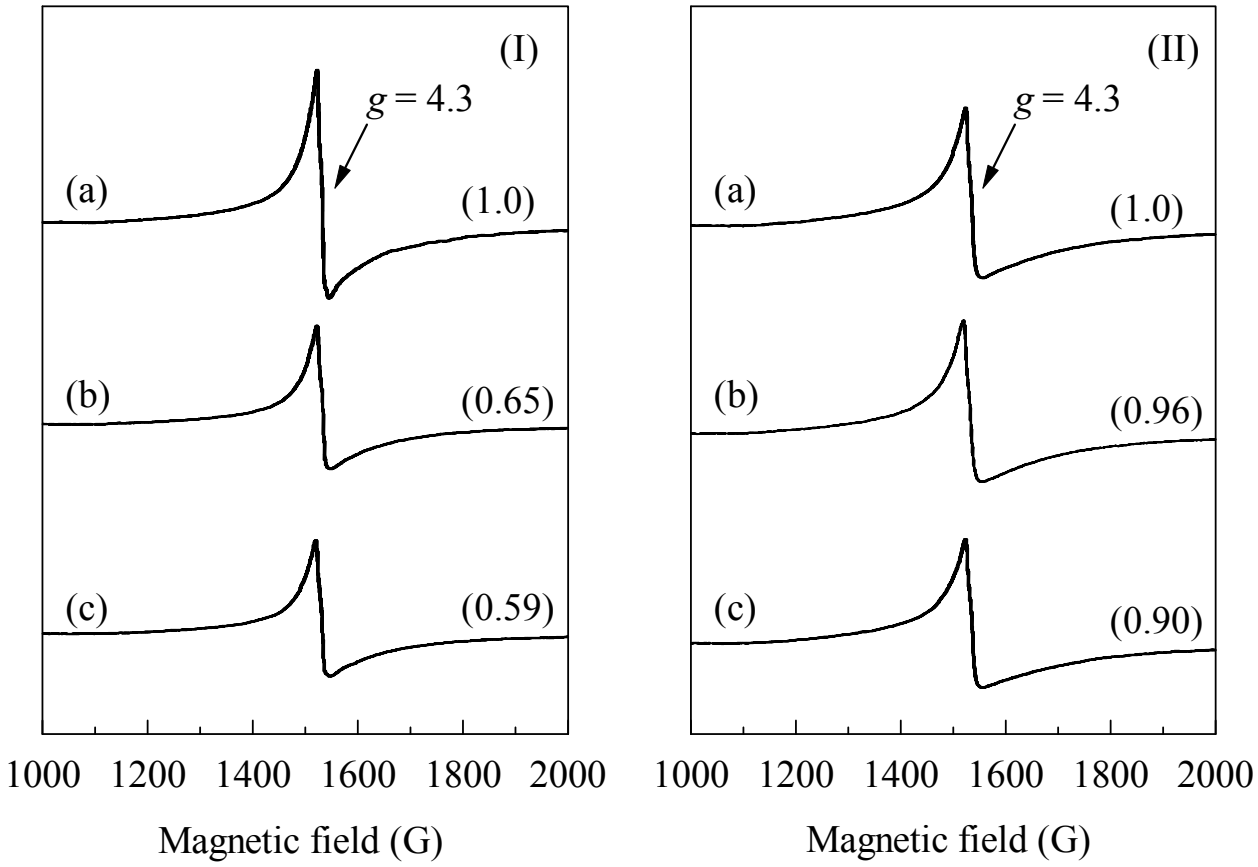

Fig. 6-8 ESR spectra of Fe(0.001)-Si(0.2)-TiO_2 measured at 123 K in vacuum (I) and in air (II); before (a) and after UV-light irradiation for: (b) 5 min and (c) 30 min. The number in parentheses indicates relative intensity of the signal to that before UV-light irradiation

UV-light irradiation for 30 min. This result suggests that electrons accepted by Fe^{3+} species are transferred quickly to oxygen molecules under the aerated condition. Similar results were previously reported [4,28].

ESR measurement was also performed on the nitrified samples. In the ESR spectrum of N-Si(0.2)-TiO_2 measured under the dark and evacuated conditions (Figure 6-9(a)), a small triplet signal (triplet-1) centered on g_1 = 1.999 (A_1 = 32.2 G) was observed. This triplet signal is due to the N species adsorbed on the surface [29,30]. On visible-light irradiation (Figure 6-9(b)), a large triplet signal (triplet-2) centered on g_2 =2.003 (A_2 = 32.3 G) appeared. Triplet-2 is assigned to the paramagnetic N species doped in the TiO_2 lattice [29–32]. The spectrum observed in the dark (Figure 6-9(a)) was apparently different from those reported previously where both triplet-1 and triplet-2 were observed [29,30]. In the present study, the sample was kept in the dark for a relatively long period at room temperature and therefore triplet-2 had disappeared before the ESR measurement.

The intensity of triplet-1 did not change even after visible-light irradiation, indicating that the N species giving triplet-2 by visible-light irradiation are closely connected with the visible-light-induced photocatalytic activity. After visible-light irradiation was stopped, a certain degree of decay of triplet-2 was observed; however, the subsequent decay rate was very slow. Even after the irradiated sample was placed in the dark at 298 K for 1 h, low-intensity signals due to triplet-2 were still observed. These results indicate that the holes formed in the dopant level by photoexcitation were transferred to localized N species yielding the ESR signals.

In the case of the sample with Fe-loading (Fe/Ti = 0.001), only low-intensity signals due to triplet-1 were observed under the dark condition as shown in Figure

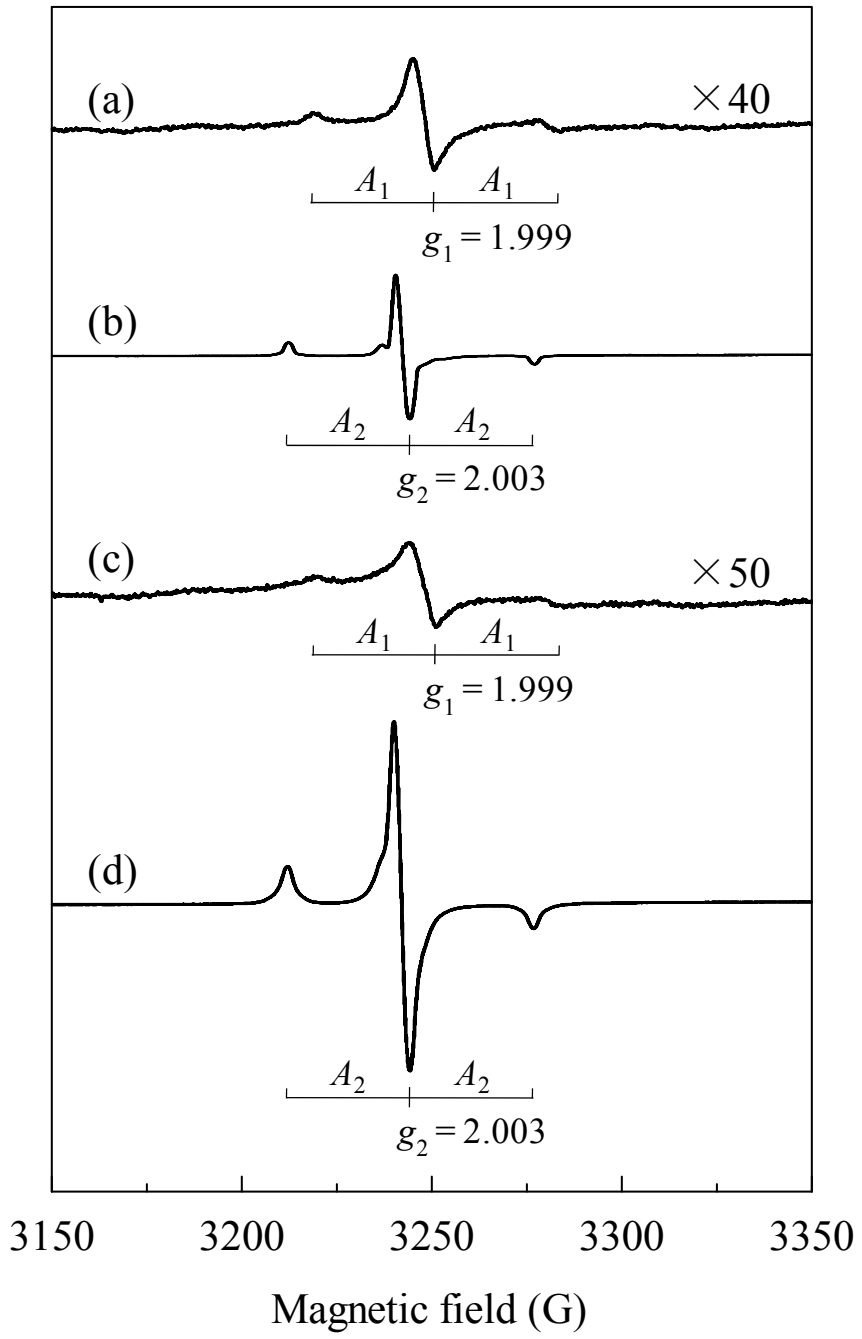

Fig. 6-9 ESR spectra of: (a) and (b), N-Si(0.2)-TiO_2; (c) and (d), Fe(0.001)-N-Si(0.2)-TiO_2; measured at 123 K in vacuum under: (a) and (c), a dark condition; (b) and (d), visible-light irradiation.

6-9(c), and triplet-2 appeared on visible-light irradiation (Figure 6-9(d)), which is quite similar to the case of N-Si(0.2)-TiO_2. Here, it should be noted that triplet-2 in the Fe-loaded sample was more than twice as intense as that observed in the sample without Fe-loading, which indicates that the Fe-loading increases the concentration of the photogenerated holes in the dopant level, thus increasing of the number of the paramagnetic N species in the Fe-loaded samples. The increase in the hole concentration can, in turn, be explained by the efficient transfer of the photogenerated electrons from the conduction band to the Fe species, thus disturbing the electron-hole recombination.

Figures 6-10(I) and 6-10(II) show the effect of visible-light irradiation on the ESR spectra of Fe(0.001)-N-Si(0.2)-TiO_2 in the magnetic field from 1000 to 2000 G measured in vacuum and air, respectively. When the measurement was performed in vacuum (Figure 6-10(I)), irradiation significantly decreased the intensity of the signal due to Fe^{3+} (g = 4.3), and the intensity of the signal decreased further as the visible-light irradiation time was prolonged. Under the aerated condition (Figure 6-10(II)), on the other hand, the intensity of the Fe^{3+} signal did not change significantly by visible-light irradiation. Similar results were reported previously [9]. These results are essentially identical with those of Fe(0.001)-Si(0.2)-TiO_2 under UV-light irradiation shown in Figure 6-8, suggesting the role of Fe species in the electron-transfer process on nitrified samples under visible-light irradiation is essentially the same as that on non-nitrified samples under UV-light irradiation. In other words, the role of Fe species on the catalysts is to accept the photoexcited electrons in the conduction band of TiO_2 efficiently and to transfer them to oxygen molecules. Through these processes, the electrons are separated from the holes effectively, and therefore, the recombination of

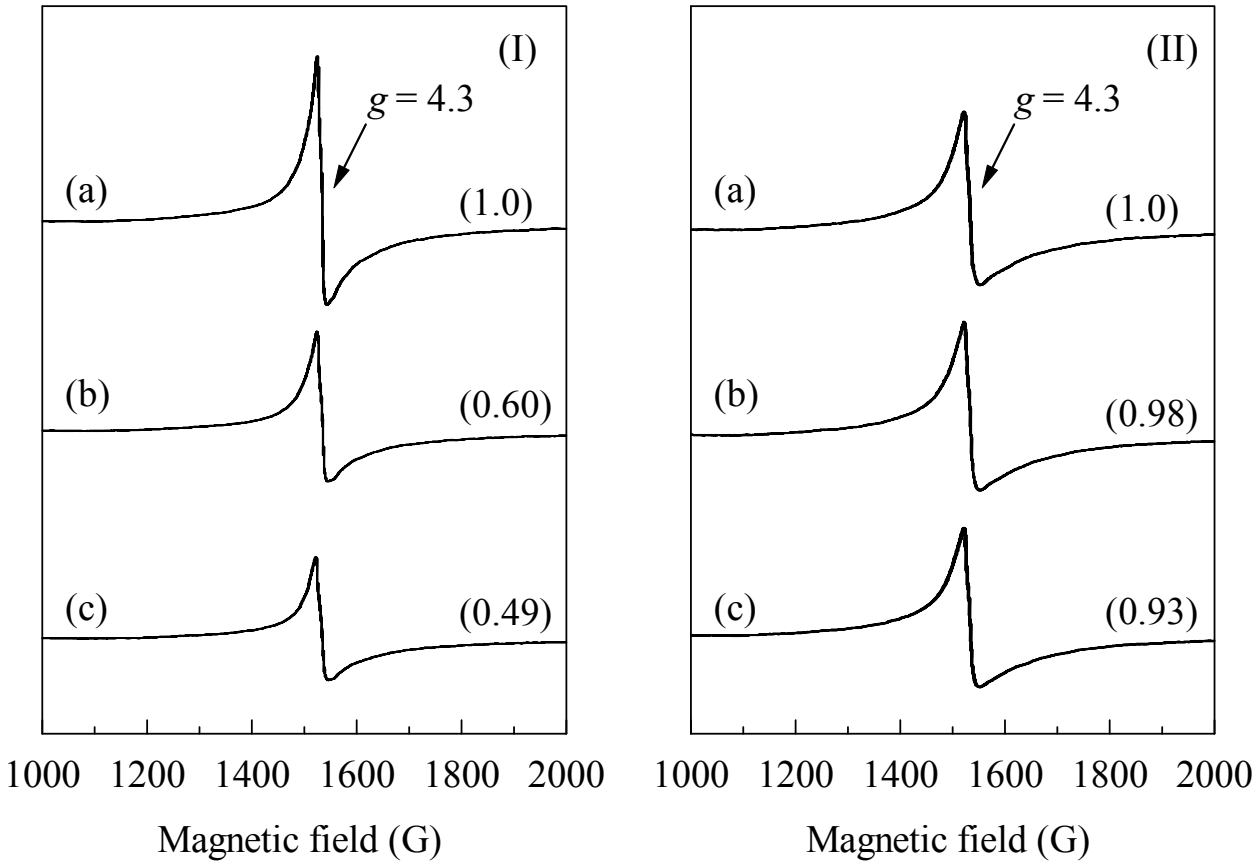

Fig. 6-10 ESR spectra of Fe(0.001)-N-Si(0.2)-TiO_2 measured at 123 K in vacuum (I) and in air (II); before (a) and after visible-light irradiation for: (b) 5 min and (c) 30 min. The number in parentheses indicates relative intensity of the signal to that before visible-light irradiation.

them is suppressed, which consequently bring about a marked improvement in the photocatalytic activity in this system.

6.4 Conclusions

The photocatalytic activities of various nitrified titania photocatalysts modified with Fe by an impregnation method were examined for decomposition of acetaldehyde under visible-light irradiation. For all the N-doped titanias, the addition of Fe caused a marked enhancement in the photocatalytic activity. Among the samples examined here, Fe-loaded N- and Si-co-doped titania showed the highest photocatalytic activity. The photocatalytic activity of the samples was well correlated to the amount of the nitrogen introduced into the TiO_2 lattice. The photocatalytic activity of N- and Si-co-doped titania was enhanced drastically by the addition of relatively small amounts of iron, and the high activities were obtained for a wide range of Fe/Ti from 0.005 to 0.07. The highest photocatalytic activity was attained by Fe(0.03)-N-Si(0.2)-TiO_2 which was about 12 times as high as that of N-Si(0.2)-TiO_2. ESR analysis clearly showed that Fe species accepted the photoexcited electrons and transferred them to oxygen molecules. These processes conduced to an effective separation of electrons and holes, thus contributing to the enhanced photocatalytic activity.

References

[1] W. Choi, A. Termin, and M. R. Hoffman, *J. Phys. Chem.* **1994**, *98*, 13669.

[2] M. I. Litter and J. A. Navío, *J. Photochem. Photobiol., A* **1996**, *98*, 171.

[3] G. N. Schrauzer and T. D. Guth, *J. Am. Chem. Soc.* **1977**, *99*, 7189.

[4] J. Soria, J. C. Conesa, V. Augugliaro, L. Palmisano, M. Schiavello, and A. Sclafani, *J. Phys. Chem.* **1991**, *95*, 274.

[5] A. Milis, J. Peral, X. Domènech, and J. A. Navío, *J. Mol. Catal.* **1994**, *87*, 67.

[6] Z. Luo and Q.-H. Gao, *J. Photochem. Photobiol., A* **1992**, *63*, 367.

[7] S. Ikeda, N. Sugiyama, B. Pal, G. Marcí, L. Palmisano, H. Noguchi, K. Uosaki, and B. Ohtani, *Phys. Chem. Chem. Phys.* **2001**, *3*, 267.

[8] A. D. Paola, G. Marcí, L. Palmisano, M. Schiavello, K. Uosaki, S. Ikeda, and B. Ohtani, *J. Phys. Chem. B* **2002**, *106*, 637.

[9] T. Ohno, Z. Miyamoto, K. Nishijima, H. Kanemitsu, and F. Xueyuan, *Appl. Catal., A* **2006**, *302*, 62.

[10] B. Gao, Y. Ma, Y. Cao, W. Yang, and J. Yao, *J. Phys. Chem. B* **2006**, *110*, 14391.

[11] H. Ozaki, S. Iwamoto, and M. Inoue, *Catal. Lett.* **2007**, *113*, 95.

[12] S. Iwamoto, K. Saito, M. Inoue, and K. Kagawa, *Nano Lett.* **2001**, *1*, 417.

[13] S. Iwamoto, W. Tanakulrungsank, M. Inoue, K. Kagawa, and P. Praserthdam, *J. Mater. Sci. Lett.* **2000**, *19*, 1439.

[14] Sh. Iwamoto, Se. Iwamoto, M. Inoue, H. Yoshida, T. Tanaka, and K. Kagawa, *Chem. Mater.* **2005**, *17*, 650.

[15] Y. Nosaka, M. Matsushita, J. Nishino, and A. Y. Nosaka, *Sci. Technol. Adv. Mater.* **2005**, *6*, 143.

[16] N. D. Shinn and K. L. Tsang, *J. Vac. Sci. Technol., A* **1991**, *9*, 1558.

[17] N. C. Saha and H. G. Tompkins, *J. Appl. Phys*. **1992**, *72*, 3072.

[18] M. I. Litter and J. A. Navío, *J. Photochem. Photobiol., A* **1994**, *84*, 183.

[19] L. A. Marusak, R. Messier, and W. B. White, *J. Phys. Chem. Solids* **1980**, *41*, 981.

[20] H. Yamashita, M. Harada, J. Misaka, M. Takeuchi, B. Neppolian, and M. Anpo, *Catal. Today* **2003**, *84*, 191.

[21] X. H. Wang, J.-G. Li, H. Kamiyama, Y. Moriyoshi, and T. Ishigaki, *J. Phys. Chem. B* **2006**, *110*, 6804.

[22] J. Zhu, F. Chen, J. Zhang, H. Chen, and M. Anpo, *J. Photochem. Photobiol., A* **2006**, *180*, 196.

[23] W. Y. Teoh, R. Amal, L. Mädler, and S. E. Pratsinis, *Catal. Today* **2007**, *120*, 203.

[24] M. Sadeghi, W. Liu, T-G. Zhang, P. Stavropoulos, and B. Levy, *J. Phys. Chem.* **1996**, *100*, 19466.

[25] M. Okumura, J. M. Coronado, J. Soria, M. Haruta, and J. C. Conesa, *J. Catal.* **2001**, *203*, 168.

[26] Y. Nakaoka and Y. Nosaka, *J. Photochem. Photobiol., A* **1997**, *110*, 299.

[27] R. F. Howe and M. Grätzel, *J. Phys. Chem.* **1987**, *91*, 3906.

[28] M. Grätzel and R. F. Howe, *J. Phys. Chem.* **1990**, *94*, 2566.

[29] R. D. Iyengar and R. Kellerman, *J. Colloid Interface Sci.* **1971**, *35*, 424.

[30] S. Livraghi, M. C. Paganini, E. Giamello, A. Selloni, C. D. Valentin, and G. Pacchioni, *J. Am. Chem. Soc.* **2006**, *128*, 15666.

[31] Y. Yamamoto, S. Moribe, T. Ikoma, K. Akiyama, Q. Zhang, F. Saito, and S. Tero-Kubota, *Mol. Phys.* **2006**, *104*, 1733.

[32] Y. Wang, C. Feng, Z. Jin, J. Zhang, J. Yang, and S. Zhang, *J. Mol. Catal., A* **2006**, *260*, 1.

General Conclusion

In this thesis, the photocatalytic properties of the xerogels of Si-modified titanias prepared by the glycothermal method under UV-light irradiation and the visible-light-induced photocatalytic activities of nitrified Si-modified titanias are described.

In chapter 1, the physicochemical properties of Si-modified titania xerogels and their photocatalytic activities for the degradation of several organic dyes are described. Xerogels of nanocrystalline Si-modified titanias having large surface areas and superior thermal stabilities were obtained by the glycothermal method, followed by the removal of the organic phase by flash evaporation. With an increase in the amount of Si addition, the crystallite size of the sample decreased and BET surface area increased. The zeta potential shifted to a more negative value due to the Si addition, which affected the adsorbability of dyes. The obtained xerogels of Si-modified titanias were effective photocatalysts for the decomposition of organic dyes and exhibited higher activities as compared to JRC-TIO-4. The xerogel samples were highly dispersed in aqueous solutions because the coagulation, which could have occurred during the drying stage in the sample preparation, was effectively prevented; this feature is one of the critical factors responsible for the high activities of the xerogel catalysts. Their effectiveness for the photocatalytic decomposition of cationic dyes was remarkable since the negative surface charge of the catalysts enhanced the adsorbability for these dyes.

Chapter 2 discusses the visible-light-induced photocatalytic activities of Si-modified titanias (Si/Ti = 0.1) obtained by NH_3 treatment at high temperatures. As

compared with the NH_3-treated TiO_2 without Si modification, the NH_3-treated Si-modified titanias showed a stronger absorption in the visible region (400–500 nm) and exhibited a larger peak at 396 eV in the N 1s XPS spectrum, indicating that a larger amount of nitrogen was stably doped in the Si-modified titania. The nitrified Si-modified titania exhibited a higher photocatalytic activity for the degradation of Rhodamine B and decomposition of acetaldehyde under visible-light irradiation than the nitrified titania.

In chapter 3, the author examined the effects of the amount of Si addition and annealing treatment on the photocatalytic activities of N- and Si-co-doped titanias under visible-light irradiation. It was found that the extent of Si modification significantly affected the amount of doped nitrogen and visible-light-induced photocatalytic activity. The annealing treatment subsequent to the NH_3 treatment also significantly affected the photocatalytic activities. Higher annealing temperature (500 °C) decreased the population of oxygen vacancies and increased the photocatalytic activity despite the fact that the amount of doped nitrogen was reduced by the annealing at that temperature. The Si-modified titania with a Si/Ti ratio of 0.3, nitrified at 600 °C for 1 h and annealed at 500 °C, exhibited the highest photocatalytic activity.

Chapter 4 deals with the photocatalytic activities of NH_3-treated titanias modified with elements other than Si. Among the six modifiers (B, Mg, Al, P, Zn, and Ga) examined, the addition of P was the most effective for the photocatalytic decomposition of acetaldehyde under visible-light irradiation. The N- and P-co-doped titanias showed stronger absorption in the visible region (400–550 nm) and exhibited a large peak at 396 eV in the N 1s XPS spectrum. It was found that the photocatalytic activity was related to the amount of nitrogen atoms doped in the anatase structure.

In chapter 5, the effect of the addition of a small amount of V on the photocatalytic

activities of N- and Si-co-doped titanias under visible-light irradiation was discussed. It was found that a very small amount of V loading (V/Ti = 0.0001–0.001) significantly enhanced the photocatalytic activity under visible-light irradiation. Highly dispersed vanadium species located on the surface of the N- and Si- co-doped titanias play a critical role as the electron trap sites. These trap sites contribute to an effective separation of photoinduced electrons and holes; consequently, they improve the photocatalytic activity under visible-light irradiation.

Chapter 6 discusses the visible-light induced photocatalytic activities of various nitrified titania photocatalysts modified with Fe by an impregnation method. Si-modified titanias synthesized by the glycothermal method and three types of TiO_2 without Si modification, i.e., TiO_2 prepared by the glycothermal method and the commercially available TiO_2, P-25 and ST-01, were nitrified by heating in an NH_3 flow at high temperatures, followed by annealing in air. Small amounts of Fe were loaded onto these samples, and their photocatalytic activities for the decomposition of acetaldehyde under visible-light irradiation were investigated. For all the N-doped titanias, the addition of Fe caused a marked enhancement in the photocatalytic activity. Among the samples, the Fe-loaded N- and Si-co-doped titanias showed the highest photocatalytic activity. The addition of small amounts of Fe (Fe/Ti = 0.005–0.7) to N- and Si-co-doped titanias enhanced the visible-light-induced photocatalytic activity by more than 10 times. The ESR studies of the Fe-loaded N- and Si-co-doped titanias suggested that the Fe(III) species loaded on the nitrified samples accepted the photoexcited electrons, and then transferred them to the oxygen molecules. These processes facilitated the electron-hole charge separation, thus suppressing the recombination of the photogenerated electrons and holes, and consequently, contributed to the improvement in the photocatalytic

activity.

The visible-light-responsive photocatalysts presented in this thesis can be obtained with relative ease, and they are composed of inexpensive and safe elements such as Ti, Si, N and Fe; therefore, they are expected to be practically employed in the field of environmental purification.

List of Publications

Chapter 1

“Photocatalytic activities of nanocrystalline Si-modified titania xerogels prepared by the glycothermal method”

H. Ozaki, K. Saito, S. Iwamoto, M. Inoue,

Journal of Materials Science, *in press*

Chapter 2

“Enhanced visible light sensitivity of nitrogen-doped nanocrystalline Si-modified titania prepared by the glycothermal method”

H. Ozaki, S. Iwamoto, M. Inoue,

Chemistry Letters, 34 (2005) 1082-1083.

“Improved visible-light responsive photocatalytic activity of N and Si co-doped titanias”

H. Ozaki, S. Iwamoto, M. Inoue,

Journal of Materials Science, 42 (2007) 4009-4017.

Chapter 3

“Effects of amount of Si addition and annealing treatment on the photocatalytic activities of N- and Si-co-doped titanias under visible-light irradiation”

H. Ozaki, S. Iwamoto, M. Inoue,

Industrial & Engineering Chemistry Research, *submitted*.

Chapter 4

"Photocatalytic activities of NH_3-treated titanias modified with other elements"

H. Ozaki, N. Fujimoto, S. Iwamoto, M. Inoue,

Applied Catalysis B: Environmental, 70 (2007) 431-436.

Chapter 5

"Effect of the addition of a small amount of vanadium on the photocatalytic activities of N- and Si- co-doped titanias under visible-light irradiation"

H. Ozaki, S. Iwamoto, M. Inoue,

Catalysis Letters, 113 (2007) 95-98.

Chapter 6

"Marked promotive effect of iron on visible-light-induced photocatalytic activities of nitrogen- and silicon-codoped titanias"

H. Ozaki, S. Iwamoto, M. Inoue,

Journal of Physical Chemistry C, 111 (2007) 17061-17066.

Acknowledgments

The present thesis summarizes the author's studies performed at the Department of Energy and Hydrocarbon Chemistry, Graduate School of Engineering, Kyoto University.

First of all, the author wishes to express his greatest gratitude to Professor Masashi Inoue for his invaluable advice and suggestion throughout the course of this work.

The author is also grateful to Professor Koichi Eguchi and Professor Tsunehiro Tanaka for their kind guidance and comments that helped him in the completion of this thesis.

A special word of thanks is conveyed to Dr. Shinji Iwamoto for his valuable discussion and support.

Sincere gratitude is also expressed to Dr. Hiroyoshi Kanai, Dr. Seiichiro Imamura, Dr. Kenji Wada, Dr. Masaru Takahashi, and Dr. Saburo Hosokawa for their kind advice and encouragement.

The author also thanks all the members of Professor Inoue's Laboratory who worked together from 2002 to 2008 for their kind encouragement, support, and collaboration.

Finally, the author would like to thank his family immensely, particularly, his parents Akihiro and Michiko Ozaki, for their understanding, support, and encouragement.

Hirotaka Ozaki

2008